COMPARTMENTALIZED HYDROGEL MICROCAPSULES AND THEIR APPLICATIONS IN MICROTISSUE ENGINEERING

A Dissertation

Presented to the Faculty of the Graduate School

of Cornell University

In Partial Fulfillment of the Requirements for the Degree of

Doctor of Philosophy

by

Yen-Chun Lu

December 2018

COMPARTMENTALIZED HYDROGEL MICROCASPULES AND THEIR APPLICATIONS IN MICROTISSUE ENGINEERING

Yen-Chun Lu, Ph. D.

Cornell University 2018

Three-dimensional (3D) cell culture has been broadly used to mimic the *in-vivo* microenvironment. Compared with traditional methods for 3D culture in which cells are embedded within a bulk extracellular matrix, compartmentalized hydrogel microcapsules, such as those with a core-shell structure, provide better mass transfer due to higher surface-to-volume ratio. In addition, such capsules can be fabricated by a multi-fluidic electrostatic co-spraying technique at a high production rate (> 10,000 capsules/min) with nearly monodisperse spherical shape and tunable size, and they can be cultured in suspension for scalable biomanufacturing applications. In this dissertation, I first proved the feasibility of producing complex microcapsules by using the electrostatic co-spraying technique. Then, I demonstrated the applications of core-shell decoupled microcapsules in large-scale production of microtissues, for example, tumoroids, hepatocyte/stromal aggregates, and small intestinal organoids, all of which could be used for applications such as drug screening and disease modeling. Lastly and most importantly, I used the core-shell microcapsules to study the effect of physical confinement on mammary tumorigenesis. It has been known that physical microenvironment, including matrix stiffness, plays an important role in cancer initiation and progression. In this work, I discovered that confinement – a new

physical parameter unlike stiffness - can also induce malignant transformation in mammary epithelial cells. I found that MCF10A cells, a benign mammary cell line that forms growth-arrested polarized acini in Matrigel, transforms into cancer-like cells within the same Matrigel material following confinement in alginate shell hydrogel microcapsules. The confined cells exhibited a range of tumor-like behaviors, including uncontrolled cellular growth and invasion. Additionally, 4-6 weeks after transplantation into the mammary fad pads of immunocompromised mice, the confined cells formed large palpable masses that exhibited histological features similar to that of carcinomas. Taken together, my findings not only suggest confinement as a previously unrecognized mechanism for malignancy induction in mammary epithelial cells but also provide a new, microcapsule-based, high throughput platform in therapeutic development for breast cancer.

BIOGRAPHICAL SKETCH

Yen-Chun was born and raised in Taipei, Taiwan, and he has a lovely family with parents and one younger brother. Since he was a child, he has a dream to be a doctor to cure every disease that suffers people in the world. Later, he attended the best high school in Taiwan, Taipei Municipal Jianguo High School where he realized that biomedical engineer is a great choice as his career, because research in this field not only enhance patients' life quality but also save lives in the world by developing new medicines or techniques. After high school, he studied in National Taiwan University (NTU) with double majors in Chemical Engineering and Civil Engineering, and minor in Economics. In NTU, he joined a protein engineering lab to study how an inhibitor, TCEP prevents amyloid formation in Alzheimer's Disease. After graduation from NTU, he served in military for 11 months at a small island called Dongyi which is closed to Mainland China. To chase his dream, he then attended his Master of Engineering program in Biomedical Engineering at Cornell University. During M. Eng. Program, he joined Professor Michael Shuler's lab to establish in-vitro brain model in "body-on-the-chip" project and developed his interests in biomaterials. Luckily, he started to pursue his Ph.D. degree with Professor Minglin Ma in Biological and Environmental Engineering at Cornell University after the master program. While he focused on research in biomanufacturing and breast cancer formation, he met a lovely woman, Jessica Huang at Cornell University and got married in 2018. Besides devoting himself in the exciting research, he served as President of Cornell Taiwanese Student Association for one year to help the

Taiwanese community and also volunteered in many public scientific educations, for example, scientific show in Sciencenter at Ithaca and program facilitator in NYS 4H Stem career exploration. After six years at Cornell University, he is now ready to move to Boston for his new journey.

To my family and friends

ACKNOWLEDGMENTS

I would like to express my appreciation to my Ph.D. advisor and my committee chair, Professor Minglin Ma for his great guidance and advice in my professional development. Although Minglin is super busy, he always spends time discussing research with me every week. With his continuous help and support, I could finish this dissertation and develop my expertise in biomedical engineering and cancer biology. Also, I would like to thank my committee members, Professor Scott Coonrod and Professor Claudia Fischbach for their great and constructive advices in my research projects. In addition, I would like to thank Professor Charles Danko for his help in bioinformatics. Without his help, I cannot learn this novel technique in two weeks.

Furthermore, I would like to acknowledge my labmates and my collaborators, especially Duo An, Alan Chiu, Longhai Wang, Wei Song, Yudi Pardo, Kai-Yuan Chen, Kuei-Ling Tung, Yitian Xu, Lihua Wang, Pengcheng Bu, Da-Jiun Fu, Shao-Pei Chou, Tinyi Chu, Ed Rice, Matthew Hall, Beum Jun Kim, Yi-Chun Yeh, Rebecca Harman, Chieh-Ren Hsia, Chinatsu Mukai and Lynne Anguish for their help, suggestion and discussion in my research.

Last but not the least, I would like to thank my wife, Jessica Huang, for the love and the happiness she brings; moreover, she always supports me to chase my dream and encourage me whenever I feel depressed. Also, I would like to thank my parents, Jen-Fu Lu and Feng-Chin Wang for their endless love and supports, so I could devote myself to the research at Cornell University. Finally, I want to thank my hamster, Jerry and my cats, Dodo and Mumu for their company.

TABLE OF CONTENTS

LIST OF FIGURES

LIST OF TABLES

CHAPTER 1: INTRODUCTION

1.1 Three-Dimensional Cell Culture

Three-dimensional (3D) cell culture has been broadly used for *in-vitro* studies, such as drug discovery, tissue engineering, and stem cell-based organoid research. In traditional two-dimensional (2D) cell culture, the cells are usually grown on a rigid substrate, for instance, polystyrene culture flasks or petri dishes (Figure 1a). The culture flasks/dishes allow cells attach to the flat surface and form monolayer. However, *in-vivo*, cells are surrounded by an extracellular matrix (ECM) in a 3D environment. 3D cell culture provides a more realistic model of the natural environment and therefore more accurate predictions of cell behavior (gene expression) for *in-vivo* drug discovery, tissue engineering, tumorigenesis research[1]. In addition, 3D culture better represents the mass transport of nutrients or drugs and metabolism. To date, many methods have been developed for 3D cell cultures, for example, seeding cells on/in ECM gel[1], hanging drop plate[2,3], microwells[4,5], microfluidics[6–8], and rotating flasks[9]. Here we introduce some conventional methods for 3D cell culture.

1.1.1 3D scaffold

The most common method for 3D cell culture is to seed cells on the surface of an ECM gel or mixed within ECM matrix (Figure 1b), where the ECM typically consists of type I collagen, reconstituted basement matrix (Matrigel™), or fibrin gel. The chosen ECM matrix plays a supporting role in hemidesmosome formation for interaction between integrin on cell surface and protein. This method provides a

convenient way to grow cells in 3D matrix.

1.1.2 Hanging Drop Plate

Hanging Drop Plate[2,3] (Figure 1c) is designed to use gravity force to form cell aggregations in 3D culture. Moreover, the culture is not only used for one single cell type but also cell co-culture by mixing different types of cells in medium before seeding to wells. It is easy to change medium from top of the well and the initial number of cells controls the size of the cell aggregations.

1.1.3 Microwells

Microwells[4,5] (Figure 1d) developed from microtechnology are typically designed in the micrometer size range to create microliter-volume space to trap cells. Microwells are typically fabricated via soft lithography from an elastomeric mold cast off a master pattern. To form the master pattern photoresist is deposited on a silicon wafer and exposed it to UV light through a mask to impart the desired pattern. Poly(dimethylsiloxane) (PDMS) precursor is poured on the master mold and polymerized by thermal curing. After removing the PDMS from the mold, the structure of silicon wafer mold is imprinted in the PDMS, making it ready for 3D cell culture. Similar to the hanging drop plate, the size of cell aggregation is determined by the cell density in the original medium used to fill the microwells, because the cells were dropped into microwell by gravity force.

1.1.4 Hydrogel Encapsulation

Hydrogels consist of a hydrophilic polymer matrix, which is swollen with water to mimic the *in-vivo* microenvironment for cell culture. There are two major

categories of hydrogel, natural and synthetic hydrogels. Natural hydrogels consist of extracellular matrix (ECM) (e.g., type I collagen, reconstituted basement matrix (Matrigel™), fibrin gel) and polysaccharides from nature (e.g., alginate, chitosan and hyaluronan). On the other hands, synthetic hydrogels, such as acrylic acid, polymethyl methacrylate, polyethylene glycol are also used for cell encapsulation in 3D culture. The advantages of natural hydrogel are that they are more biocompatible and degradable than synthetic hydrogels. However, synthetic hydrogels tend to be more consistent in quality assurance.

Different ECM materials support cell attachment, proliferation and cellular function for different types of cells. For instance, fibrin gel supports angiogenesis in cultures of human umbilical vein endothelial cells (HUVECs), collagen matrices provide stiff fibers for cell migration studies, and laminin-rich reconstituted basement membrane matrices (Matrigel™) support stem cell-based organoid growth or mammary epithelium development in human benign mammary epithelial cells (MCF10A). While these protein-based matrices are effective scaffolds for *in-vitro* 3D cell culture they are not appropriate for transplantation in immunocompetent animals. To protect the cells from immune response, polysaccharides, such as alginate or chitosan and some synthetic hydrogels are better choices. However, although these hydrogels can isolate cells from the immune systems, they cannot fully support the cellular functions.

1.2 Designing compartmentalized hydrogel microcapsules

Hydrogel microcapsules have been used extensively for cell encapsulation, culture and transplantation[10–15].The microcapsules protect the cells from the

environment, or the immune system when transplanted, while simultaneously allowing facile mass transfer necessary for the cellular survival and function. They have therefore found tremendous applications in tissue engineering[16,17] and cell therapy[10,15,18]. However, in many cases, the microcapsules have no internal structure and the cells are encapsulated randomly in whatever material that forms the microcapsules, most commonly alginate[14,19]. It has now been increasingly recognized that controlling the structure and composition of these microcapsules will significantly expand their applications. For example, alginate-based core/shell microcapsules were made to improve the immunoprotective property of the capsules[20], liquid-core microcapsules were reported for confined 3D cell culture[21,22], and janus microcapsules were used for co-encapsulation[23,24]. While they had enhanced properties and functions, these structured microcapsules had no natural extracellular matrix (ECM) support. In their natural state, cells are supported architecturally by ECM, and surrounded by other cell types. Furthermore, many cells require a specific microenvironment to perform physiologically relevant functions[25–27]. For example, collagen particles have been shown to induce osteogenic differentiation of the encapsulated mesenchymal stem cells[28]. Thus, it is highly desirable to control the cellular environment within the microcapsule platform[6,29].

In this dissertation, we developed complex hydrogel microcapsules with controlled ECM internal compartments for efficient and scalable 3D cell culture. Compared with conventional 3D culture methods where the cells are embedded in bulk ECM hydrogels (e.g. collagen), the microcapsules have a larger surface-to-volume ratio for mass transfer and can be potentially cultured in suspension in stirred

bioreactors for scale-up. We made the microcapsules and encapsulated the cells by a one-step electrospray-based, multi-fluidic cell micropackaging technique. The method allowed a high rate production (> 10,000/min) of compartmentalized hydrogel microcapsules with a uniform spherical shape and nearly monodisperse size distribution. The process is relatively simple and does not involve surfactants,[7] oils[6–8] or acids[7,8] that are typically used in microfluidic flow focusing approaches.

1.2.1 Production of compartmentalized hydrogel microcapsules

We made the compartmentalized hydrogel microcapsules by adopting a multi-fluidic electrostatic spraying technique. (Figure 2) A similar technique has been previously used to prepare structured solid polymer particles[30,31]. However, here we used it to produce spherical, nearly monodisperse hydrogel microcapsules including a novel triple-layer concentric configuration for cell encapsulation. Figure 3 shows three different microcapsule designs (core-shell, side-by-side and triple-layer), all from Ca^{2+} /Ba^{2+} - crosslinked alginate hydrogel. The alginate in different compartments was labeled with a different fluorescent color for visualization purpose. Using model cells (MDA-MB-231 expressing GFP, normal human lung fibroblasts (NHLFs) with RFP and MCF-10A stained with Hoechst), we demonstrated that different types of cells could be encapsulated in distinct compartments within individual microcapsule. With a uniform spherical shape, a nearly monodisperse size distribution and a high production rate, these hydrogel microcapsules are in contrast with those made previously by the high flow rate jetting[21] or centrifuge-based[23] approaches that produced non-uniform microcapsules or the sequential deposition method that was difficult to scale up.[32] Moreover, the complex hydrogel microcapsules described here

are also unlike the previously reported structured particles that were made of solid polymers and might not be suitable for cell encapsulation applications.

1.2.2 Preparation of ECM-supported core-shell hydrogel microcapsules

To incorporate ECM into the hydrogel microcapsules, we simply replaced one or more inner alginate fluids with ECM hydrogel precursor solutions while keeping the outer alginate fluid the same. (See Figure 4a, Figure 5a, b and Figure 6a, b for schematics.) The microcapsules were formed by an ionic crosslinking of alginate outer layer followed by a thermal (37 ºC) crosslinking of ECM inner layers. ECM hydrogels such as Matrigel^{TM} provide physiologic growth environments and it is often desired to process them into robust microcapsules for cell encapsulation applications. By using the multi-fluidic electrostatic cell micropackaging, we can encapsulate and culture various types of cells in different ECM compartments inside microcapsules. (See Table 1 for a summary.) The microcapsules not only have large surface area for mass transfer but can also be suspended in stirred bioreactors for large scale cell culture and expansion. Figure 4b-d shows the hierarchical structures of core-shell microcapsules with a cell-containing ECM inner layer (collagen). (Also see Figure 5c-e for particles with an alginate outer layer and two different ECM cores, and Figure 6c-e for triple-layer concentric particles with an alginate outer layer and two different ECM inner layers.) In Figure 4d, the type I collagen fibers surrounding the cells in the microcapsule were observed by the second-harmonic generation microscopy.[33]

1.2.3 Scalable production of tumor aggregates with controlled size in core-shell microcapsules

Next, we demonstrated the ECM-containing microcapsules represented an excellent platform to generate size-controlled tumor microtissues. Tumor microtissues have many applications in drug screening, cancer modeling and therapeutic development.[34,35] Several approaches have been successfully used to make the tumor microtissues; for example, the hanging-drop method.[3] However, this method requires manual seeding of droplets and is difficult to scale up. In contrast, the microcapsules can be continuously produced and suspended in stirred bioreactors for large-scale microtissue production. Previously, liquid-core microcapsules made via the high flow rate jetting approach were proposed as a new platform to produce tumor microtissues and study the effect of confinement on their invasiveness.[21] However, more than half of the produced particles had poor shapes, making the control of microtissue size difficult.[21] Here we demonstrate the scalable production of microtissues from two different breast epithelial cells, nonmalignant MCF-10A (Figure 8a) and invasive MDA-MB-231 (Figure 8b) using our alginate/ECM core-shell microcapsules. Interestingly, the cells grew in the Matrigel inner layer and stopped growing (or grew with a much slower rate) after they filled the inner layer and reached the alginate/Matrigel interface (Figure 8c). This is consistent with the observation that these cells did not proliferate in microcapsules composed of alginate alone. (Figure 9) The confined growth in the microcapsules enabled us to control the microtissue size, from 95 μm to 725 μm, by simply changing the size of the Matrigel inner layer (Figure 8d and Figure 10). Previously, large size (up to 600 μm) tumor microtissues were

considered to better mimic the primary tumor before vascularization, but were difficult to produce using conventional microfabricated cell culture platforms[36]. The 3D confinement of microcapsules also made structurally defined microtissues comparing with other unconfined systems such as bulk hydrogel or microwells for the E-cadherin-lacking MDA-MB-231 cells (Figure 11)[37,38]. After formation in within the capsules, the microtissues were easily recovered by dissolving the alginate outer layer using an ethylene diamine tetraacetic acid (EDTA) solution (Figure 8a4, b4). As expected, the cells in the microtissues exhibited a size-dependent, heterogeneous viability. While the small size microtissues had mostly live cells, the large ones had necrotic centers (Figure 12), typical of non-vascularized primary tumors.[39,40] During the course of microtissue growth, the hydrogel microcapsules were stable with limited swelling (Figure 13), consistent with previous report that the addition of Ba^{2+} into the Ca^{2+} crosslinking bath made the alginate microcapsules stronger.[41] It should be noted that for some other types of cells such as Ins-1 cells (Figure 14), the microtissues may continue to grow after they fill the ECM core and eventually break the microcapsules.

1.2.4 Co-cultures in core-shell hydrogel microcapsules

Another application of these microcapsules is for studying cell-cell interactions in confined 3D co-cultures. Two or more different types of cells at different ratios can be encapsulated together in the ECM inner layer of individual microcapsules. As an example, we encapsulated the MDA-MB-231 cells and the MCF-10A cells at a ratio of 1:1 in the alginate/Matrigel microcapsules. Remarkably, a random mixture of cells evolved over time into a well-defined, core-shell structure with the MDA-MB-231 cells (expressing dTomato fluorescence) enclosing the MCF-10A cells. (Figure 15a)

The segregation and formation of boundaries between different cell populations are common and essential in tissue development and morphogenesis.[37,42,43] Here the core-shell microcapsules provide a robust platform to study the cell segregation in a 3D confined space. One question was why the benign cells (MCF-10A) aggregated in the center, while the more invasive ones (MDA-MB-231) were segregated to the periphery. According to the differential adhesion hypothesis (DAH), the different degrees of surface adhesion induce spontaneous cell reorganization to minimize the interfacial free energy.[44] It was also shown that two types of cells with differential E-cadherin expression segregated spontaneously with lower E-cadherin expression level cells enveloping higher expression level ones.[45] In our case, the MDA-MB-231 cells lack the E-cadherin and the MCF-10A cells express higher levels of E-cadherin, leading to the unique segregation within the microcapsules.

1.2.5 Hepatocytes co-culture in compartmentalized hydrogel microcapsules

In addition to cell segregation, cell-cell interactions also play an essential role in cellular functions. Using the ECM-supported microcapsules, we co-cultured hepatocytes and stromal cells and obtained drastically improved survival of hepatocytes. *In vitro* culturing of primary hepatocytes, particularly in a scalable fashion, has important applications in drug screening and toxicity testing for pharmaceutical industries.[46,47] However, the cell viability and hepatic function decline rapidly *ex vivo*, under conventional culture conditions.[48,49] Previous studies[50–52] have shown that a combination of ECM substrate and stromal cell support could enhance the hepatocyte survival and stabilize their functions. Although several techniques[53,54] have been reported to realize this combination, most of them were essentially two-

dimensional (2D) cultures. Our ECM-supported microcapsules offer a 3D, miniaturized culture environment with a great potential for scalability and parallel cell culture. We first encapsulated the rat hepatocytes alone in the alginate/Matrigel microcapsules (Figure 15b1) and after 14 days of culture the cells appeared either dead or loosely dispersed in Matrigel (Figure 15b2, b3). By contrast, when we co-encapsulated the hepatocytes and the non-proliferating, mitotically inactivated mouse 3T3-J2 fibroblast stromal cells at a ratio of 3:1 (Figure 15c1), the cells were aggregated together and appeared mostly healthy (Figure 15c2, c3) after 14 days. The measurement of secreted albumin via ELISA (enzyme-linked immunosorbent assay) confirmed the significant improvement in hepatocyte viability in the co-culture, as shown in Figure 15d. The live/dead staining from a separate experiment also confirmed the improved survival of hepatocytes when co-encapsulated with stromal cells (Figure 16).

1.2.6 3D paracrine cell co-culture by combining hydrogel microcapsules with microwell system

Finally, to demonstrate the applications of the microcapsules for potential screening and 3D paracrine (non-contact) cell co-cultures, we combined them with an individually addressable microwell system.[4,42,55] We seeded the microcapsules (~470±30 μm) into PDMS microwells (500 μm depth and 500 μm diameter). Figure 17a shows a schematic and representative image of the fluorescently labeled alginate microcapsules seeded in microwells. Microcapsules with GFP-expressing HUVECs (human umbilical vein endothelial cells) encapsulated in the fibrin hydrogel were similarly seeded in the microwells (Figure 17b). HUVECs are widely used for

vascular engineering[56,57] and studies of angiogenesis and vascular biology.[56,58,59] They are typically cultured in ECM such as fibrin hydrogels. Here we culture the HUVECs in fibrin within arrayed microcapsules, which may find applications for screening of angiomanipulatory drugs.[56,60] (Note that the HUVECs could not survive in conventional, alginate alone microcapsules – see Figure 18.) Furthermore, the "microcapsules in microwells" configuration represents a new, potentially scalable platform for 3D paracrine cell co-culture[61,62] where one type of cells are cultured in microcapsules and the second type of cells are seeded in microwells. To provide a proof of concept, we first aggregated the RFP-expressing normal human lung fibroblast (NHLF) in the microwells and then seeded the microcapsules with HUVECs, as shown in Figure 16c. One advantage of this system compared with previously published ones such as the InVERT molding[53] or suspending microcapsules in bulk hydrogel[61] is that the microcapsules and the microwells are detachable and switchable. Thus, this approach provides opportunities for reconfigurable cell co-cultures.

1.3 Significance of this dissertation

This dissertation focuses on developing a high-throughput method for compartmentalized hydrogel microcapsules production which is relevant to many biological applications such as cell therapy for biomanufacturing in tumor aggregates and stem cell-based organoids, and tumorigenesis under physical confinement. First, we developed a multiple fluidic electrostatic co-spraying technique for complex structure hydrogel microcapsules production. For example, we developed core-shell structures where the core is a desired ECM protein matrix to support the encapsulated cells in cell attachment, proliferation, morphogenesis, janus (i.e. side-by-side)

structures to encapsulate two different types of cells for cell-cell interaction studies and more complicated structures such as two cores or a triple layer structure hydrogel capsules that could also be used in co-culture studies. In this dissertation, we only focus on the application of core- shell structure microcapsules. By using this technique, we were able to produce around 13,000 core-shell microcapsules per minute with nearly monodisperse size and uniform spherical shape. Furthermore, these core-shell structured capsules were applied to efficiently expand intestinal organoids with higher proliferation and stem cell marker expression. Last, we used the same structure to study how physical confinement affect mammary tumorigenesis. The hydrogel shell layer creates a physical confinement on human mammary epithelial cells, MCF10A embedding in soft Matrigel core. In the microcapsules, the hydrogel layer could simulate the dense collagen fibers imposing on mammary epithelium in basement membrane matrix. Results show that, following removal of the MCF10A cells from physical confinement, the cells exhibited tumor-like behavior, such as uncontrolled growth and invasion. Additionally, approximately 4-6 weeks after transplantation of the confined cells into immunocompromised mice, these mice formed carcinomas, thus confirming their malignancy. Taken together, our findings suggest that physical confinement alone can induce a malignant transformation of mammary epithelial cells. In summary, this platform to produce core-shell microcapsules by a high-throughput electrostatic co-spraying technique is applicable in both biological research and bio-manufacturing.

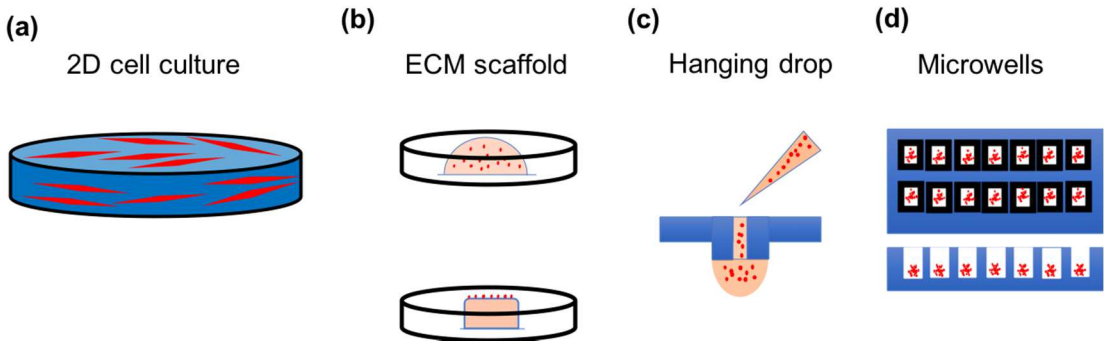

Figure 1, In-vitro cell culture methods.

(a) Traditional 2D cell culture in a petri dish. (b) 3D cell cultures by using ECM scaffold. (c) Using a hanging drop plate to generate 3D cell aggregations. (d) Microwells are also used for 3D cell culture.

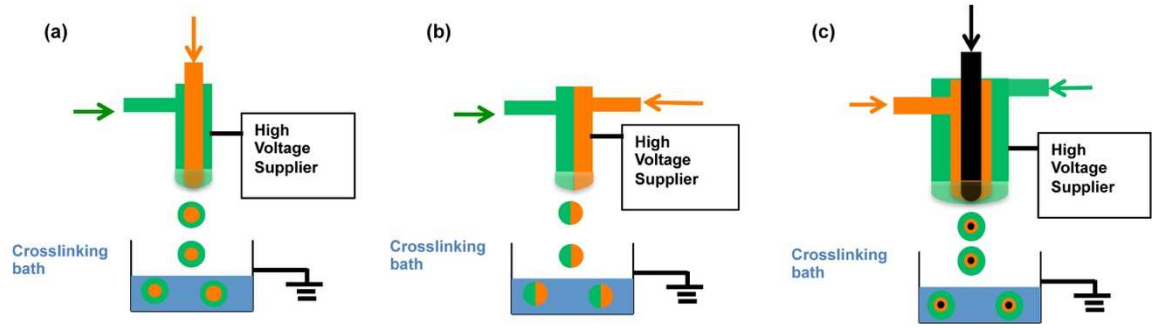

Figure 2, Schematics for the multi-fluidic electrospraying to produce the three different configurations of structured alginate hydrogel microcapsules.

(a) Core-shell; the nozzle has an inner tube (I.D. ~200 μm, O.D. ~400 μm) and an outer tube (I.D. ~750 μm, O.D. ~1200 μm) (b) Side-by-side; the nozzle has two connected tubes (I.D. ~200 μm, O.D. ~400 μm) (c) Triple layer microcapsules. The nozzle has three concentric tubes (I.D. ~150 μm, O.D. ~300 μm; I.D. ~600 μm, O.D. ~900 μm; I.D. ~1,100 μm, O.D. ~1,400 μm)

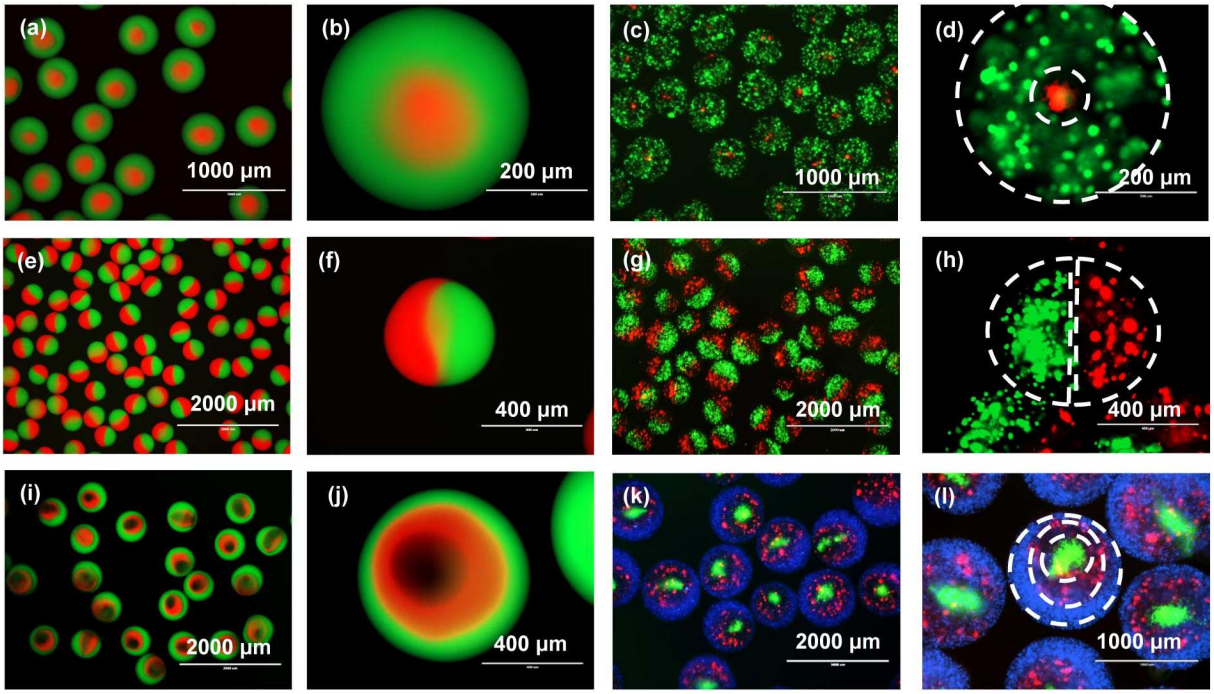

Figure 3, Hydrogel microcapsule designs and their applications for cell encapsulation.

(a-b) Core-shell hydrogel microcapsules made of fluorescently labeled alginate (Red: alginate labeled with Alexa Fluor® 594 dye; Green: alginate labeled with Alexa Fluor® 488 dye). (c-d) Core-shell alginate microcapsules encapsulating different types of cells (Green cells: MDA-MB-231 expressing GFP; Red cells: normal human lung fibroblasts expressing RFP). (e-f) Side-by-side alginate hydrogel microcapsules. (g-h) Cell encapsulation using side-by-side microcapsules. (i-j) Triple-layer hydrogel microcapsules. (The inner most layer in i and j was unlabeled alginate.) (k, l) Cell encapsulation using triple-layer particles. (The blue cells in k and l were MCF-10A stained with Hoechst).

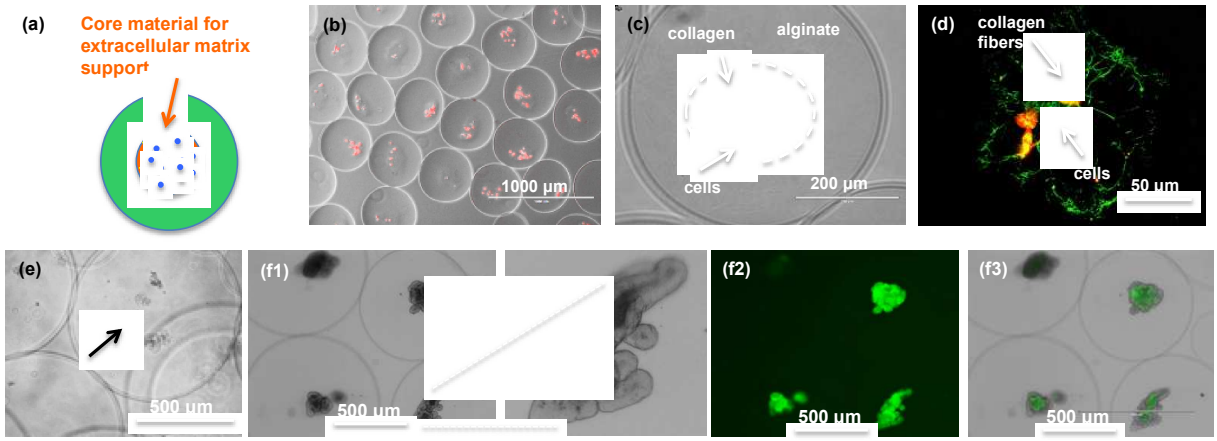

Figure 4, Hydrogel microcapsules with ECM support for scalable 3D cell culture.

(a) A schematic of an ECM-supported microcapsule. (b) MDA-MB-231 cells with tomato red expression encapsulated within collagen matrix inner layer in the alginate microcapsules. (c) A magnified view of a single microcapsule. (d) Cells in the collagen fibers (green) in the inner core of a microcapsule as imaged by second harmonic generation microscopy. (e) Mouse small intestinal crypts encapsulated in alginate-alone microcapsules failed to survive after 2 days of culture. (f) The crypts encapsulated in Matrigel inner core of the microcapsules grew into structured organoids in a week with an enriched GFP-labeled *Lgr5*+ stem cell population (f1: bright field; f2: GFP; f3: merged).

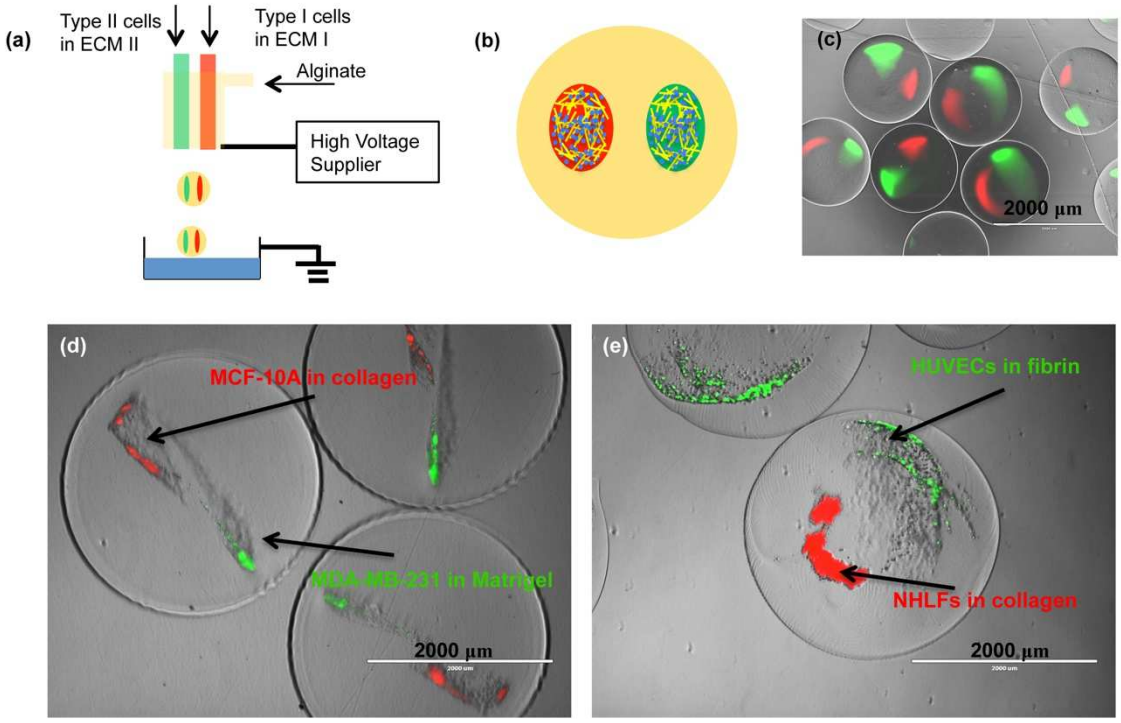

Figure 5, Hydrogel particles with an alginate outer layer and two ECM cores for cell encapsulation.

(a, b) Schematics of the setup and the microcapsules. (c) The two cores visualized by fluorescent alginates (red and green). (d) The MCF-10A (red) with collagen and MDA-MB-231 (green) in Matrigel encapsulated in the double-core microcapsules. (e) HUVECs (green) in fibrin and NHLF cells (red) with collagen encapsulated in the double-core microcapsules.

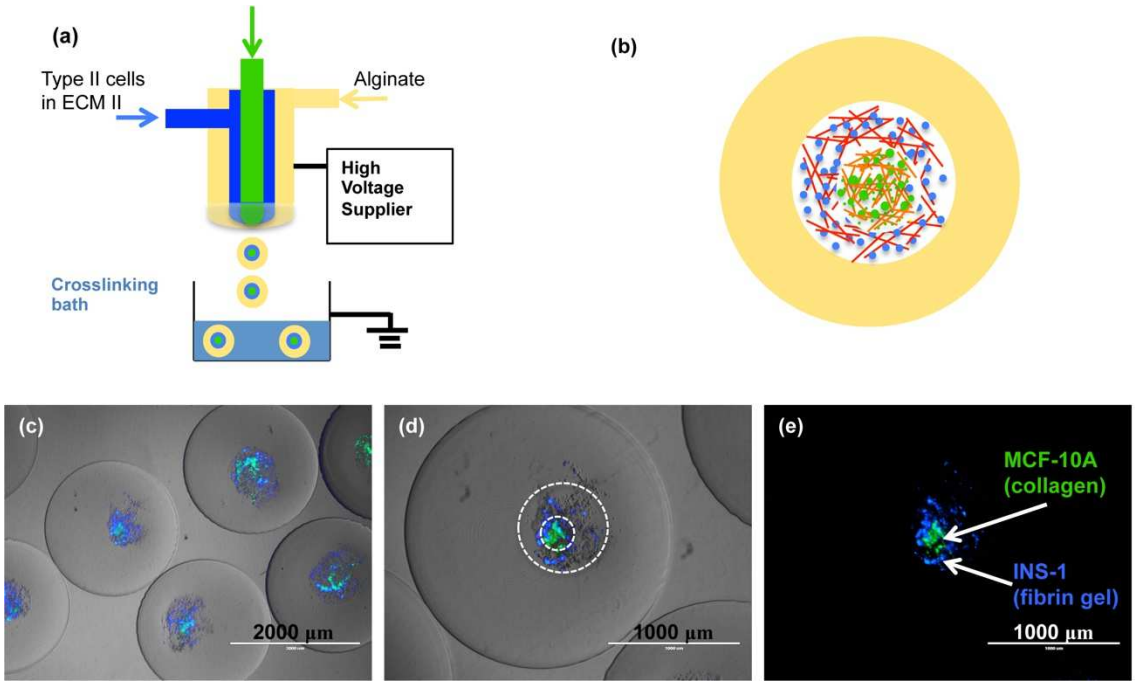

Figure 6, Triple-layer concentric hydrogel particles with an alginate outer layer and two ECM inner layers.

(a, b) Schematics of the setup and the microcapsules. (c-e) The MCF-10A (green) in collagen matrix as the innermost layer, surrounded by INS-1 cells (blue, stained with Hoechst) in fibrin within the alginate outermost layer.

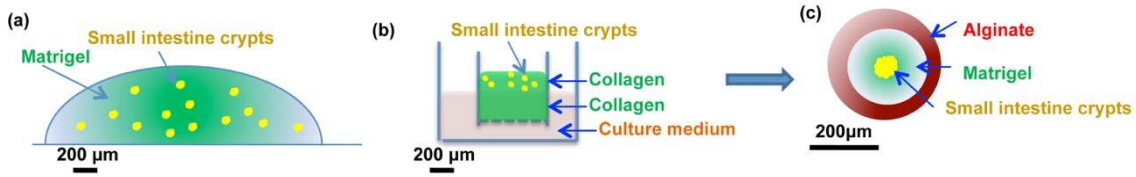

Figure 7, Schematics of different culturing methods for the small intestinal crypts.

(a) The crypts cultured in a Matrigel droplet. (b) The crypts embedded in collagen gel near air-liquid interface in first dish that was inserted in a second dish containing medium as a "dish-in-dish" configuration. (c) The crypts grown with Matrigel in microcapsules. The microcapsules have increased surface-to-volume ratio and reduced diffusion distance as compared with the bulk hydrogel.

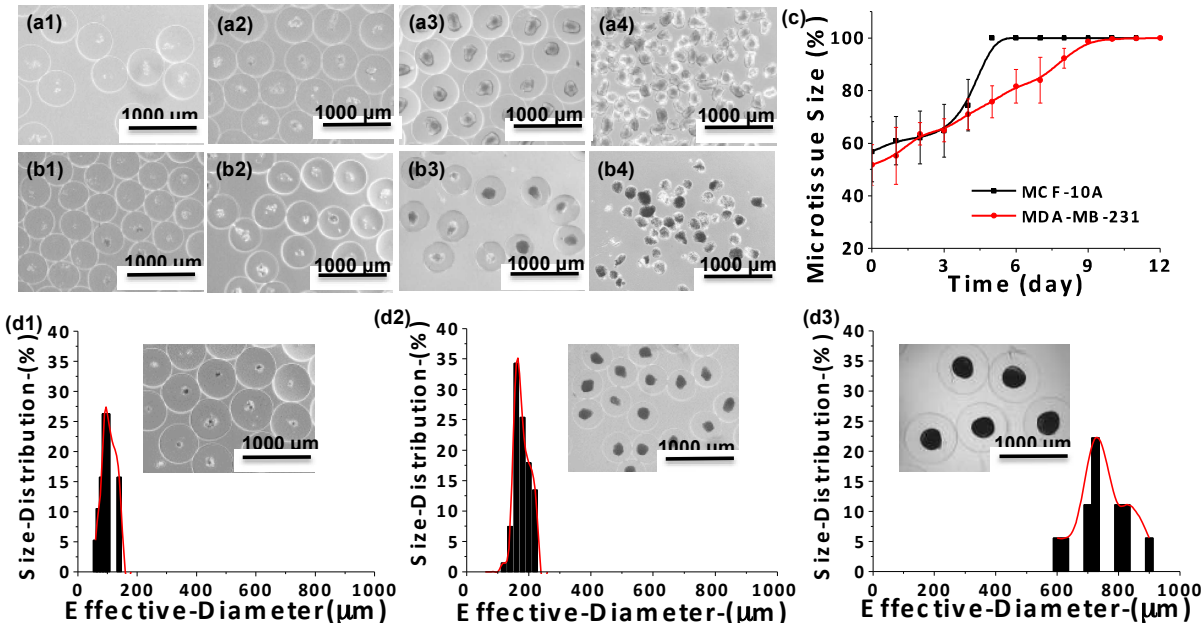

Figure 8, Scalable production of tumor microtissues with controllable sizes.

(a) MCF-10A cells within Matrigel matrix in the microcapsules, observed on day 0 (a1), day 3 (a2) and day 8 (a3). The microtissues (a4) were recovered by dissolving the microcapsules using EDTA. (b) MDA-MB-231 cells on day 0 (b1), day 2 (b2), day 19 (b3) and microtissues recovered (b4). (c) The growing curve of these two types of cells. The microtissue size is defined as the mean of the longest and shortest dimensions of the microtissue. The average size is typically taken from about 50 microtissues. (d) The control of the average microtissue sizes: 95 μm (d1), 160 μm (d2) and 725 μm (d3).

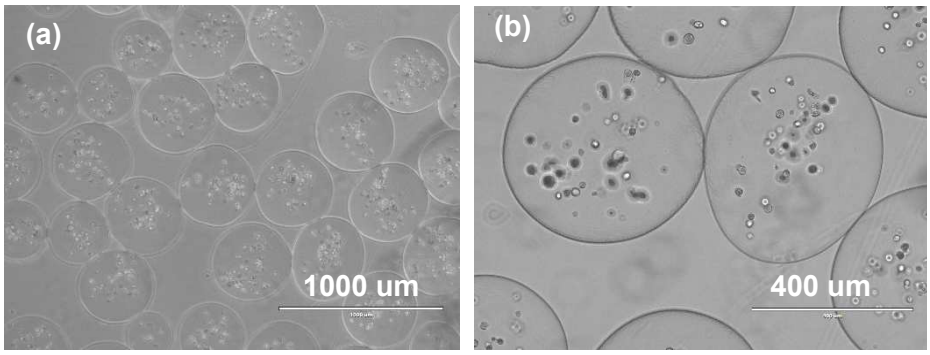

Figure 9, The MDA-MB-231 cells encapsulated in alginate alone microcapsules (day 13) did not proliferate.

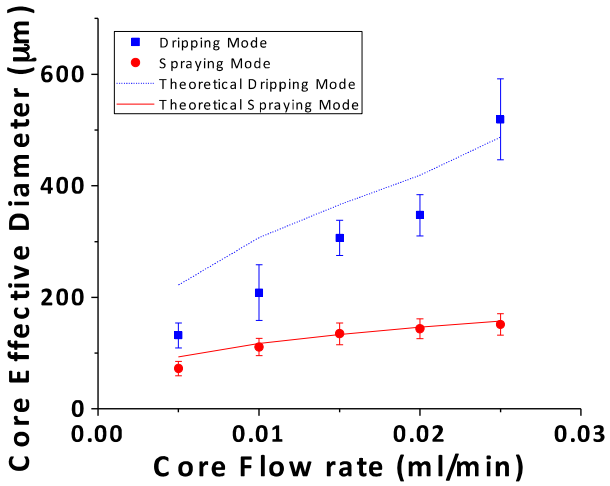

Figure 10, Controlling of the size of the ECM inner core in the core-shell microcapsules.

The plots show the core size as a function of the core flow rate given a fixed flow rate of 0.45 ml-min^{-1} for the outer, shell fluid. The experimental data (in dots) were compared with theoretical values (in lines) in both dripping and spraying modes. The effective diameter (D') of the core was approximated as the average of the longest and shortest dimensions determined by ImageJ. The theoretical values were derived as the following: The shell flow rate $Q_{shell} = \frac{4}{3}\pi(\frac{D}{2} - \frac{D\prime}{2})^3/\Delta t$ (Equation 1) where D is the overall diameter of the particles, and approximately 420 μm in the spraying mode. In the dripping mode, D was measured for each batch of particles. The core flow rate $Q_{core} = \frac{4}{3}\pi(\frac{D\prime}{2})^3/\Delta t$. (Equation 2) The ratio of the two flow rates $\frac{Q_{shell}}{Q_{core}} = (\frac{D}{D\prime})^3 - 1$ (Equation 3) The theoretical effective diameter was obtained by re-arrangement. $D' = D/\sqrt[3]{\left(\frac{Q_{shell}}{Q_{core}}\right) - 1}$ (Equation 4)

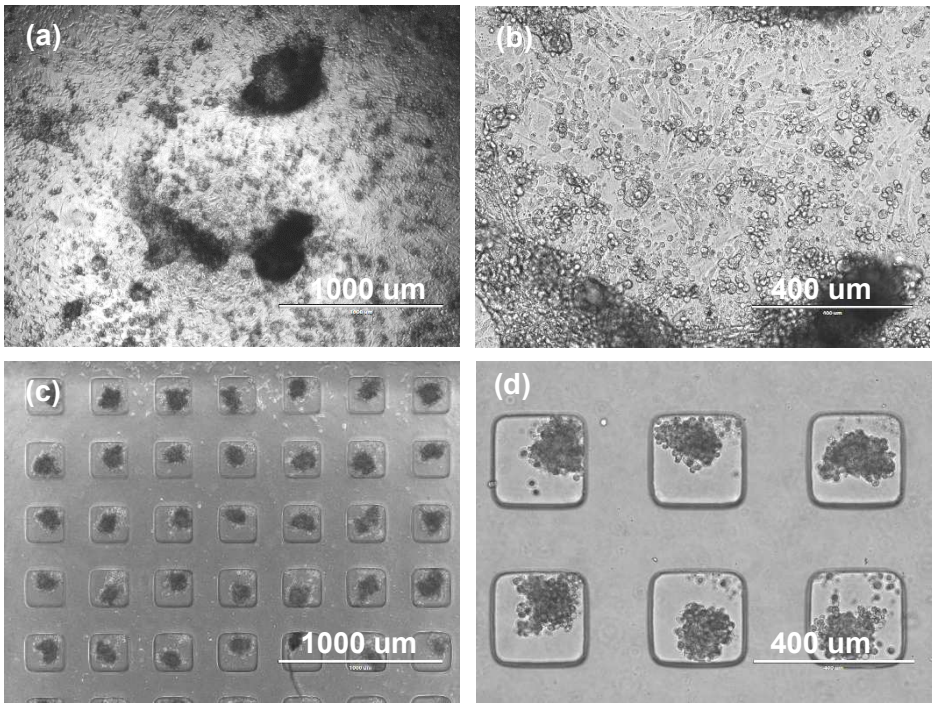

Figure 11, Assessment of microtissue formation of MDA-MB-231 cells embedded in Matrigel™

(a, b) and seeded (with Matrigel) in microwells (c, d). The Matrigel was diluted to 16.7% using culture medium, similar to the case of microcapsules. After 16 days culturing, the cells in the bulk gel randomly formed cell aggregates of several different sizes, while in the PDMS microwells the cells formed better aggregates, similar to previous studies.[3] However, the aggregates formed in the microwells seemed structurally loose, as compared to those formed in the microcapsules.

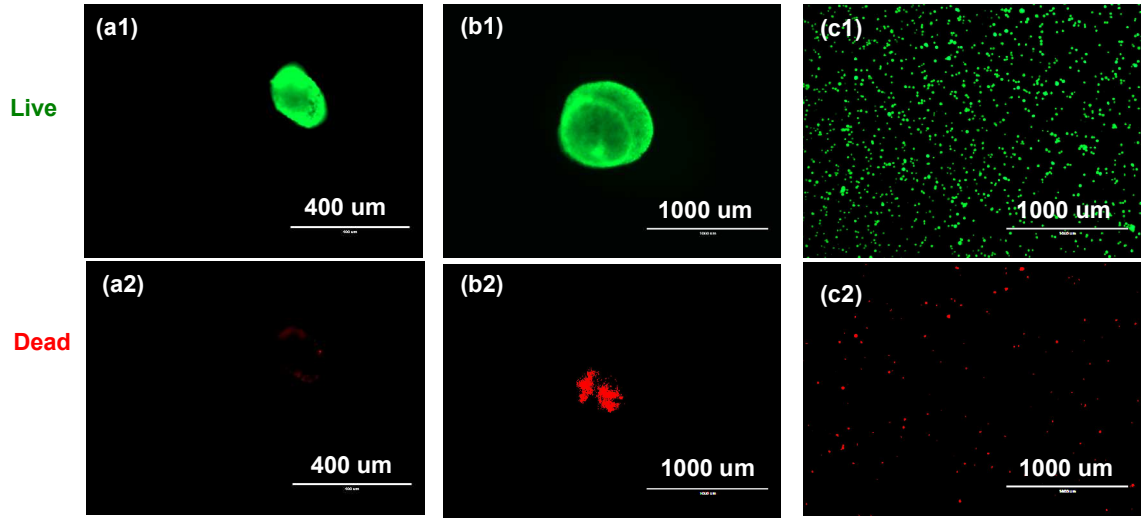

Figure 12, The viability assessment for MDA-MB-231 microtissue with two different sizes (200 μm and 700 μm).

(a) The viability of MDA-MB-231 microtissue with size around 200 μm; (b, c) The live/dead staining results of a 700 μm microtissue. In (b), the microtissue was stained directly, while in (c) the microtissue was broken into single cells before staining to show individual live/dead cells.

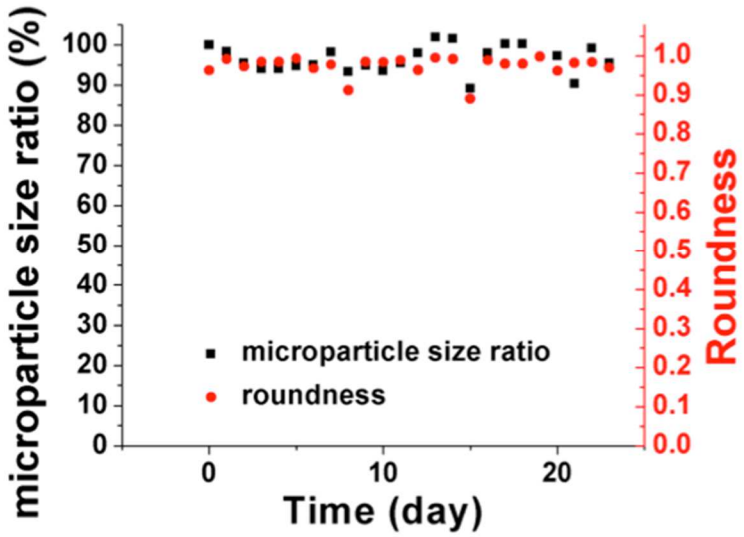

Figure 13, The morphometric characterization of a representative alginate microcapsule over time.

The size (diameter) and roundness of the alginate microcapsule (with cells) were measured from Day 0 to Day 24. (The roundness is defined by $\frac{4*(area)}{\pi*(major\ axis)^2}$ calculated through ImageJ)

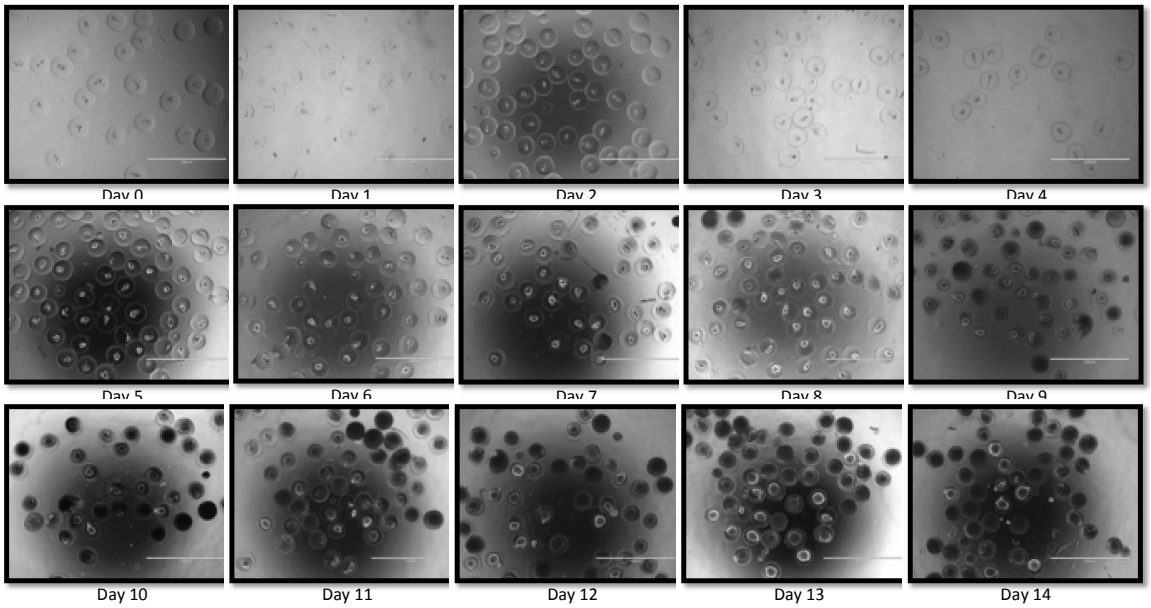

Figure 14, Ins-1 cells grow in alginate/Matrigel core-shell microcapsules over 2 weeks.

Note the darkening and breakage of microcapsule. (All images are at the same magnification and the scale bars are 2 mm.)

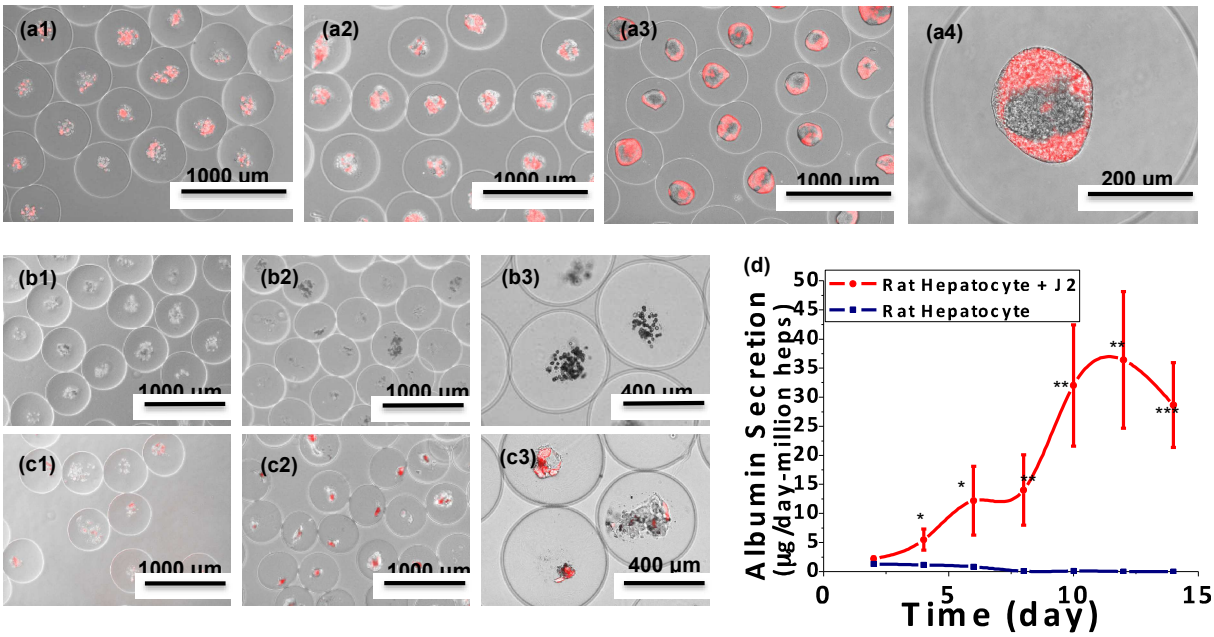

Figure 15, Cell-cell interactions in confined 3D cell co-cultures.

(a) Interactions of breast epithelial cell lines, MDA-MB-231 (with red dTomato fluorescence) and MCF-10A cells. The cells over time segregated into core-shell structures: day 0 (a1), day 4 (a2) and day 7 (a3, a4). (b) Rat hepatocytes cultured alone in the Matrigel-supported microcapsules: day 0 (b1); day 14 (b2, b3). (c) Rat hepatocytes co-cultured with stromal cells in the microcapsules: day 0 (c1); day 14 (c2, c3). The stromal cells were mitotically inactivated, non-proliferating, mCherry-expressing (red) mouse 3T3-J2 fibroblasts. (d) The co-cultured hepatocytes had improved viability over time as measured by the albumin secretion (mean ± SE; n=6; ***$p<0.01$; **$p<0.05$; *$p<0.1$).

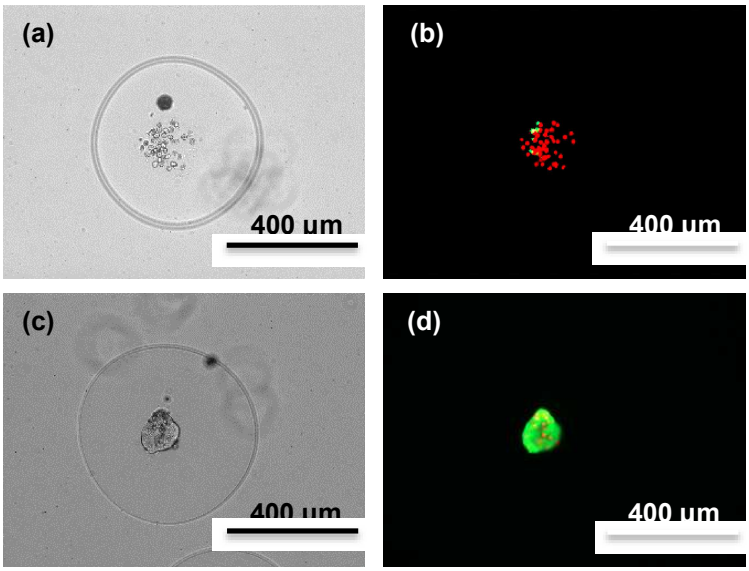

Figure 16, Rat hepatocyte encapsulated in Matrigel-supported microcapsules

(a, b) the hepatocytes appeared loosely dispersed (a) and mostly dead as indicated by live (green) / dead (red) staining on day 2. (c, d) Rat hepatocytes co-encapsulated with mouse 3T3-J2 stromal cells were better aggregated (c) and mostly alive (d).

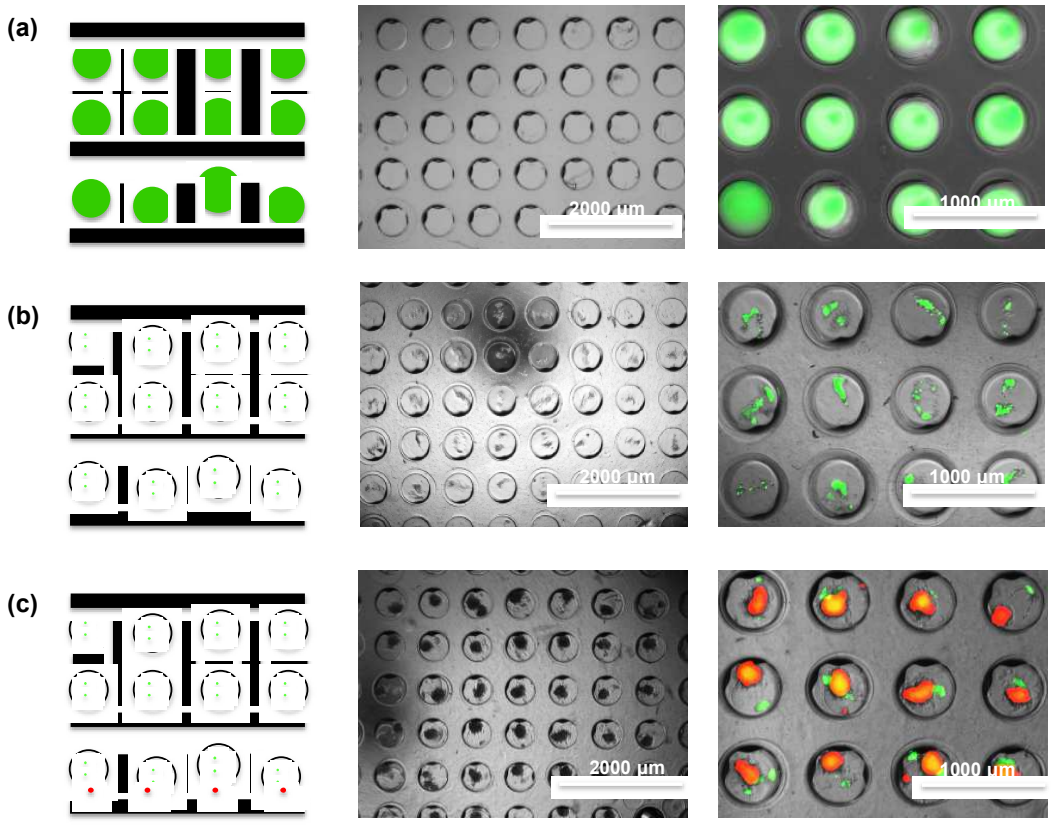

Figure 17, "Microcapsules-in-microwells" culture systems.

The schematics illustrate the configurations with both the top and side views. Both the bright field images and the merged images with fluorescent colors are shown. (a) Fluorescently labeled alginate microcapsules seeded in microwells. (b) Alginate/fibrin core-shell microcapsules encapsulating GFP-expressing HUVECs seeded in the microwells. (c) HUVECs (green)-containing microcapsules seeded in microwells that were pre-loaded with NHLF cells (red).

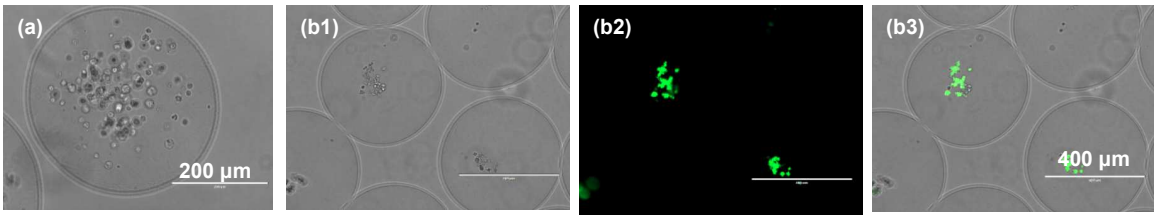

Figure 18, HUVECs with GFP expression were encapsulated in alginate alone particles and alginate/fibrin core-shell ones.

(a) The HUVECs in alginate alone particles were mostly dead after two days as indicated by no GFP expression. (b) The HUVECs in fibrin gel were still mostly alive after 10 days.

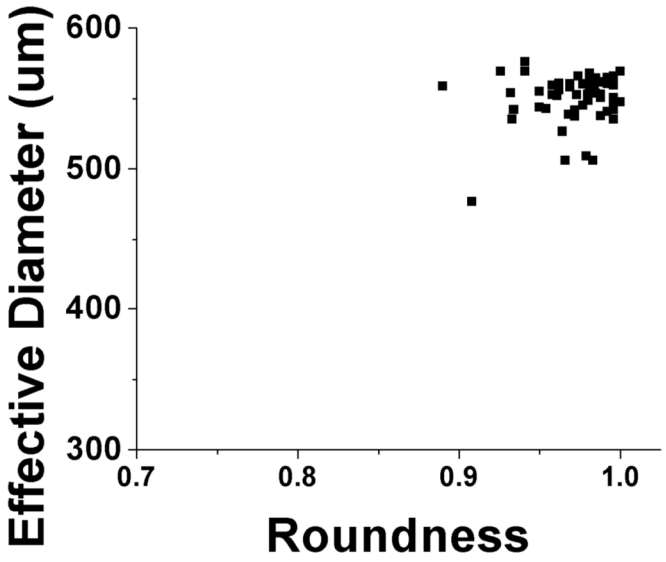

Figure 19, The morphometric characterization of alginate microcapsules.

All the alginate microcapsules (n=65) were analyzed through ImageJ. The effective diameters (average of major axis and minor axis) of this batch microcapsules varied from 540 to 560 μm except 4 smaller ones less than 510 μm. In addition, the roundness analysis $\frac{4*(\text{area})}{\pi*(\text{major axis})^2}$ of the microcapsules revealed that most of particles were close to perfect spheres.

Configuration	*Extracellular matrix component used in this study*	*Cell lines used in this study*	*Potential applications*
Core-shell	*Fibrin, collagen and Matrigel*	*HUVECs, NHLF, MDA-MB-231, MCF-10A, hepatocyte, small intestinal organoids*	*Microtissue production, co-culture, liver model, stem cell culturing*
Double-core	*Fibrin, collagen and Matrigel*	*HUVECs, NHLF, MDA-MB-231, MCF-10A*	*Paracrine co-culture*
Triple-layer	*Fibrin, collagen*	*MCF10A, INS-1*	*Paracrine co-culture, cell migration*

Table 1, A summary of different microcapsule configurations.

CHAPTER 2: SCALABLE PRODUCTION AND CRYOSTORAGE OF ORGANOIDS USING CORE-SHELL DECOUPLED HYDROGEL CAPSULES

2.1 Introduction

Organoids are stem cell-derived, lab-grown multicellular structures that closely mimic the physiology and hierarchical cell organizations in their counterpart tissues or organs *in vivo*. [63–67] Recognized recently as a major science advance[68], the organoid technology holds enormous potential for studying stem cell biology, modeling diseases, screening drugs and engineering cell therapies.[63,69–74] Organoids corresponding to several organs have been developed, including gut[75–78], lung[79,80], liver[81,82], retina[83,84], brain[69,85] and kidney[86], to name a few. For example, the culture of intestinal organoids first established by Clevers and his colleagues in a landmark paper[75] has initiated numerous follow-up investigations. Intestinal organoids not only became a prime model for studies on adult stem cells in health and disease but also represented a promising potential source for cell therapies for intestinal diseases such as microvillus inclusion disease, ulcerative colitis, and post-endoscopic mucosal resection.[64] Eiraku et al.[83] reported the autonomous formation of the optic cup (retinal primordium) structure from mouse embryonic stem cell aggregates, which opened up new avenues for the next-generation of regenerative medicine in retina degeneration therapeutics. Lancaster et al.[69] showed that cerebral organoids recapitulated features of human cortical development and could be used to model microcephaly, a brain disorder that has been difficult to study in mice. Dekkers et al.[87] used patient-derived intestinal organoids to model the cystic fibrosis. These studies and many others have

clearly shown the great potential of organoids as *in vitro* human tissue/organ surrogates for various important applications[63,64].

In almost all cases, the 3D culture in extracellular matrices such as Matrigel™ played an essential role in the formation of organoids[7,8,13,14,16,22]. Current 3D cultures are typically accomplished by embedding the cells in bulk Matrigel™ usually deposited as sessile drops on flat surfaces. While these culture methods enabled numerous insightful studies in laboratories, they were not suited for large-scale productions. This method of culture requires manual seeding and becomes extremely labor-intensive when performed at large scales; in addition, the macroscopic Matrigel™ drops or blocks have limited surface area for mass transfer and are not suitable for suspension culture (e.g., in stirred bioreactors). The scale-up of organoid culture that is critically important for high-throughput screening and clinical applications has remained challenging[90–92]. Another factor that limits the rate of organoid technology development and clinical translation is the long-term storage, such as cryopreservation of the organoids[93]. The challenge for complex tissue preservation is the potential cryoinjury from ice crystal formation during the freezing and recovery processes. Usually, a cryoprotectant (e.g., dimethyl sulfoxide (DMSO)) in combination with a slow freezing process is applied to avoid intracellular ice formation, which is the major cause to damage the cryopreserved cells. However, the recovery process usually involves de-vitrification that can still induce ice crystal formation[93–95]. The ice crystal might not only hurt the cells but also disrupt cell-cell interactions among these organized tissues. To prevent devitrification during the

warming process, hydrogels have been used to protect the cryopreserved cells/tissues in a rapid recovery procedure to enhance the viability of cells in cryopreservation[96,97].

Here, we report an efficient and scalable organoid culture and cryostorage system using hydrogel capsules. The capsules have a core-shell structure where the core consists of Matrigel™ that supports the growth of organoids (i.e., "organogenesis" in capsules), and the shell is alginate that forms robust spherical capsules, enabling suspension culture. Compared with conventional culture in bulk Matrigel™, the capsules provide better mass transfer from both diffusion and convection in a stirred bioreactor and can be continuously produced by a two-fluidic electrostatic co-spraying[98]. Using mouse stomach and small intestinal organoids as models, we demonstrated that core-shell capsules not only enable scalable, suspension culture of organoids, but also enhanced the stem cell expansion within the organoids. In addition, these core-shell capsules also allowed a higher recovery rate from cryopreservation of organoids, probably due to the protection from the mechanical damage by the hydrogel layers during freezing or thawing processes. This new, capsule-based organoid culture and cryo-storage method will likely facilitate current organoid studies and accelerate its translation into clinical or industrial applications.

2.2 Methods and Materials

2.2.1 Encapsulation of cells and crypts in core-shell alginate capsules

Cell encapsulation was accomplished using two fluidic electro-co-spraying technique described previously[98]. Briefly, the isolated cells or small intestinal crypts were dispersed in an ice-cold Matrigel™ solution, which was pumped (0.06mL min^{-1})

into an high electric field (~5.8 kV) as the core fluid, and 1.8%(w/v) sterile alginate (UPLVG FMC Biopolymer) dissolved in 0.9%(w/v) sodium chloride was pumped (0.3mL min^{-1}) as the shell fluid. The two fluids were pumped simultaneously and sprayed into small core-shell droplets under the electric field; the droplets were crosslinked in a 100mM calcium chloride solution placed ~1.8cm under the nozzle. After encapsulation, the capsules were transferred to a culturing dish or stirred bioreactor in an incubator at 37ºC with 5% CO_2 for culturing.

2.2.2 Calculation for organoid expansion efficiency

Quantification of organoid expansion: The expansion efficiency is defined by the equation below.

$$Expansion\ Efficiency = \frac{(Final\ amount\ of\ fragments - initial\ amount\ of\ fragments)}{initial\ amount\ of\ fragments} \qquad (equation5)$$

2.2.3 Statistical analysis

All quantification data are presented as mean ± SEM with at least three independent replicates, and the sample size "n" in each experiment is given in the legend of each figure. In statistical analysis, all the p values were calculated by one-way ANOVA using Prism 7. In addition, all the figures were depicted from Prism 7. (N.S.: non-significant difference, *$p<0.05$, **$p<0.01$ and ***$p<0.001$)

2.2.4 Mouse gastric organoid isolation

The stomachs were collected from 6-8 week-old $Lgr5^{tm1(cre/ERT2)Cle}$/J ($Lgr5^{EGFP\text{-}Ires\text{-}CreERT2}$) knock-in mice, washed with ice-cold PBS buffer three times to remove the remaining lumen contents, and divided into 2mm small pieces. The gastric fragments

were collected in 50 mL conical tube and incubated at room temperature for 15 minutes in a gentle dissociation buffer (Stem Cell Technologies). After removal of the dissociation buffer, the tissue fragments were vigorously suspended in and out using 10 mL pipets for 10-20 times with ice-cold 0.1%(w/v) BSA/PBS solution. The supernatants were collected to new 50mL conical tubes. The gastric epithelial cells were spun down and washed with ice-cold DMEM/F12 medium for twice. The organoid culture was modified from a previously described method.[99] Briefly, the isolated gastric cells were counted and a total of 20,000 cells were suspended in 100μL of ice-cold DMEM/F12 medium, mixed with 100μL of liquid growth factor-reduced Matrigel™ (Corning), and seeded in a dish. After solidification of Matrigel™ in the 37°C incubator for 20 minutes, a stem cell culture medium (IntestiCult™ Organoid Growth Medium supplemented with 10nM gastrin) was added into the dish and incubated until 37°C for several days until encapsulation.

2.2.5 Mouse small intestinal organoids isolation

The small intestines were collected from 6-8 weeks old wild-type (WT) or $Lgr5^{tm1(cre/ERT2)Cle}/J$ ($Lgr5^{EGFP\text{-}Ires\text{-}CreERT2}$) knock-in mice. The isolation process was modified from a previously developed method.[100] The isolated crypts and cells were mixed with growth factor-reduced Matrigel™ and seeded on a dish for 20 minutes at 37ºC before adding intestinal organoid medium.

2.2.6 Immunofluorescence (IF) and single-molecule fluorescence in situ hybridization (FISH)

IF staining for LGR5-eGFP, CD44 and CK8 were performed using a method modified from a previously published protocol[101]. For the intestinal organoids from wild-type mice, stem cell biomarker, Lgr5 was identified by FISH followed a previous method[102,103]. Several differentiation biomarkers, such as Lysozyme and MUC2 were stained by an immunofluorescent staining technique.

2.2.7 Cryopreservation

Organoids in hydrogel capsules were collected and incubated in DMEM:F12 medium with 10% (v/v) DMSO with a density of around 20-30 capsules per ml. On the other hand, the organoids in bulk were preserved in the same freezing medium with a density of around 200 organoids per ml. The decreasing rate of temperature was controlled around 1°C per minute till -80°C for cryopreservation. To recover the organoids, the cryo-vial was incubated in 37°C water bath for about 5 minutes to thaw the vial and added 10ml DMEM:F12 medium to dilute the DMSO.

2.2.8 Quantitative reverse transcription real-time PCR

Total RNA was isolated from the organoids formed by the epithelial cells of stomachs and small intestines of the $Lgr5^{tm1(cre/ERT2)Cle}/J$ ($Lgr5^{EGFP\text{-}Ires\text{-}CreERT2}$) knock-in mice using mirVana RNA isolation kit (Thermo Fisher scientific, AM1560). Reverse transcription was carried out using SuperScript III First-Strand Synthesis System (Thermo Fisher Scientific, 18080051) and quantitative PCR (qPCR) reactions were

performed using a PerfeCTa® SYBR® Green SuperMix (Quanta Biosciences, 95054). The qPCR conditions were initiated at 95°C for 3 minutes, followed by 40 cycles of 95°C for 15 seconds and 60°C for 45 seconds. The sequences of primers are listed in supplemental information (Table 2). Amplification of mouse Actb (β-actin) was used as the reference gene control.

2.2.9 Viability Assessment

The viability was characterized by live/dead staining kit including acetoxymethyl ester of calcein (calcein AM) and ethidium homodimer-1 (EthD-1) dyes (Life Technologies). To enhance the staining in capsules, the hydrogel layer was dissolved by alginase before incubating in dye. Those organoids collected from capsules were incubated with 20μM calcein AM and 14μM EthD-1 for 10 minutes at 37°C. The viability analysis is based on the total number of live cells in one whole organoid/aggregation which is calculated by total area of live cells divided by total area of organoid/aggregation. Moreover, the area is measured by ImageJ.

2.2.8 Microscopy and image analysis

The organoids in bulk and in capsules were observed and imaged by an EVOS AMF4300 imaging system. The fluorescent images were obtained by an Olympus FV1000 confocal microscope and processed by ImageJ.

2.3 Results and Discussions

2.3.1 Core-shell Hydrogel Capsules provides enhanced mass transfer in stirred bioreactor

The most common method to culture organoids is to use reconstituted basement membrane matrix (Matrigel™) as a scaffold to support the organoid growth and maintain the stemness[69,75,80,81,83,88,89]. This method is easy to implement in a small scale, for example by simply dripping a droplet of pre-gelled Matrigel™ in a dish. (Figure 20a) However, this method is not suitable for large-scale productions. In contrast, the core-shell capsules, which can be made continuously by a two-fluidic electrostatic co-spraying technique, provide a more scalable and efficient organoid culture platform (Figure 20b). During the electrospraying, the alginate shell crosslinks instantaneously when the droplets hit the Ca^{2+} solution in the grounded collector and the pre-cooled Matrigel™ core, protected by the shell, gradually gels through a temperature increase. The capsules, due to their smaller sizes, have higher surface to volume ratios than the bulk hydrogels and therefore better mass transfer even when cultured in dishes. When cultured in stirred flasks or bioreactors, the alginate shell protects the softer Matrigel™ and the cells from the shear force and importantly the mass transfer is further enhanced through convection. For example, based on a simple diffusion assay, we found that the mass diffusion reaches equilibrium in hydrogel capsules in static culture within 2 hours, while the time required to reach equilibrium in a stirred flask was merely 20 minutes. (Figure 21a) In addition, using a human breast cancer cell line, MCF10DCIS.COM, as a model, we

showed the growth of the cells in the core of each hydrogel capsule (Figure 21b, c) in the stirred flask, confirming the potential of this platform for scalable cell culture and production.

2.3.2 Hydrogel Capsules enhance expansion of stem cells in gastrointestinal organoids

To examine whether the core-shell capsule system is suitable for organoid culture, we first used gastrointestinal organoids as a model. The gastric fragments, isolated from $Lgr5^{tm1(cre/ERT2)Cle}$/J ($Lgr5^{EGFP\text{-}Ires\text{-}CreERT2}$) knock-in mouse stomach, were dispersed in Matrigel™ and then dripped in a dish (i.e. bulk culture) or encapsulated in the alginate-shell capsules. The capsules had a nearly monodisperse diameter of 1900±25μm with the Matrigel core size of 900±40μm.[98] After 9 days of culture, the tissue fragments grew into gastric organoids in both bulk and core-shell capsules (Figure 22a). The stem cell markers within the organoids, CD44 and LGR5-eGFP[104], were measured by immunofluorescence (Figure 22b). Interestingly, the LGR5-eGFP expression seemed to be higher and the columnar differentiation marker (CK8) expression lower in hydrogel capsules than in the bulk Matrigel™.[104,105] These biomarker expressions suggest that the hydrogel capsules might enhance the expansion of stem cells in the organoids, probably due to the mechanical confinement effect from the alginate shell. It was previously reported that the mechanical heterogeneity in core-shell capsules composed of softer ECM core and harder alginate shell enhanced the development of ovarian follicles[6,106].

We also tested the culture of another type of organoids, mouse small intestinal organoids (crypts), in core-shell capsules and compared that to the bulk culture (Figure 22c-g and Figure 23). In both methods, the small intestinal crypts isolated from mice formed organoids after a few days of culture (Figure 22c). The organoids had lumen structures with apoptotic inner cells as shown by the caspase-3 staining (Figure 22d). The intestinal stem cells in the organoids were identified by CD44 and LGR5-eGFP. Using a quantitative real-time PCR (polymerase chain reaction), we found that the organoids grown in the capsules had similar Cd44 but significantly higher Lgr5 expression than those grown in bulk (Figure 22e, f). This observation of enhanced stem cell expansion in capsules was consistent with our observed results from the gastric organoids. In a recent study, it was found that stiff matrix in the microenvironment effectively improved intestinal stem cell expansion, and softer matrix supported the intestinal differentiation and organoid formation.[107] In our core-shell capsules, the shell hydrogel layer may provide a mechanical confinement to enhance the stem cell expansion, while the Matrigel™ core, with unaltered composition and mechanical property, supports the organoid formation. This is consistent with earlier reports that core-shell hydrogel capsules might be used to simulate the microenvironment of early-stage embryos to enhance the pluripotency.[22,108–110] The expression of proliferation marker, Ki67, was also higher in capsules than in bulk (Figure 22g), suggesting again that the core-shell capsules were not only suitable for organoid culture but might also improve the efficiency of organoid expansion.

2.3.3 Hydrogel Capsules provide scalable production for intestinal organoids

Next, to demonstrate the culture of organoids in core-shell capsules was scalable, we performed repeated encapsulation, expansion, dissociation and re-encapsulation. First, small intestinal crypts were encapsulated in the capsules; the crypts grew into organoids in 6 days. Then, we used alginase to dissolve the alginate hydrogel shell and EDTA to remove alginate residues and dissociate organoids. The dissociated organoids were broken into smaller fragments through physical pipetting, and the fragments were re-encapsulated in core-shell capsules for the next round of culture (Figure 24a). After re-encapsulation and culture, these intestinal organoids maintained their stem cell population with expression of LGR5-eGFP and CD44 (Figure 24a). Furthermore, after 4 passages, the organoids contained not only stem cells with Lgr5 expression but also normal intestinal niches, such as Paneth cells with Lysozyme expression and intestinal goblet cells with MUC2 expression based on the fluorescence in situ hybridization (FISH) and immunofluorescent staining (Figure 24b). To demonstrate the scalability and feasibility of suspension culture in bioreactors, we transferred the capsules from culture dishes to a stirred flask. (Figure 24c and 24d) The small intestinal organoids grew and expanded efficiently in the stirred bioreactor and after a 6-day culture, we obtained ~15,000 organoids from a 100-ml stirred flask. In principle, we may produce a much larger or potentially any number of organoids using larger reactors. In contrast, to produce the same large number of organoids using the conventional bulk Matrigel™ culture, it would require many plates or dishes and become laborious. It is also worth mentioning that when we compared the expansion efficiency (or the increase of organoid numbers after an

expansion) between cultures in bulk Matrigel™ and in capsules, we found that the efficiency from capsules was on average 1.5 times higher than the bulk culture. (Figure 24e) (The efficiency could be ever higher as expansion continues due to the higher stem cell population in organoids grown from capsules.)

2.3.4 Hydrogel Capsules protect the encapsulated organoid in cryopreservation

Lastly, we investigated whether the core-shell capsules could also be used for the cryo-storage of the organoids. Tissue/organ preservation is a challenge for tissue engineering in clinical application, especially for complex tissues or organs which constitute different cell types in an organized structure[93–95]. The most common methods for cryopreservation involve a slow freezing process and a penetrating cryoprotectant, such as DMSO to avoid intracellular ice formation, which is the major cause of cell death during vitrification. However, during warming process, the ice crystal formation might still be induced by devitrification[96,97,111]. In current methods[112–114], organoids are frozen in medium with high concentrations of serum and a cryoprotectant, and the cooling temperature is controlled at a rate of 1ºC per minute. These steps can prevent ice formation inside the cells in the freezing process, but crystal formation from devitrification, which might disrupt the cell alignment within tissues or organs, cannot be avoided during the conventional cryopreservation procedure. Here, we combined core-shell hydrogel capsules and cryoprotectant together to protect organoids from both vitrification and devitrification[94,96,97,111]. Compared with the bulk Matrigel™, the capsules had a much higher recovery of cryo-preserved organoids (Figure 25a-c and Figure 26a-c). In bulk, only small cell

aggregates could grow into organoids after thawing and re-culturing in Matrigel™ (Figure 25a and Figure 26a); larger ones failed to survive (Figure 25b and Figure 26b). The recovery efficiency (i.e., the fraction of viable cells recovered after thawing) was only around 20%. In contrast, in capsules even whole organoids could survive and grow after recovery from the cryo-storage (Figure 25c and Figure 26c). The cell viability was improved to 80%. (Figure 25d, e), suggesting that the core-shell hydrogel structure might suppress the ice formation during cryopreservation. The recovered organoids showed the stem cell markers, LGR5-eGFP and CD44 after being cultured for a week after thawing. (Figure 25f, g) Although the alginate shell deformed due to the mechanical force generated during freezing or thawing process, the capsules clearly played a protective role in the cryo-storage of organoids.

2.4 Conclusion

In summary, we reported here a new, capsule-based platform for scalable production and cryo-storage of organoids. The key to this platform is the core-shell decoupled design of the capsules, which can be continuously produced through a two-fluidic electrospraying, where the Matrigel™ core creates a permissive environment for organoid growth while the alginate shell enables the formation of mechanically robust capsules. Compared with the conventional droplet or bulk Matrigel™ currently used for organoid culture, the new capsules provide a higher surface area for mass transfer, support enhanced expansion of the stem cell population within organoids and can be suspended in stirred bioreactors for large-scale production. The alginate shell, which could be easily dissolved to harvest the organoids, protects the organoids from

shear force during suspension culture and potential mechanical damage during the cryopreservation process. Given the significance of organoid technology, our core-shell decoupled hydrogel capsules would be a useful platform for many laboratory studies and potential clinical or industrial applications.

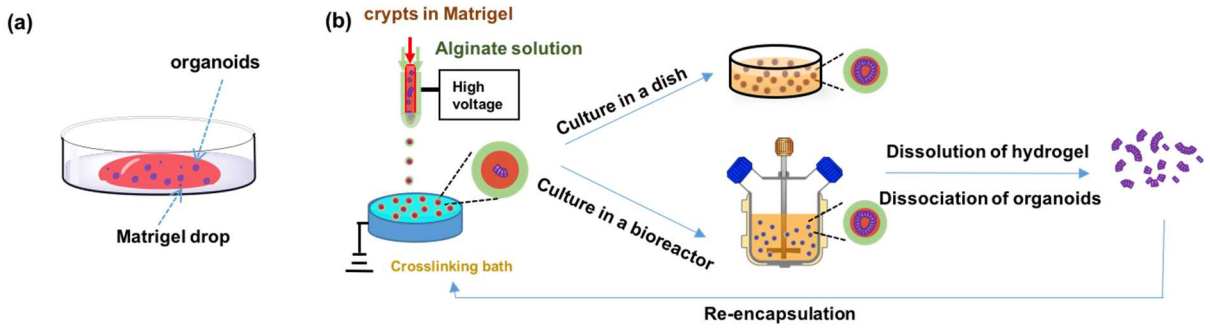

Figure 20, A Schematic comparison between a conventional organoid culture and the more scalable, capsule-based culture.

(a) Conventional method using Matrigel™ drops placed in a dish. (b) A schematic of the capsule-based organoid culture and expansion process. The cells or cell aggregates (e.g. crypts) dispersed in Matrigel™ is first encapsulated in core-shell capsules through a two-fluidic electrospraying; the capsules may then be cultured in a dish or a stirred bioreactor. For expansion, the capsule shell (i.e. alginate) may be dissolved and the organoids dissociated and re-encapsulated.

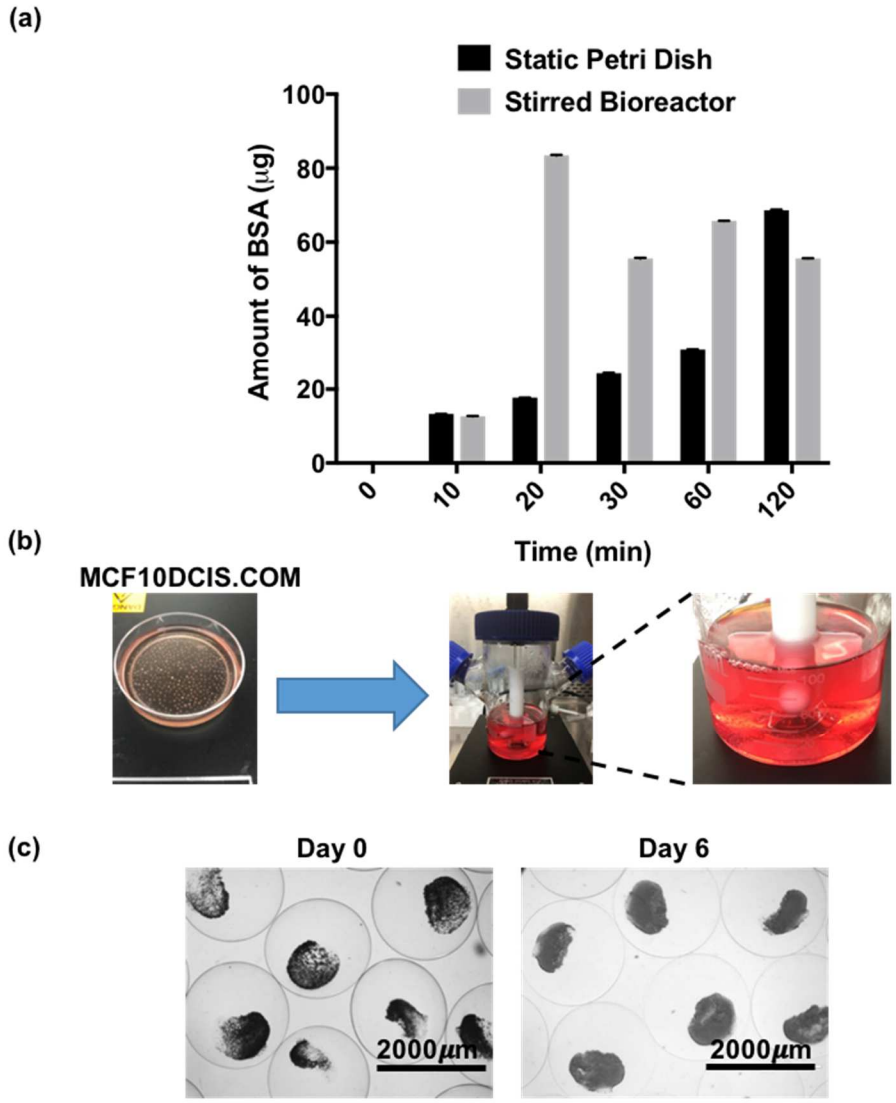

Figure 21, Mass transfer in hydrogel capsules in stirred bioreactors.

(a) A diffusion assay by BSA conjugated with Alexa fluor® 488 for static culturing and dynamic culturing in bioreactors (n=3 for each group). (b, c) The cell growth within hydrogel capsules in a stirred flask using a MCF10DCIS.COM cancer cell line as a model.

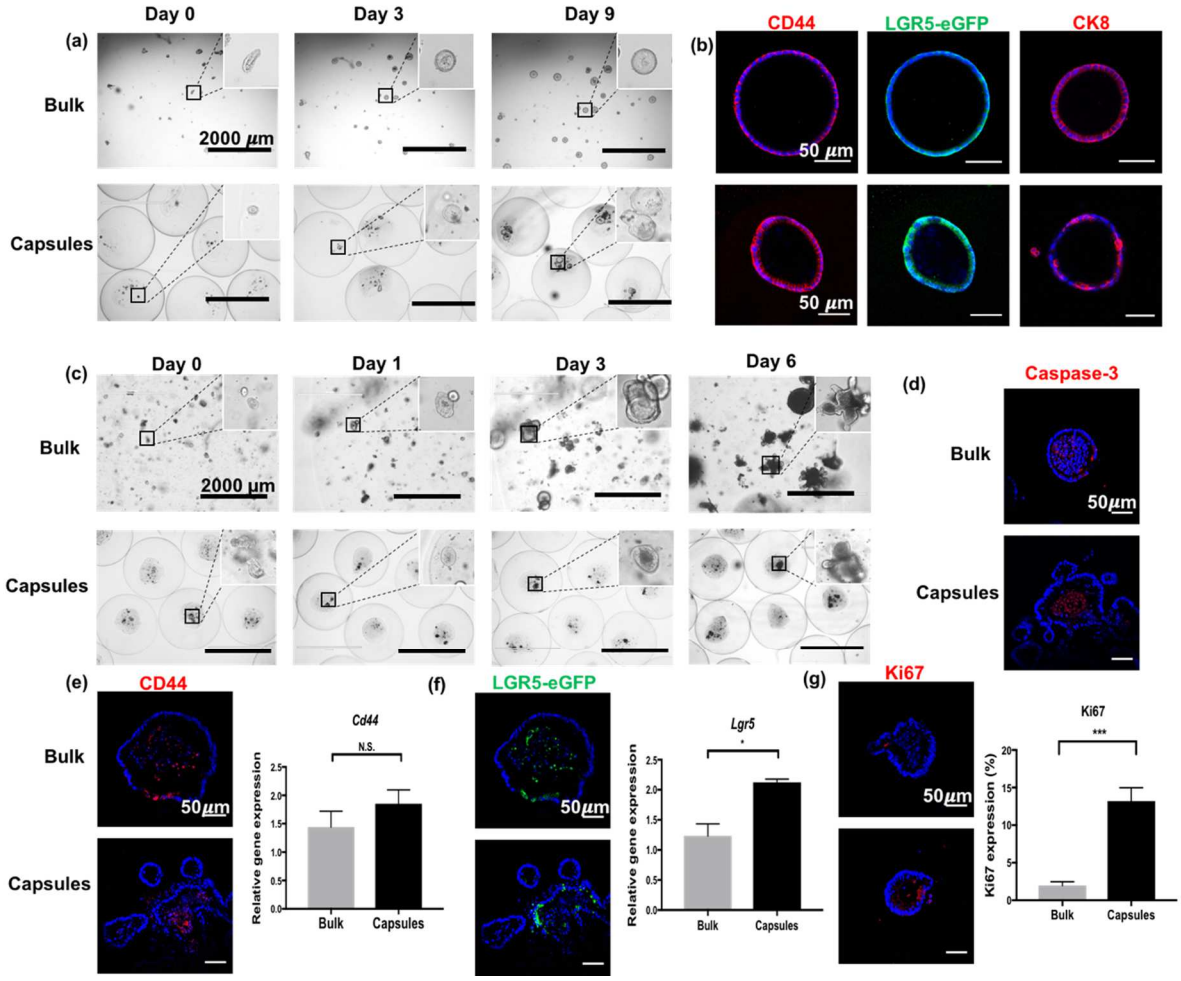

Figure 22, Culture of Gastrointestinal organoids in bulk Matrigel™ and core-shell decoupled capsules.

(a) Growth of mouse gastric organoids in bulk Matrigel™ and capsules during a 9-day culture period. (b) Whole mount staining for stem cell markers, CD44 and LGR5, and columnar differentiation marker, CK8 in bulk Matrigel™ and capsules. (c) Growth of mouse small intestinal organoids in bulk Matrigel™ and capsules during a 6-day culture period. (d) Immunofluorescent (IF) stainings from paraffin-embedded sections for apoptosis marker, caspase-3. (e, f) IF staining and qPCR analysis of stem cell markers (Cd44 and Lgr5) (n=3 for bulk and capsules). (g) IF staining of the proliferation marker, Ki67 and quantitative analysis based on the staining (n=3 for both bulk and capsules).

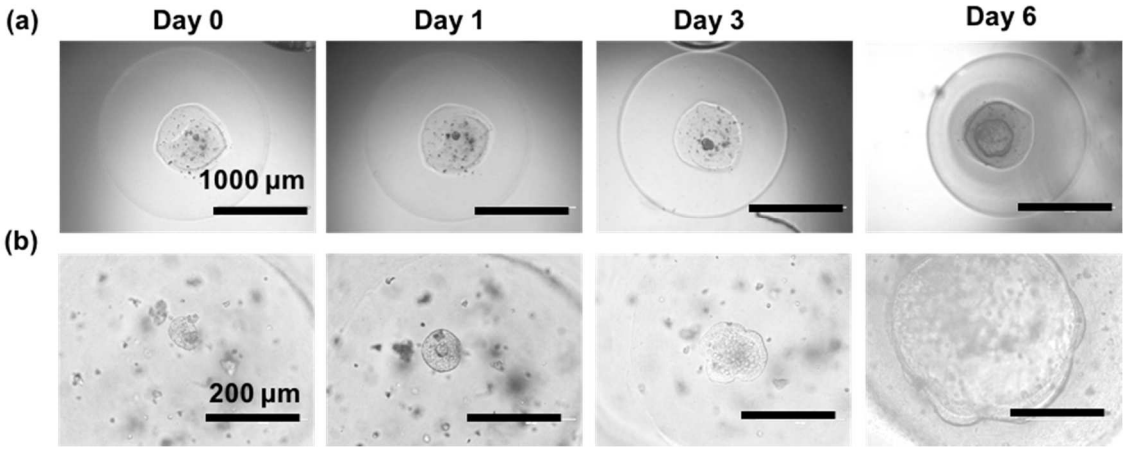

Figure 23, Growth of a mouse small intestinal organoid in a single capsule.

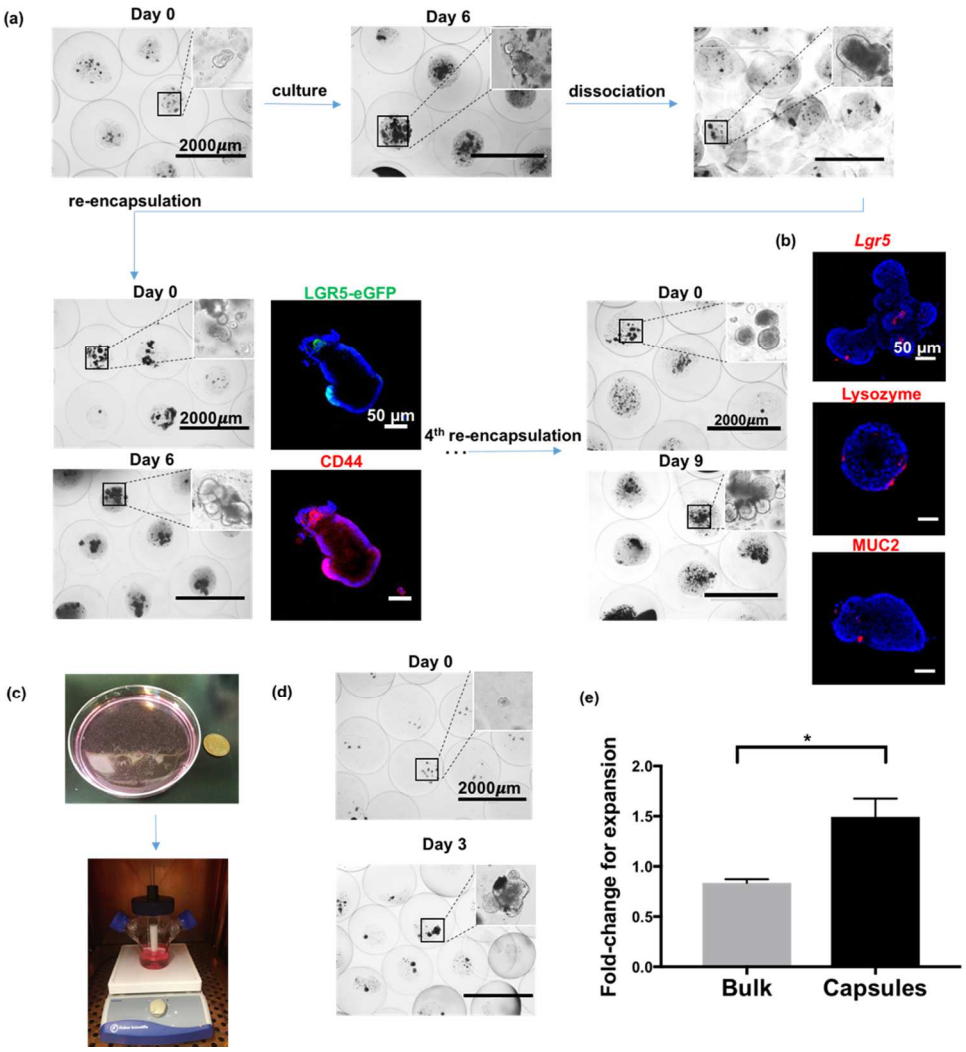

Figure 24, Expansion of mouse small intestinal organoids within hydrogel capsules and suspension culture in a stirred flask.

(a) The process of organoid expansion in hydrogel capsules including encapsulation, culturing, dissociation and re-encapsulation. Whole mount staining for LGR5-eGFP and CD44 in capsules confirms the presence of stem cells. The whole process may be repeated multiple times. (b) The stem cell biomarker, Lgr5, and two intestinal cell markers, *Lysozyme* and *MUC2* identified by fluorescence in situ hybridization (FISH) and immunofluorescent staining, confirming that the key features of stem cell such as self-renewal and multi-differentiation capabilities remained stable in hydrogel capsules after 4 times of passaging. (c) Capsules containing growing crypts being transferred from a dish to a stirred flask for suspension culture. (d) Growing organoids in capsules in a stirred flask. (e) A quantitative comparison of expansion efficiency between cultures in bulk and in hydrogel capsules (n=4 for each group). The expansion efficiency is defined as the fold-increase over the initial number of organoids.

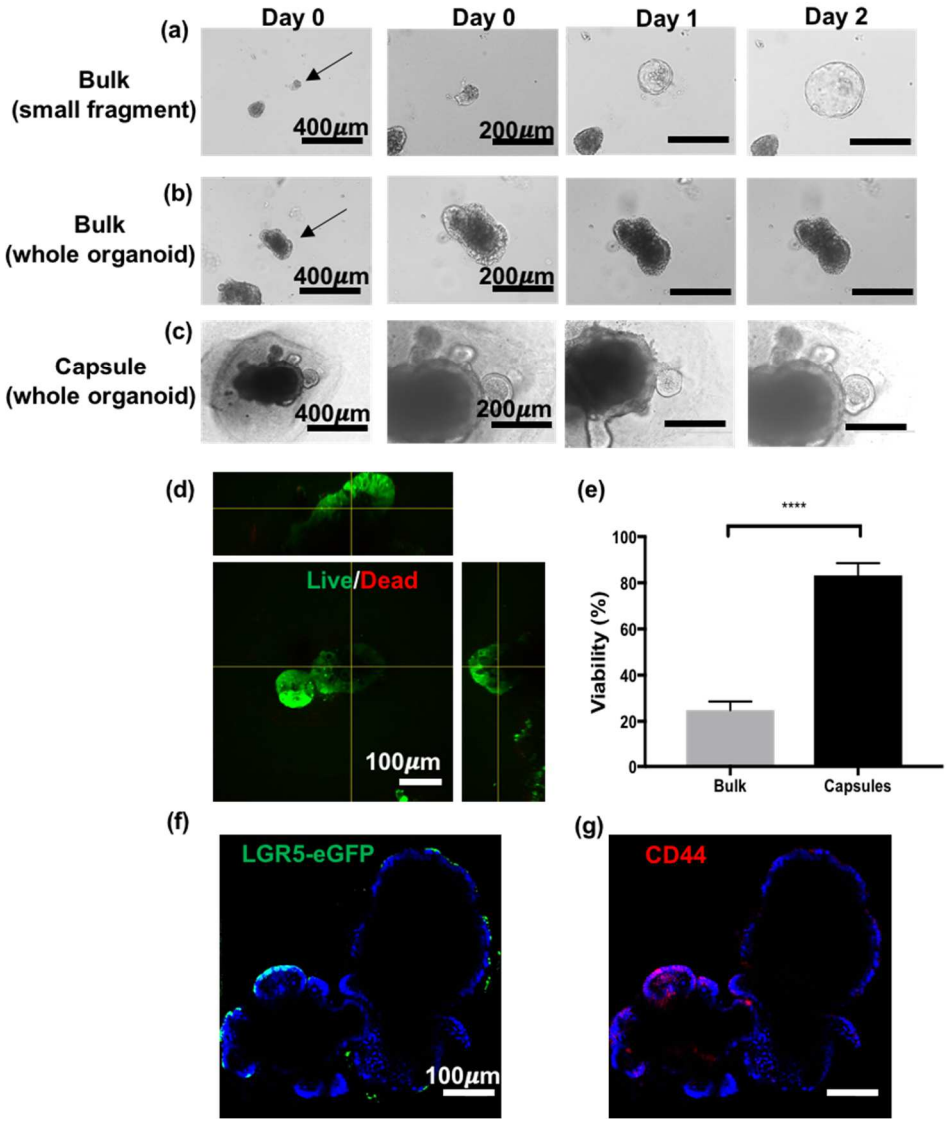

Figure 25, Improved cryostorage of organoids in hydrogel capsules.

(a) Small fragments of organoids thawed from bulk Matrigel™ were re-suspended in growth medium/Matrigel for culturing. (b) Large fragments or structured organoids thawed from bulk Matrigel™ were re-suspended in growth medium/Matrigel for culturing. (c) Organoids thawed from capsules were re-suspended in growth medium/Matrigel for culturing. (d) Live/dead staining for re-cultured organoids from capsules with z-stack imaging. (e) A quantitative comparison of the cell viability in organoids recovered from bulk and capsules (n=3 for each group). (f, g) Expression of stem cell markers, LGR5-eGFP and CD44, in the organoids that were thawed from capsules and re-cultured for a week after freezing at -80°C for 6 weeks.

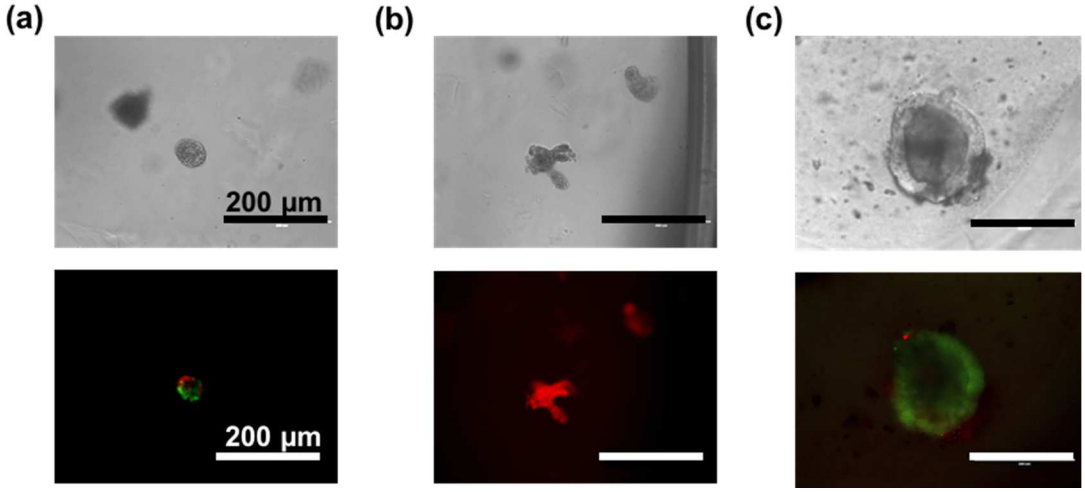

Figure 26, Recovery of mouse intestinal organoids from cryopreservation.

(a, b) In bulk, the viability of intestinal organoids depended on the size of aggregations: Higher viability in smaller crypts or organoid fragment, and lower viability for organoids with well-organized structures. (c) In capsules, organoids mostly survived after the thawing procedure.

Targeted gene	*forward*	*reverse*
Lgr5	*5'-TCTTCTAGGAAGCAGAGGCG-3'*	*5'-CAACCTCAGCGTCTTCACCT-3'*
Cd44	*5'- CCACGACCCTTTTCCAGAG-3'*	*5'- CGGCAGGTTACATTCAAATCG-3'*
Actb	*5'-GATTACTGCTCTGGCTCCTAGC-3'*	*5'-GACTCATCGTACTCCTGCTTGC-3'*

Table 2, The primer sequence of Lgr5, Cd44 and Actb (β-actin) for qPCR

CHAPTER 3: PHYSICAL CONFINEMENT INDUCES MALIGNANT TRANSFORMATION IN MAMMARY EPITHELIUM

3.1 Introduction

Breast cancer (BC) is the second leading cause of cancer-related deaths in women[115] and its progression is categorized from benign to malignant[116–118]. Ductal carcinoma in situ (DCIS) represents an early, pre-invasive stage of breast cancer in which neoplastic epithelial cells begin to fill the mammary duct[119]. Invasive BC occurs when the neoplastic cells within the duct break through the basement membrane, invade into the neighboring stromal tissues, and begin to spread to other organs[119]. In BC research, the non-malignant MCF10A basal cell line is commonly used to study how normal epithelial cells become transformed into triple negative BC[120] (estrogen receptor, progesterone receptor, and human epidermal growth factor receptor 2 negative[121]). Previous studies have shown that, upon in vitro culture in Matrigel™ (a reconstituted basement membrane matrix[122,123]), MCF10A cells grow into hollow acinar-like structures which resemble the normal acinar architecture in mammary glands[123]. Additionally, studies have shown that stable incorporation of specific oncogenes into these cells causes severe disruption of the acinar structure, uncontrolled growth, and loss of polarity[124,125].

In the breast, mammary ducts are composed of a thin layer of luminal cells surrounded by myoepithelial (basal) cells which are constrained by a basement membrane (BM). Outside of the BM, collagen fibers and other extra-cellular matrix (ECM) components are secreted by stromal cells, such as fibroblasts, to provide, amongst other things, structural support for the mammary ducts[126,127]. However, when the neighboring collagen matrix becomes overly dense, the imposing physical confinement of this matrix on the mammary epithelial cells, is thought to play a role in

the transformation of normal mammary epithelial cells to DCIS[127] (Figure 27a). While the connection between tissue density and malignant transformation has been widely studied, the precise mechanisms linking these two events remains to be fully defined. Previous studies investigating the relationship between mechanics of ECM and tumorigenicity have cultured MCF10A cells in a type I collagen matrix that had been modified by glycation to tune ECM stiffness[128]. Alternatively, collagen has been added directly to Matrigel to increase its stiffness[129]. However, type I collagen is not normally found in the mammary basement membrane matrix[130]. Therefore, adding collagen changes both the composition of the matrix and the density of binding sites, making it difficult to identify the cause of malignant transformation. To alter matrix stiffness without changing the density of binding sites, in another study[130], Matrigel was mixed with alginate, a naturally derived hydrogel that lacks adhesive binding sites, in a fixed composition and crosslinked with varying calcium concentrations to control its mechanical properties[130]. In this system, mechanical stiffness could be altered without affecting Matrigel concentration, however, the addition of alginate does not closely parallel the microenvironment that cells normally encounter in vivo.

In order to document the effects of a confined microenvironment on tumorigenicity in a more biologically relevant setting, we developed a model system whereby we embedded MCF10A cells in Matrigel and then encapsulated these cells in alginate shell hydrogel microcapsules. The core-shell encapsulation allowed us to examine how confinement of MCF10A cells within unaltered Matrigel affects the proliferative and migratory potential of these cells. Results show that, following removal of the MCF10A cells from physical confinement, the cells exhibited tumor-like behavior, including uncontrolled growth and invasion for a minimum of 6 passages. Additionally, approximately 4-6 weeks after transplantation of the confined cells

into immunocompromised mice, these mice formed carcinomas, thus confirming their malignancy. Taken together, our findings suggest that physical confinement alone can induce a malignant transformation of mammary epithelial cells.

3.2 Methods and Materials

3.2.1 Materials

In hydrogel microcapsules, the sterile alginate (UPLVG) was purchased from FMC Biopolymers and dissolved in saline, 0.8% (w/v) sodium chloride (Sigma-Aldrich). Matrigel (growth factor reduced with phenol red free, 356237) was purchased form Corning. The crosslinking buffer was prepared in 100mM calcium chloride (Sigma-Aldrich) with 5mM barium chloride (Sigma-Aldrich). For immunohistochemistry and immunofluorescence, the following antibodies and fluorescent dyes were used: anti-integrin β1(TS2/16) (Santa Cruz Biotechnology, sc-53711), anti-integrin β4 (EMD Millipore, MAB1964), anti-laminin 111 conjugate with dylight550 (Life technologies, PA5-22903), Anti-KI67 (Genetex, GTX20833), cleaved caspase-3 (Cell Signaling, 9661S), Anti-E-cadherin (Santa Cruz Biotechnology, sc-7870), anti-p63 (Genetex, GTX102425), anti-cytokeratin (EMD Millipore, MAB3412) and Alexa Fluor 488® phalloidin conjugate (Life technologies, A12379). For drug inhibition, the following drugs and antibodies were used: LY294002 (Life technologies, PHZ1144), NSC23766 (Toris Bioscience, 2161), Y27632 (Santa Cruz Biotechnology, sc3536), Blebbistatin (Cayman chemicals, 13013), ML-7 (Tocris Bioscience, 4310), FAK Inhibitor 14 (Tocris Bioscience, 3414), pp1 for Src inhibitor (Tocris Bioscience, 1397), AG1024 (Santa Cruz Biotechnology, sc205907), TGF-β RI kinase inhibitor (EMD Millipore, 616451), GM6001 MMP inhibitor (EMD Millipore, CC1010) and anti-integrin β4 (EMD Millipore, MAB2059Z).

3.2.2 Animals

We used scid-beige female mice (CBSCBG-F, C.B-Igh-1b/GbmsTac-Prkdc^{scid}-Lyst^{bg} N7) for xenograft from Taconic Farms. The xenograft transplantation procedure was approved by the Cornell Institutional Animal Cate and Use Committee.

3.2.3 Cell Culture

MCF-10A mammary epithelial cells were maintained in DMEM:F12 supplemented with 5% horse serum, 0.5 mg/ml hEGF, 10 mg ml1 insulin (Sigma-Aldrich), 100 ng /ml cholera toxin, and 100 units/ml penicillin and 100 mg/ml streptomycin. Madin Darby Canine Kidney (MDCK) cells were cultured in Dulbecco's modified Eagle's medium (DMEM) with 4.5 mg/ml glucose, 1 mM sodium pyruvate supplemented with 10% heat-inactivated fetal bovine serum (FBS), 5 mM L-glutamine, 100 units/ml penicillin and 100 mg/ml streptomycin. MCF10DCIS.COM mammary cancer cells were maintained in DMEM:F12 supplemented with 5% horse serum and 100 units/ml penicillin and 100 mg/ml streptomycin. Human primary mammary epithelial cells were grown in Mammary Cell Basal Medium (ATCC PCS-600-030) supplemented with the Mammary Epithelial Cell Growth Kit (ATCC PCS-600-040). These cells were incubated at 37^{o}C in 5% CO_2.

3.2.4 3D culture and invasion assay

Bulk Matrigel samples were prepared by mixing cells with Matrigel and dripping them into a 96 well-plate or petri dish as a comparison with microcapsules. The medium was changed every 2-4 days until the 40-day end point. For the invasion assay, the encapsulated MCF10A cell aggregations were collected from microcapsules by dissolving the hydrogel layer, and the MCF10A acini were obtained from bulk Matrigel. Before being embedded in collagen gel, the

aggregations and acini were washed by cold PBS to remove alginate or Matrigel residues. Type I collagen from rat tail was dissolved in 0.1% (v/v) 0.1% acetic acid at 4°C for 3 days at the desired concentration (5mg/ml). It was diluted with growth medium and neutralized by 1N sodium hydroxide at 4°C at final concentration of collagen of 1.5 mg/ml before mixing with cells or aggregations. The collagen gel/fibers were formed at 37°C for 30 minutes.

3.2.5 Cell Encapsulation

Cells were diluted in pure reconstituted basement membrane matrix (Matrigel™) to the desired cell density. The cells were encapsulated in sterile alginate (UPLVG FMC Biopolymers) crosslinked with calcium chloride mixing with barium chloride by core-shell electrospray under an electrical voltage ranging from 5.8 to 7.2kV.

3.2.6 Immunohistochemistry & immunofluorescent

Both *in vitro* and *in vivo* samples were fixed by 10% formalin in PBS before processing for paraffin-embedded sectioning by Cornell Histology Core Facility or whole mount staining. In addition, the paraffin sections were stained with hematoxylin/eosin by the core facility at Cornell University. Paraffin sections with 10mm thickness were processed by de-paraffin and rehydration procedure under sequential incubation and washing steps: xylene, 100% ethanol, 95% ethanol, 70% ethanol and water before immunohistochemistry or immunofluorescent staining. In immunohistochemistry, the rehydrated section was first incubated with citrate buffer for antigen retrieval before blocking in 10% normal goat serum and 1% bovine serum albumin (BSA) in Tris-buffered saline (TBS) for 2 hours at room temperature (RT). The primary antibodies in 1% BSA in TBS were incubated at 4°C overnight before the peroxidase block with 0.3% hydrogen peroxide for 15 minutes and biotinylated secondary antibody incubation. We

incubated the samples with NovaRED (SK-4805, Vector labs) as an enzyme substrate for 5-10 minutes and Hematoxylin as a counter stain. Finally, the sections were dehydrated by incubating in 75% ethanol, 95% ethanol, 100% ethanol and xylene before mounting in cytoseal XYL. The slides for immunochemistry and H&E staining were imaged by Aperio Scanscope (CS2) by 40x and processed by Aperio eSlide Manager. For immunofluorescent staining, the rehydrated sections or fixed samples for whole-mount staining were washed by PBS and incubated in 1% BSA in phosphate buffered solution (PBS) before applying the primary antibody in 1% BSA in PBS for 30-60 minutes at RT. After washing with PBS three times, the secondary antibodies (sometimes mixed with phalloidin for F-actin staining) in PBS were incubated for 30-60 minutes at RT. Lastly, the fluorescent stained slides were mounted in Fluoroshield with DAPI(4',6-Diamidino-2-Phenylindole, Dihydrochloride). The fluorescent images were captured by a Zeiss LSM710, LSM880 confocal microscope, or Olympus FV1000 confocal microscope.

3.2.7 Xenograft preparation

The encapsulated MCF10A cells were extracted from microcapsules by alginate lyase to dissolve the hydrogel layer. Half of the cell aggregations were incubated in 0.25% Trypsin with 2.21mM EDTA in Hank's Balanced Salt Solution to obtain single MCF10A cells. For control groups, acini were prepared by culturing MCF10A cells in bulk Matrigel for 40 days. MCF10A cells and MCF10DCIS.COM cells were detached from culture flasks by 0.25% Trypsin with 2.21mM EDTA in HBSS. For xenograft experiments, all the cells/aggregations were spun down in 1.5mL microcentrifuge tubes and suspended in 100μL Matrigel solution before injection. The cells in Matrigel were injected into mammary fat pad via a 25G needle (BD) in 10 weeks-old female Scid-beige mice.

3.2.8 Clinical anatomic pathological analysis

The xenograft tumors collected from mice were fixed by 10% formalin before embedding in paraffin for sectioning. The H&E staining slides were analyzed by diagnostic histology laboratory and stem cell pathology unit at Cornell University. The tumor grade was determined by the Nottingham grading system.[118,131]

3.2.9 Tracking Cell Generated 3D ECM Displacements

Cell-generated 3D displacements of the ECM were tracked as described previously.[132] Briefly, 1.0μm diameter carboxylated green fluorescent (excitation wavelength:580nm and emission wavelength:605nm) microspheres (Thermo Fisher) were embedded in the extracellular matrix at 5-7μm spacing. Next, a three-dimensional image stack of the cells and fluorescent beads was acquired every 20 minutes using a 40x with N.A.=1.1 water immersion lens of a Zeiss 710 Confocal Point Laser Scanning Microscope. The 3D position of each bead at each time-point was determined using a weighted centroid method and the bead positions were subsequently paired into tracks across time using a feature-vector-based relaxation method[133] both implemented in MATLAB. 3D displacements were exported from MATLAB and rendered with the open-source Paraview software (Kitware).

3.2.10 RNA sequencing process- Differential Expression Analysis (DESeq2)

We quantified transcription activity of encapsulated and non-encapsulated control using RNA-seq. Adapters were trimmed from the 3' end of reads using cutadapt at 10% error rate. Transcript quantification was done using salmon[134] with indexed human cDNA transcriptome (assembly GRCh19). Two encapsulated data and two controls were treated as replicates for

differential expression analysis. The analysis was conducted using deSeq2.[135] Estimated abundance level of transcription was round up to the nearest integer for deSeq2 input. Differentially expressed genes were defined as those with a false discovery rate (FDR) less than 0.01.

3.2.11 Mechanical characterization for alginate hydrogel

All the tensile tests and compression tests were measured by Instron 5965 and analyzed by the software Bluehill 3.0 SOP.

3.2.12 MCF10A loss function of cytoplasmic tail in integrin β1 and β4

For integrin tail-less cell lines, tail-less integrin cDNA (1-853 amino acids for β4 and 1-762 amino acids for β1) was fused with monomer green fluorescent protein (GFP) at C-terminal and inserted into a piggyback backbone (SBI: system biosciences) expressing a tetracycycline transactivator protein (rTA) and drug resistance gene hygromycin under EF1 promoter. The plasmid was then co-transfected with a super piggybac transposase plasmid into MCF10A cells with Neon eletrapolation system (Invitrogen). Positive cells were selected under hygromycin for 1 week to generate a stable cell line.

3.2.12 Microscopy and image analysis

The hydrogel capsules were observed and imaged by an EVOS AMF4300 imaging system. The fluorescent images were obtained through the EVOS inverted fluorescent microscope, Zeiss LSM710 confocal microscope operated by ZEN software v. 2010, Carl Zeiss, and Olympus FV1000 confocal microscope. All fluorescent images were processed using ImageJ.

3.2.13 Statistical analysis

All quantification data are presented as mean ± SEM (standard error of the mean) with at least three independent replicates, and the sample size "n" in each experiment is given in the legend of each figure. In statistical analysis, all the p values were calculated by Student's t-tests followed by a Mann-Whitney test or two-way ANOVA followed by a Tukey post hoc test using Prism 7 or BMP. In addition, all the figures were created in Prism 7. (N.S.: non-significant difference, *$p<0.05$, **$p<0.01$ and ***$p<0.001$)

3.3 Results and Discussions

3.3.1 Malignant transformation of mammary epithelium in microcapsules

In an effort to mimic the confining effect of high density collagen fibers on the mammary epithelium in vivo, here, we developed a core-shell hydrogel microcapsule platform that contains a pure Matrigel matrix with MCF10A cells (Figure 27b). The microcapsules were produced by a two fluidic electrostatic co-spraying technique at a high production rate from 120 to 4,000 capsules/min depending on capsule size) with nearly monodisperse spherical size and tunable core diameter (~100 to 600 μm)[98]. The core, containing MCF10A cells in soft Matrigel (~450 Pascal (Pa) [136], Figure 28, red Matrigel, blue Hoechst stained cells), was separated from the stiffer alginate shell (~1252 kPa, Figure 29). In addition to providing a soft environment, the Matrigel supports mammary epithelium development. When in Matrigel, single MCF10A cells proliferate into a small aggregate and following apoptosis of the inner mass, forming hollow structures called acini[127]. In vitro, integrin β1 is localized on the surface of the acini, suggesting hemidesmosome formation which is a key element for acinar formation (Figure 27c). In contrast, within the confinement of an alginate shell, multiple MCF10A cells failed to form acini in

Matrigel and, instead, underwent uncontrolled growth as demonstrated by the loss of integrin β1 surface localization (Figure 27d and Figure 30a). However, the cellular overcrowding in microcapsules might contribute to the proliferation. To clarify the observed effects of confinement on acini formation were not simply due to cellular overcrowding, we cultured MCF10A cells with different initial cellular concentrations in Matrigel for 40 days and measured the percentage of acini formation as well as the size of the acini. We found that, regardless of the initial cellular concentration, the proportion of MCF10A cells that formed acini remained the same, with only the size of the acini changing (Figure 31). Although these data suggested that the cellular concentration is likely not a key determinant of the observed malignant growth within the microcapsules, we nevertheless used only single cells for the physical confinement experiments in order to simplify the model. When single MCF10A cells were confined in the microcapsules, the cells again grew uncontrollably (Figure 27e), eventually invading the alginate layer (Figure 32). These results suggest that physical confinement may disrupt the mammary morphogenesis by uncontrolled growth.

To test the hypothesis that decreased oxygen and nutrient diffusion across the microcapsule hydrogel layer may be the cause of the observed proliferative effects[137], we developed a sandwich layer assay to control for the effect of diminishing diffusion. For this assay, cells were embedded in Matrigel covered by a layer of alginate having a similar thickness to that of the microcapsules. Results show that, similar to Matrigel alone, polarized acini structures were observed after 40 days of culture (Figure 33). Lastly, we confirmed there was no significant mixing of Matrigel and alginate hydrogel at the core-shell interface in the microcapsules by using immunofluorescent staining for laminin and fluorescent alginate (Figure 28); and even in a bulk mixture of Matrigel and alginate, the MCF10A cells still formed acini (Figure 34),

excluding the possibility that the mixing caused the malignancy in microcapsules. Taken together, these *in vitro* experiments support the hypothesis that physical confinement is sufficient to promote the transformation of mammary epithelial cells.

3.3.2 Confinement results in increased cell proliferation, reduced apoptosis and promotes epithelial-mesenchymal transition

To more quantitatively characterize the malignant growth caused by the confinement, we performed indirect immunofluorescence using antibodies against a proliferation marker, Ki67, and an apoptosis marker, caspase-3. Results showed that, compared with cells in bulk Matrigel, confined cells showed a higher proliferative signal and lower apoptosis, potentially explaining the lack of lumen formation in microcapsules (Figure 30a-b). Moreover, as with integrin β1, we found that integrin β4 localization was also disrupted, further suggesting that hemidesmosome formation did not proceed appropriately (Figure 30c).

A key characteristic of carcinoma development is the epithelial-mesenchymal transition (EMT) in which epithelial cells display mesenchymal or fibroblast-like behavior with reduced intercellular adhesion and increased cell motility.[138] We found that the confined cells in our study partially lost surface expression of E-cadherin which is one of the features in EMT (Figure 30d). To further investigate the ability of confinement to promote the EMT, the invasiveness of confined cells was measured through an invasion assay (Figure 30e). After culturing in type I collagen gel for 9 days, 83% of the total aggregates from microcapsules grew and migrated into the collagen matrix. By contrast, the majority of the acini from bulk Matrigel (~98%) maintained the stable state without proliferation (Figure 30f). Similar behavior was observed when the aggregates or acini were re-embedded in Matrigel (Figure 35). Moreover, E-cadherin was absent

from the aggregates from microcapsules during the invasion assay and integrin β1 was expressed throughout the invasive cluster. By contrast, integrin β1 was localized at the periphery of the acini (Figure 30e). The result suggests that physical confinement may have transformed the MCF10A into cells with cancerous properties.

When we collected the confined cells from microcapsules and re-cultured them in a cell culture flask, these cells (MCF10A-PC) maintained the tumor-like behavior, such as rapid growth and invasion into bulk Matrigel even after 6 passages (Figure 36). This result suggests that the physical confinement might not only transform the confined cell into invasive state but also allow the cells maintained the confined effect for at least 6 passaging time possibly due to epigenetic change. We also examined the universal effect of the physical confinement on different types of cells, specifically, breast tumor cells, MCF10DCIS.COM (Figure 37), human primary mammary epithelial cells (hPMEC) (Figure 38) and kidney epithelial cells (MDCK) (Figure 39). These cells all responded to the confinement but in different ways. For example, the MCF10DCIS.COM cells displayed accelerated growth, the hPMEC cells showed disruption of the mammary epithelium morphogenesis, and MDCK exhibited increased apoptosis.

3.3.3 RNA sequencing suggests that physical confinement might activate insulin/insulin-like growth factor pathways

In order to better understand the mechanisms by which confinement induces tumorigenesis, we analyzed the gene expression profiles of confined cells using RNA-seq. We prepared four different groups; confined MCF10A cells, which were cultured in microcapsules for 40 days, MCF10A, MCF10DCIS.COM cells, and MCF10A-PC cells at the 9^{th} passage from bulk Matrigel at the same culturing condition as the confined cells. Results show that around

8000 genes are differentially expressed (adjusted $p<0.01$) in confined cells compared to those from bulk Matrigel (Figure 40a-b). In MCF10DCIS.COM and MCF10A-PC cells, around 8000 and 3000 genes are differentially expressed compared to the control MCF10A cells, respectively (Figure 40). Without physical confinement, the MCF10A-PC cells (9^{th} passage) maintained differential expression from normal MCF10A cells in bulk Matrigel (Figure 41). Even when the microcapsule was first dissolved, removing the physical confinement one day before RNA extraction, there were nevertheless around 4500 differentially expressed genes (Figure 42). These results suggest that the effect of confinement could be maintained for 9 passages after the confined layer was removed. GO enrichment analysis[139] of these samples identified ~161 potential signaling pathways that were altered by culturing the MCF10A cells in microcapsules. Among these pathways, we inferred two potential pathways that promote cell proliferation and prevent apoptosis under physical confinement. The insulin/insulin-like growth factor (IGF) pathway and the mitogen activated protein kinase/MAP kinase cascade (MAPK/MAP) pathway. Moreover, these two pathways were confirmed by molecular inhibition experiments by drugs and antibody (Figure 43-46). These results suggest that the complex formation of IGF1R and integrin β4 due to the disruption of hemidesmosome might induce the malignancy by activating IGF pathway[140] (Figure 47).

3.3.4 Confinement restricts matrix fluctuation to disrupt acini formation

Next, to better understand how physical confinement by microcapsules might affect ECM remodeling, we prepared microcapsules in which the MCF10A expressed EGFP and the Matrigel matrix was tagged with fluorescent microbeads (red). This approach enabled analyzing fluctuations in the matrix that were caused by cellular traction forces and movement (Figure 48a-b). Time-lapse images were then taken to simultaneously track cell movement and bead

displacement using Matlab (Figure 49). We found that, immediately after encapsulation, there was no significant difference between cell movements in the bulk Matrigel group when compared to the cells contained within the microcapsules (Figure 48c). However, under confinement, matrix fluctuation was restricted, and bead displacement was decreased in the microcapsule group when compared with the bulk group (Figure 38d). This result suggested that the restricted matrix fluctuation might hinder hemidesmosome formation which could further promote integrin β4 and IGF1R[140] complex formation (Figure 48e). Such an outcome fits well with our RNA-seq data and could explain how physical confinement transforms MCF10A cells.

We also found that the observed confinement effect depends on cell position in the Matrigel core with the cell growth rate being inversely proportional to the distance between the confined cell and the alginate shell (Figure 48f). Additionally, we found that increasing the diameter of the Matrigel core actually decreased the growth of confined MCF10A cells. For example, we found that, when the core size increased to 500μm in diameter, the confined cells would grow into small aggregates devoid of luminal structures and reminiscent of pre-malignant breast cancer (Figure 50). When the core size reached 600μm, the confined cells formed hollow acini in capsules, which is similar to that of non-confined cells. In the large-core capsules, the MCF10A cells formed growth-arrested polarized acinar structures and expressed high levels of E-cadherin and localized integrins, suggesting hemidesmosome formation in these structures is more similar to normal acini (Figure 48g). This result suggests that the effect of physical confinement on cellular growth is inversely proportional to the distance between confined cells and the alginate shell. Additionally, when the diameter of core size reaches 600μm, the effect of physical confinement nearly vanishes.

3.3.5 Confined cells form carcinomas in Scid-Beige mice

Lastly, to verify that the malignant characteristics observed in vitro were indicative of a true malignant transformation, we tested whether the confined MCF10A cells could form tumors in immunodeficient Scid-Beige mice (which lack T and B lymphocytes and contain defective cytotoxic T cells, macrophages, and natural killer cells). Five different types of cell preparations were injected into the nude mice: confined MCF10A cell aggregates from microcapsules (CMA), dissociated cells from the confined MCD10A cell aggregates in suspension (DCMA), MCF10A acini from bulk Matrigel, MCF10A cells in suspension and MCF10DCIS.COM cells (which, as opposed to MCF10A cells, form tumors in immunodeficient mice) in suspension. For the xenografts, cell aggregates were collected, suspended in 100μL Matrigel, and $1x10^6$ cells were injected into the mammary fat pad tissue using a 26G needle as described in the Materials and Methods and previously[141,142]. After 4-6 weeks, the acinar and MCF10A single cell groups did not form tumors in mice, however, the other three groups (CMA, and DCMA as well as MCF10DCIS.COM) all formed palpable masses in the mice (Figure 51a). We note that we did not remove skin and hair from the negative control groups because lesions in these groups were either not present or were so small that they could not be dissociated from the skin. Therefore, weight for negative control groups was given a value of zero. For the rest of groups, these masses were weighed (Figure 51b), fixed and embedded for histological analysis using hematoxylin and eosin and for immunohistochemistry using antibodies against the differentiation markers, p63 for myoepithelial cells, and cytokeratin for luminal cells (Figure 51c). Based on the Nottingham grading system, three different histopathology grades were scored by histologic pattern (Figure 52), mitotic rate and amount of necrosis (Figure 53): low grade (I), intermediate grade (II), and high grade (III). Results from this blinded study show that the confined cell

groups (CMA and DCMA) and the control MCF10DCIS.COM group were scored by the pathologist as intermediate (II) and high grade (III) carcinomas by the pathologist. (Figure 51d). Furthermore, Integrin β1, β4 and E-cadherin were also characterized for these samples. (Figure 54). Interestingly, these biomarkers were lost in the confined groups.

3.3.6 Discussion

Mammographic density is an important factor for predicting risk of early stage breast cancer in women[143,144]. Here, we developed a core-shell microcapsule platform as an in vitro model system to mimic the physical confinement effect of dense stromal tissue on the mammary epithelium. MCF10A cells seeded in Matrigel within microcapsules grew faster and resulted in larger aggregates after 3 days compared to cells grown in bulk Matrigel. After a total of 6 days in the microcapsules, signs of uncontrolled growth in the microcapsule group were apparent (Figure 55). Moreover, when fully formed acini were collected from bulk Matrigel at day 40 and re-encapsulated, we observed a similar result on the confined acini. Although each acinus was in a growth-arrested state, the polarized structure was disrupted in microcapsules and the cells filled the core and eventually escaped the microcapsules completely, suggesting that encapsulation can successfully transform MCF10A cells after they have fully differentiated into acinar epithelial cells (Figure 56).

The ability of MCF10A cells to differentiate into acini is thought to depend on hemidesmosome formation.[145,146] Hemidesmosomes are important connections between the extracellular matrix and the cytoskeleton, and these connections are mediated by integrins on the cell surface. In previous studies, increasing Matrigel matrix stiffness either through the addition of collagen to Matrigel or by mixing Matrigel with alginate, promoted uncontrolled growth in

MCF10A cells and caused the disruption of integrin β1 or β4[128–130]. The disordered localization of integrins observed in microcapsules in this study suggests that the formation of hemidesmosomes were disrupted. However, unlike previous studies, in which a similar phenomenon was caused by changes in the biochemistry, composition, and/or mechanics of ECM, here the Matrigel matrix was unmodified with the only other variable being the stiff outer alginate capsule.

To determine whether new DNA sequence changes might play a role in malignant transformation, we derived the genetic mutations in exons from RNA-seq data via variant discovery. 26 candidates were randomly selected for DNA sequencing to determine if the mutations were indeed present (Table 3). However, a lack of confirmation indicated that mutations in RNA-seq data were sequencing errors and did not occur in the genome. Tumor formation is caused by an accumulation of mutations in somatic cells due to a variety of environmental factors that result in the accumulation of mutations over time[147]. Over the relatively short period of time the confined cells were grown in the capsules, they are extremely unlikely to undergo significant new genetic mutations that are common between different replicates. Taken together, these results suggest that new DNA sequence changes are unlikely to explain the transformation of MCF10A cells in capsules.

Our RNA-seq analysis found that the expression of approximately 8000 genes were altered under physical confinement. We observed changes in expression 9 passages after removing the encapsulation, suggesting that changes in expression last for an extended duration. This result implies that confinement changes gene expression in lasting ways that prevent MCF10A cells from reverting back to their normal state. Changes in gene expression that alter the gene expression regulatory state that cells are present in can have the potential to lock in new

cellular states[148]. This type of change in expression could be a key factor in allowing MCF10A-PC to "remember" the confinement and continue to generate excess growth signaling for uncontrolled growth and invasion even after removal from the microcapsules. Based on the RNA-seq and DNA sequencing, we propose a model in which alterations in gene expression such as gene regulation changes.

Furthermore, the RNA-seq data suggests that growth does not come from mechanotransduction which is induced by the integrins interacting with the intracellular signaling molecules, focal adhesion kinase (FAK) and Src kinase to upregulate Rho and MAPK signaling pathways to enhance proliferation; however, the inhibitors for them failed to stop the growth in microcapsules (Figure 43b). In addition, while engineered MCF10A cells lost the expression of cytoplasmic tail of integrin β1 or β4, these cells still continuously grew in microcapsules (Figure 43c-d). On the other hand, the IGF pathway could activate PI3K and MAPK/MAP pathways as transforming growth factor beta receptor for cell proliferation and ceasing apoptosis. To confirm it, inhibitors for ROCK, PI3K, MLCK and Myosin II were applied to decrease the growth and stimulate localization of integrin β4. (Figure 43e-i) Moreover, with inhibitor for IGF1R, the MCF10A cell form acini-like structure again. It is interesting to mention when the cells form acini-like structure in microcapsules, they also lost the expression of integrin β4 (Figure 43h-j). When the receptor of integrin β4 was blocked by antibody, the growth was controlled without filling the core (Figure 43k). It indicated that the drug or antibody could stop the uncontrolled growth in microcapsules without disrupting the acini formation. Based on the results of RNA-seq and molecular inhibitors, one potential mechanism is that integrin β4 might form a complex with IGF1R when the hemidesmosome is disrupted, inducing PI3K signaling mediated by insulin receptor substrate[149,150].

The in-vivo xenograft data indicated that the confinement-induced changes in MCF10A cellular behavior observed in vitro could potentially result in malignant carcinomas. In normal mammary gland architecture or in DCIS, tubules are composed of a single, proliferative layer of polygonal cells lining a central lumen[151,152]. On the other hand, nests and trabeculae, which are solid structures without lumens, were observed in MCF10A cells exposed to physical confinement (Figure 52) and is characteristic of invasive ductal carcinoma. Moreover, the cells forming nests and trabeculae were often larger with more cytoplasm than the ones forming tubules. These cells are less similar to the normal mammary epithelial cells and probably reflect de-differentiation in the xenograft. Also, some nests developed areas of central necrosis similar to more aggressive tumors. Ordinarily, MCF10A cells do not grow or survive in in vivo xenografts. In fact, in order to form malignant MCF10A cell lines (e.g. MCF10AT), they typically must be transformed to stably overexpress the H-Ras gene. Importantly, these transformed MCF10A cells tend to form tumors in mice more slowly (over ~3 months vs. 40 days) and at a lower rate (~40% vs. 90%) compared to MCF10A cells grown in our microcapsules[125].

3.4 Conclusion

In conclusion, not only does this study provide interesting insights into how physical confinement of the breast epithelium can induce tumor formation, but also, the mini-tumors formed in microcapsules could be useful for breast cancer research and treatment development. The high-throughput nature of the electrospray encapsulation technique allows hundreds or thousands of microcapsules to be rapidly produced for drug screening with tumor pressure or other industrial applications.

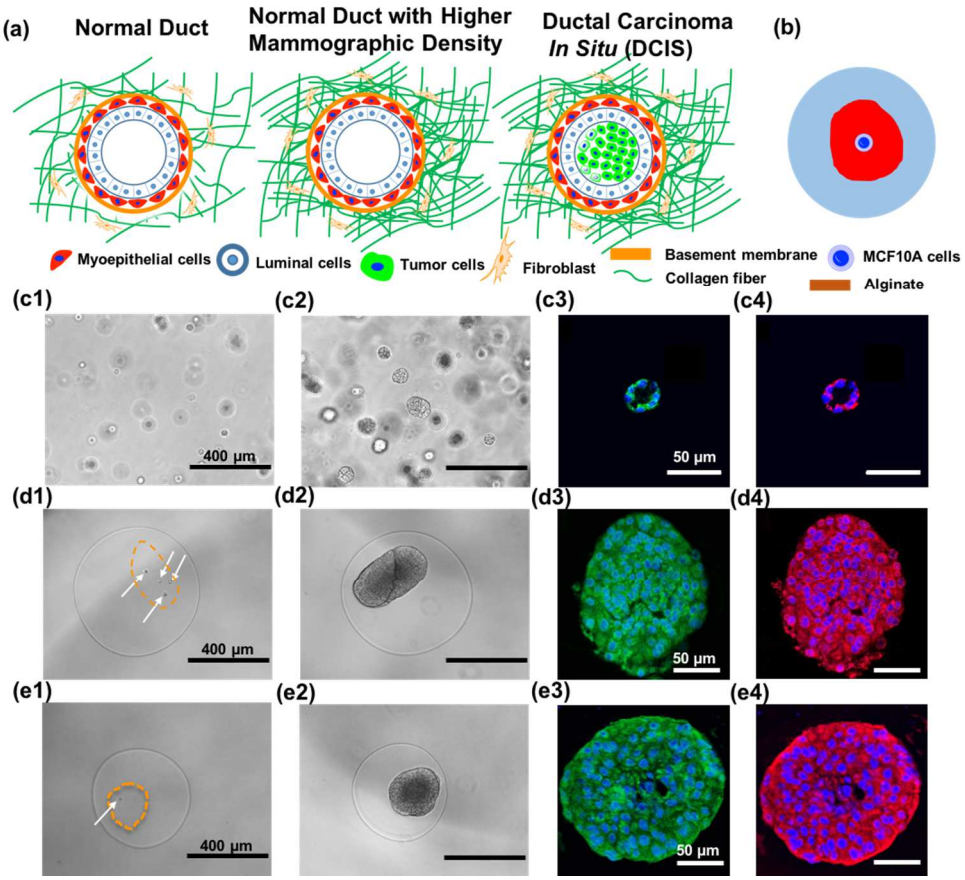

Figure 27, Mammary epithelium tumorigenesis with high mammographic density which could be simulated by core-shell hydrogel decoupled microcapsules.

(a) the mammary epithelium consists a single layer of luminal cells surrounding by myoepithelial cells in basement matrix. The microenvironment including stromal cells and collagen fibers support the mammary epithelium, however, higher mammographic density became a risk factor for breast cancer progression with more and thicker collagen fibers. In DCIS, the malignant cells usually fill the hollow of mammary duct before invasion. (b) A core-shell microcapsule composes of single MCF10A cell in basement matrix confined by a stiffer a hydrogel layer to simulate the in-vivo mammary epithelium tumorigenesis under high mammographic density. (c) (d) (e) MCF10A cells were cultured in bulk Matrigel and in microcapsules for 40 days. Cytoskeleton, F-actin and integrin β1 were stained by immunofluorescent. (c) The acini from bulk presents clear F-actin and localized integrin β1. (d) Multiple cells in a microcapsule continuously grew to fill the core. The F-actin became blurred and the localization of integrin β1 was disrupted. (e) Single cell was encapsulated in microcapsule, but uncontrolled growth might be induced by disruption of hemidesmosome, integrin β1. The unclear F-actin suggested that the de-polymerization occurred under physical confinement for epithelial-mesenchymal transition.

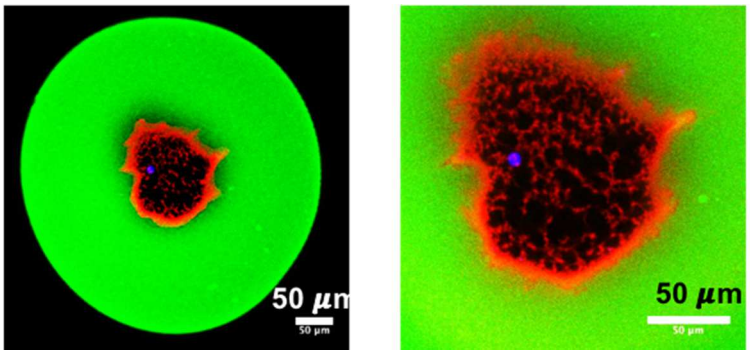

Figure 28, The laminin (red) which is the primary component in Matrigel was stained by antibody with a single MCF10A cell whose nucleus was stained by Hoechst 33342 (blue).

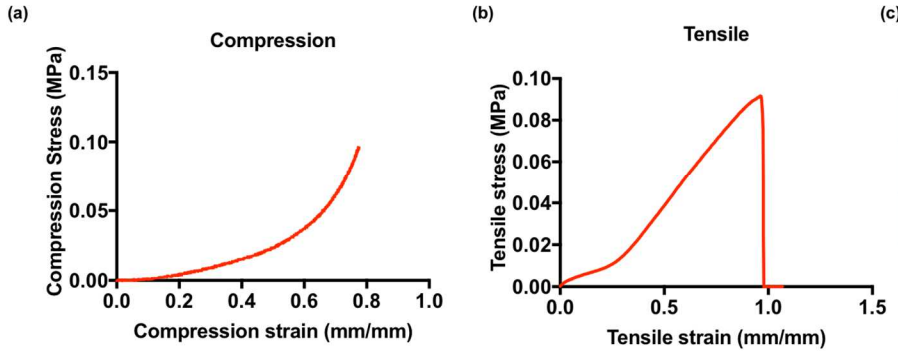

(c)

	Modulus (MPa)
Compression	0.0484 ± 0.0280
Tensile	0.1252 ± 0.0723

Figure 29, The mechanical properties of alginate in compression and tensile modulus measurement.

(a) Compression curve of alginate hydrogel cylinder (b) Tensile curve of alginate hydrogel cylinder (c) The modulus was calculated by 10 samples for compression and tensile tests.

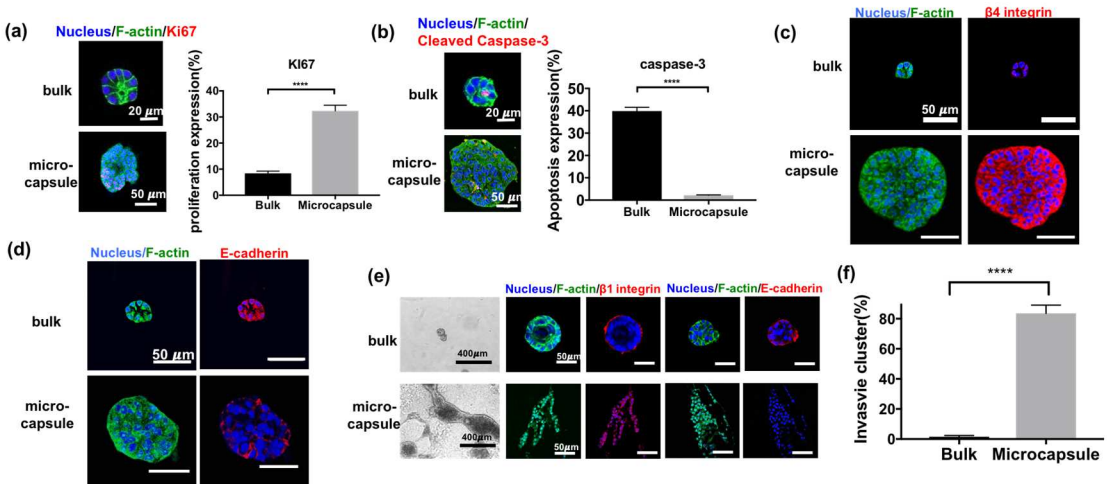

Figure 30 , Characterization for confined cells.

(a) The proliferation marker, KI67 was stained in bulk and in microcapsules and measured as proliferation expression. The proliferation expression in bulk and in microcapsules are 8.37%±0.87% and 32.36%±2.17%. (n=427, 259 stacked all six independent experiments, $p<0.0001$) (b) The apoptosis marker, cleaved caspase-3 was stained for the hollow structure formation. The apoptosis expression in bulk and in microcapsules are 39.87%±1.70% and 2.15%±0.19%. (n=321, 248 stacked all six independent experiments, $p<0.001$) (c) The sections from cells in bulk and in microcapsules were stained for integrin β4. (d) E-cadherin was detected in bulk and in microcapsules. In acini from bulk, the E-cadherin was fully expressed, but partially lost in microcapsules. With loss of E-cadherin and blurred F-actin, it suggested that these encapsulated cells might under EMT. (e) An invasion assay was conducted in collagen gel. Acini from bulk could maintain its structure after 7 days, but the aggregations from microcapsules grew and invaded into surrounding matrix in collagen matrix. (f) The invasive cluster was measured in bulk (1.47%±0.83%) and in microcapsules (83.60%±5.46%). (n=130, 116 stacked all three independent experiments, $p<0.0001$)

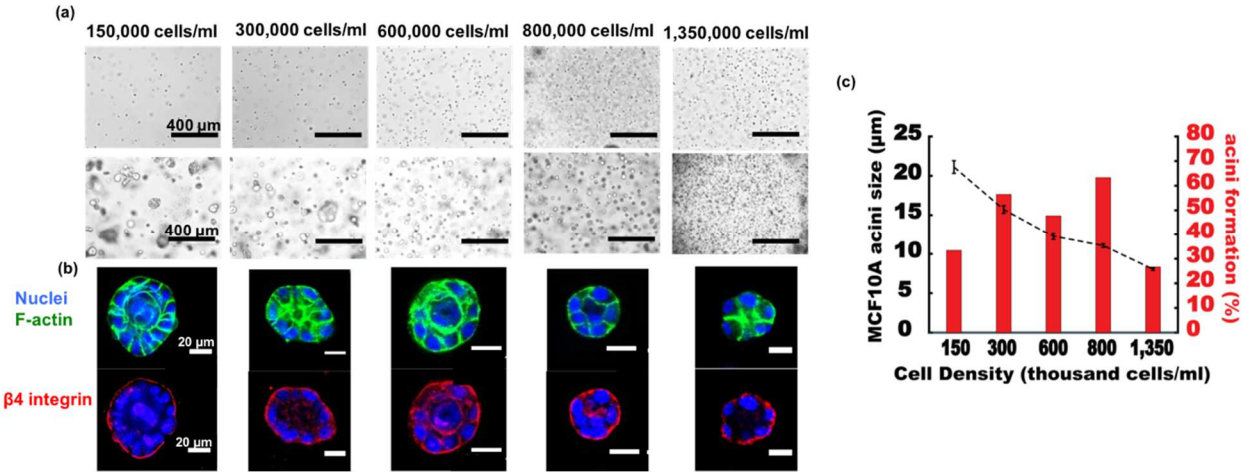

Figure 31, The relationship between acini formation and cellular concentration.

(a) The MCF10A cells were seeded in bulk Matrigel with different cellular concentration from 150,000-1,350,000 cells/ml for 40 days. (b) Acini were observed in all the groups, and integrin β4 was likely localized on the surface. (c) The relationship for acini formation, cell density and acini size. The black dash line showed the acini size in diameter from different cell density. The red bar indicated the acini formation ratio with cell density.

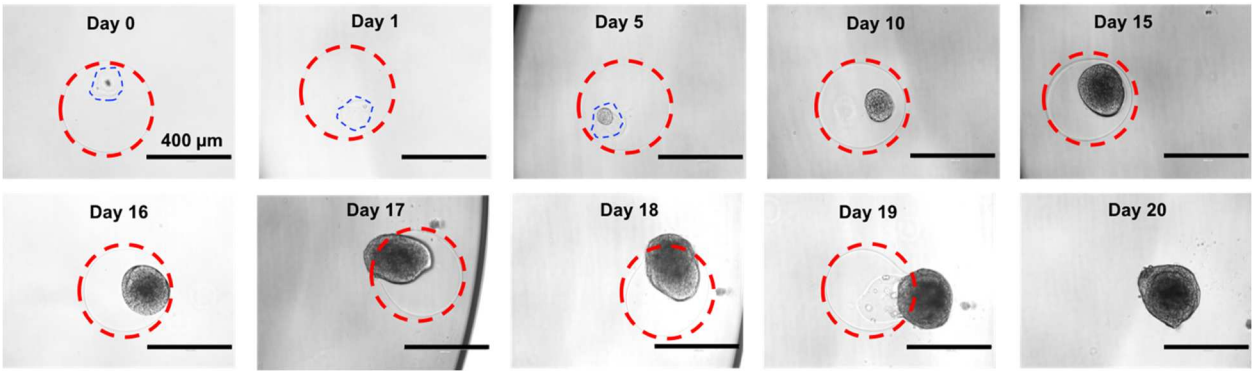

Figure 32, The single MCF10A cell in microcapsule continuously grew with time and broke the alginate microcapsules.

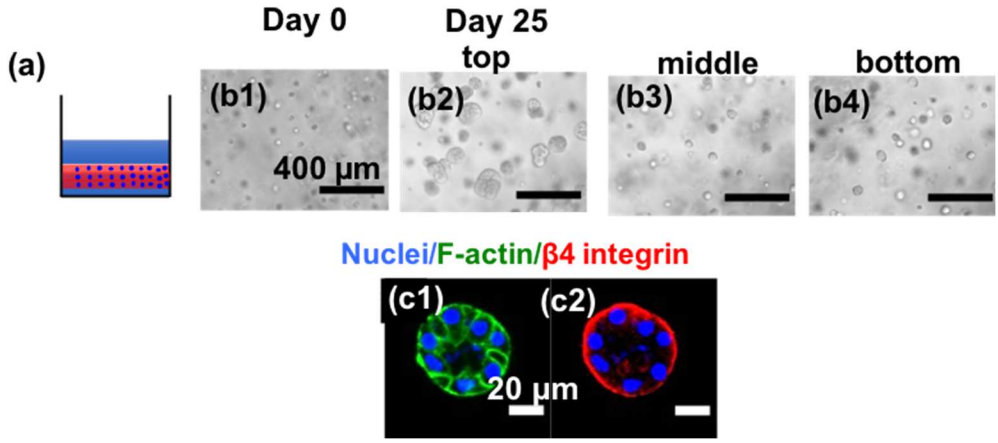

Figure 33, The sandwich model to simulate the mass diffusion in microcapsules.

(a)The sandwich model is composed of three layers: alginate, MCF10A cell in Matrigel, and alginate layer. The thickness alginate layer is similar as microcapsules. (b) The Matrigel layer could be imaged by three different layers from top to the bottom part close to alginate layer. They all formed acini in three different layers, but the size became smaller in middle or bottom layer due to mass diffusion. (c) The polarized acini were observed with integrin β4 localization on the surface.

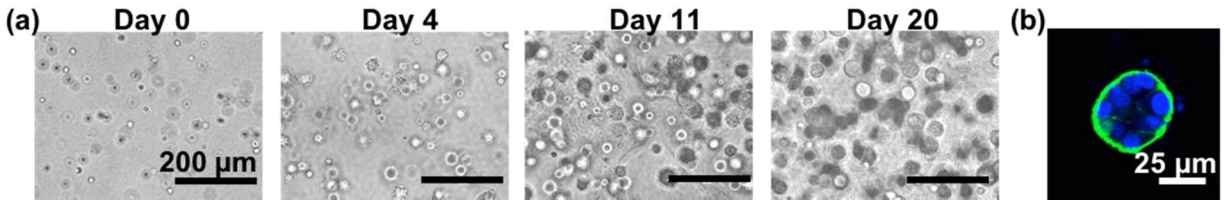

Figure 34, MCF10A cells were cultured in mixture of Matrigel and alginate crosslinked with calcium and barium.

(a) The MCF10A could form acini after 20 days. (b) The acini with polarized structure was stained for nucleus (blue) and F-actin (green).

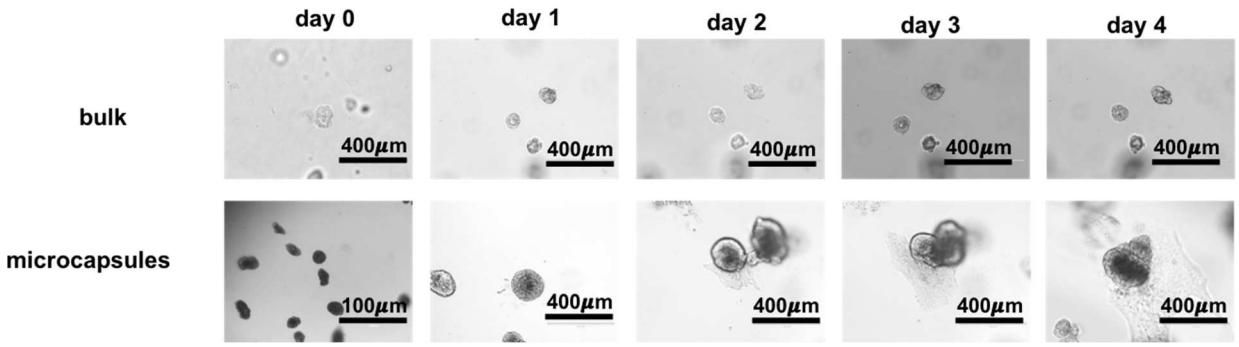

Figure 35, The acini from bulk and cell aggregates from microcapsules were re-suspended in Matrigel.

The acini maintained the polarized structure, but the aggregations grew and invaded in 3 days.

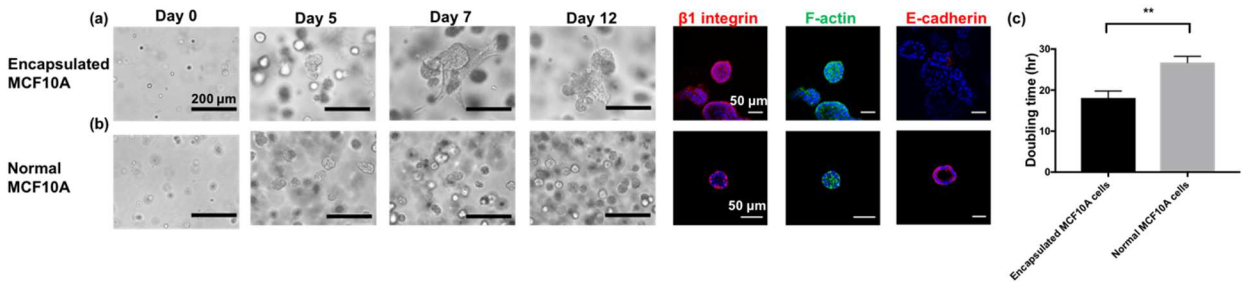

Figure 36, Re-suspension of confined MCF10A cells in Matrigel.

(a) The encapsulated cells were obtained from microcapsules and passaged in culture flask for 6 times before seeding in bulk Matrigel. The encapsulated MCF10A behaved similar as normal MCF10A cell in first 5 days, then became invasive as cancer cells. The localization of integrin β1 is disrupted, and E-cadherin was completely lost. (b) Normal MCF10A cells were seeded in the Matrigel as a control. The integrin β1 localized on the surface and E-cadherin was fully expressed. (c) The doubling time of encapsulated MCF10A cells (18.08hr ± 0.99hr) is significantly short than normal MCF10A cells (26.7hr ± 0.88hr). (n=3, 3. p=0.003)

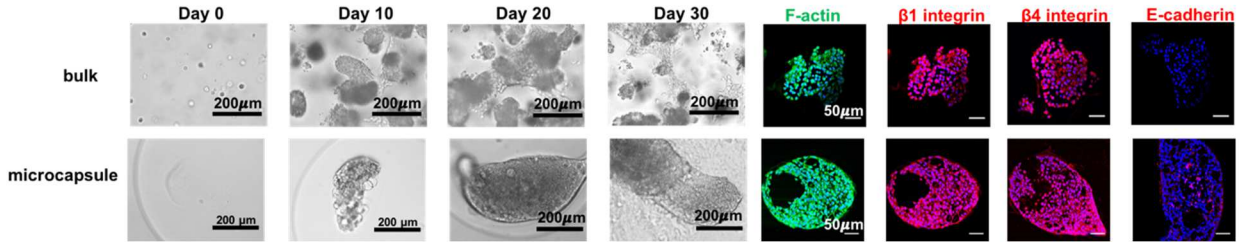

Figure 37, Malignant breast cancer cell, MCF10DCIS.COM were seeded in bulk and in microcapsules.

The cells in bulk and in microcapsules grew rapidly and became invasive after 20 days. The integrin β1 and integrin β4 were all disrupted, and E-cadherin was lost in both conditions.

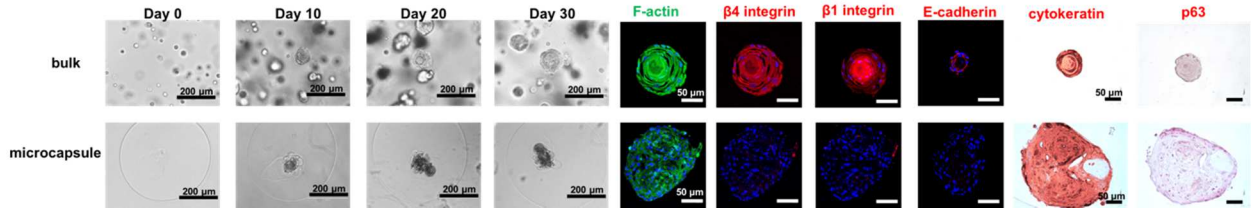

Figure 38, The human primary mammary epithelial cells were cultured in bulk Matrigel and in microcapsules.

The primary cells could form multiple layer structure with integrin β1, integrin β4 and E-cadherin expression, however, the encapsulated cell in microcapsule lost integrin β1, integrin β4 and E-cadherin. Moreover, the F-actin was strong in bulk but blurring in microcapsules. In bulk, the structure consists of lumen cells (expressing cytokeratin) surrounding by myoepithelial cells (expressing p63). In microcapsules, only luminal cells were observed by immunohistochemistry.

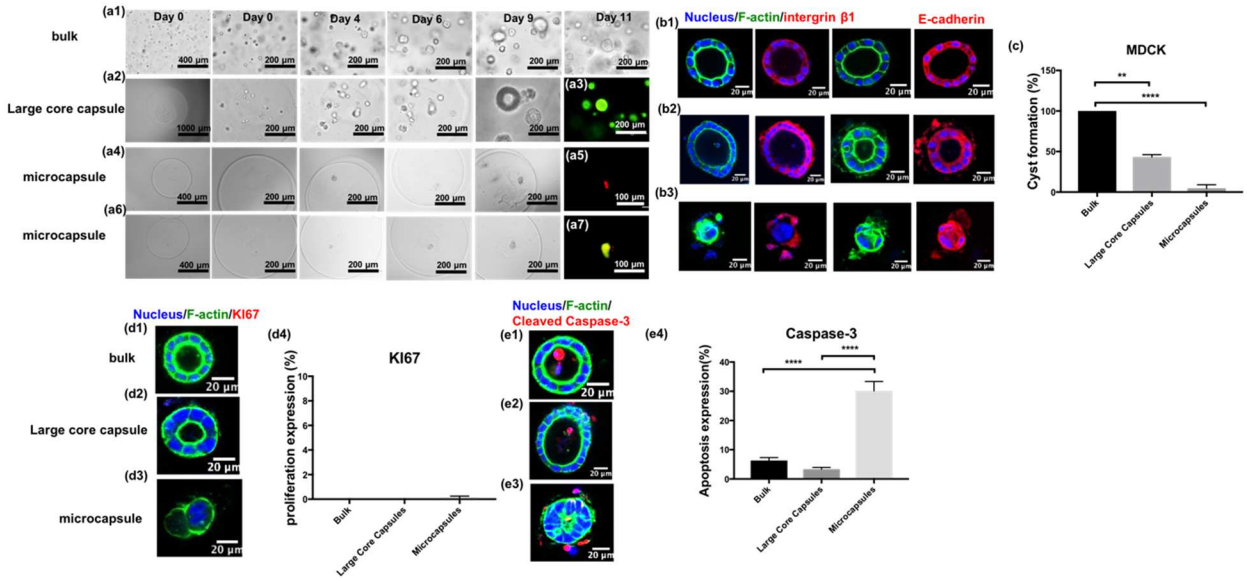

Figure 39, MDCK cyst formation in bulk, in microcapsules and large core capsules.

(a1) The cysts were formed in bulk Matrigel after 6 days. (a2)(a3) The cells in large core capsules could grow into polarized structure, and these cells were alive at day11. (a4)(a5) The MDCK cell in microcapsule might be under apoptosis after encapsulation. The cells were dead at day9 by live/dead staining (a6)(a7) The cell in microcapsules might slightly grow without polarized structure. (b) The cysts/aggregations were stained for F-actin, integrin β1 and E-cadherin in bulk, microcapsules and large core capsules. (b1) The polarized cysts from bulk express integrin β1 and E-cadherin. (b2) The cysts were observed in large core capsules with polarized structure. (b3) The cells in microcapsules did not form hollow structures but random shape of aggregations. (c) The cyst formation were calculated for bulk, large core capsules, microcapsules. (n=64, 29, 100 $p<0.0001$) (d)(e) The proliferation marker, KI67 and apoptosis marker were stained at day 11 for cells in bulk, large core capsules and microcapsules.

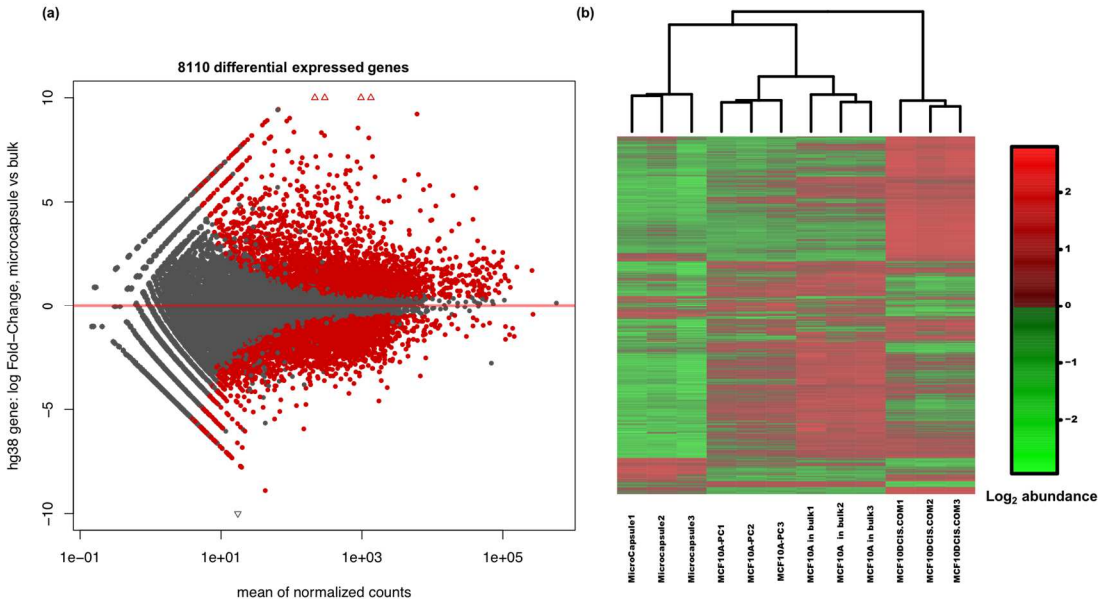

Figure 40, RNA-seq from cells in microcapsules and in bulk.

(a) The MA plot for differential gene expression in fold-change of microcapsules over bulk. There are 8110 genes which are differentially expressed in microcapsules comparing with bulk. ($p<0.01$) (b) The heat map for the samples with 3 microcapsules, 3 MCF10A-PC (9^{th} passage) in bulk, 3 normal MCF10A cells in bulk and 3 MCF10DCIS.COM cells in bulk.

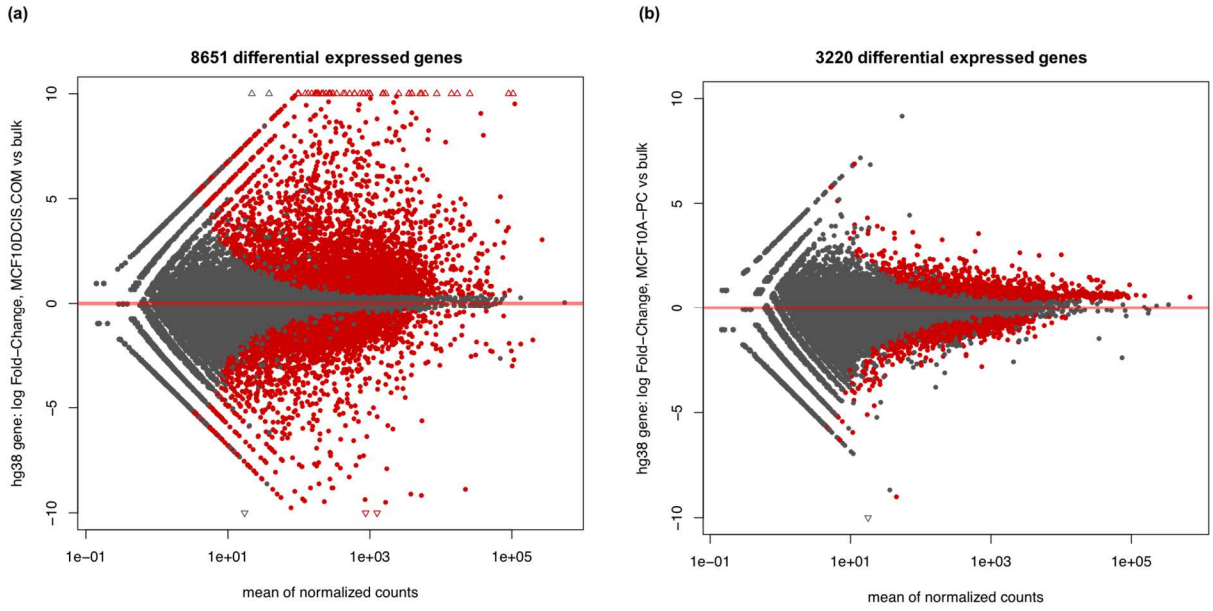

Figure 41, RNA sequencing from MCF10A, MCF10DCIS.COM and MCF10A-PC cells in bulk Matrigel.

(a) The MA plot for differential gene expression in fold-change of MCF10DCIS.COM over MCF10A cells. There are 8651 genes which are differentially expressed in microcapsules comparing with bulk. ($p<0.01$) The heat map for the samples with 3 MCF10DCIS.COM and 3 MCF10A was depicted by the differential expressed transcriptomes. (b) The MA plot for differential gene expression in fold-change of MCF10A-PC over MCF10A cells. There are 3220 genes which are differentially expressed in microcapsules comparing with bulk. ($p<0.01$) The heat map for the samples with 3 MCF10A-PC and 3 MCF10A was depicted by the differential expressed transcriptomes.

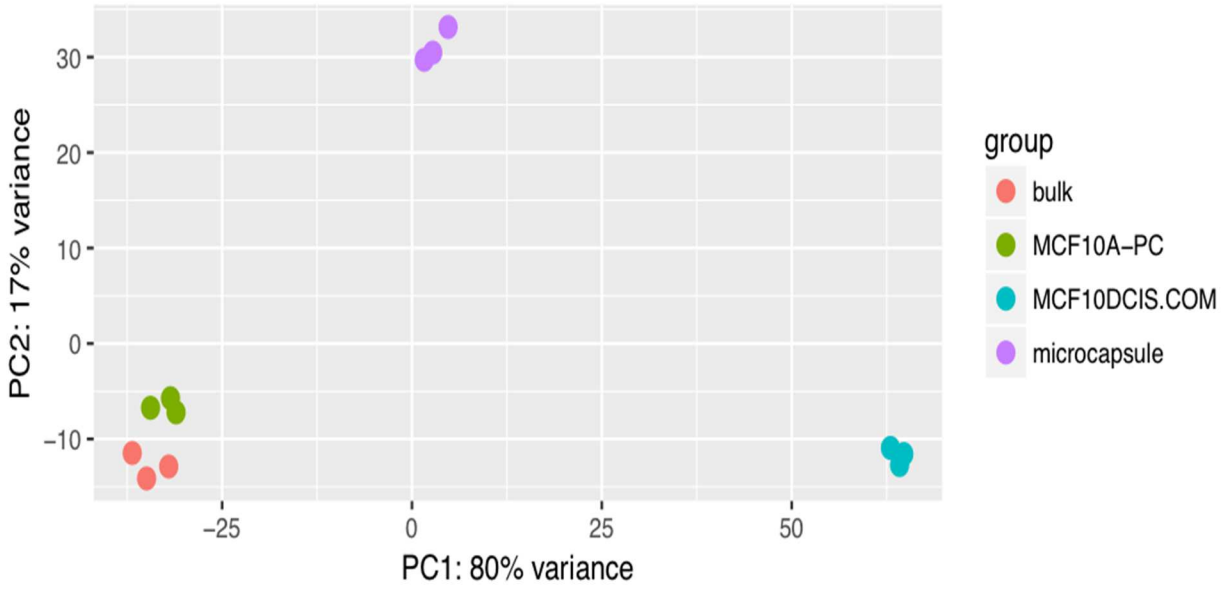

Figure 42, The principal component analysis of RNA-seq from four different groups, MCF10A in microcapsules, MCF10A, MCF10A-PC and MCF10DCIS.COM in bulk Matrigel.

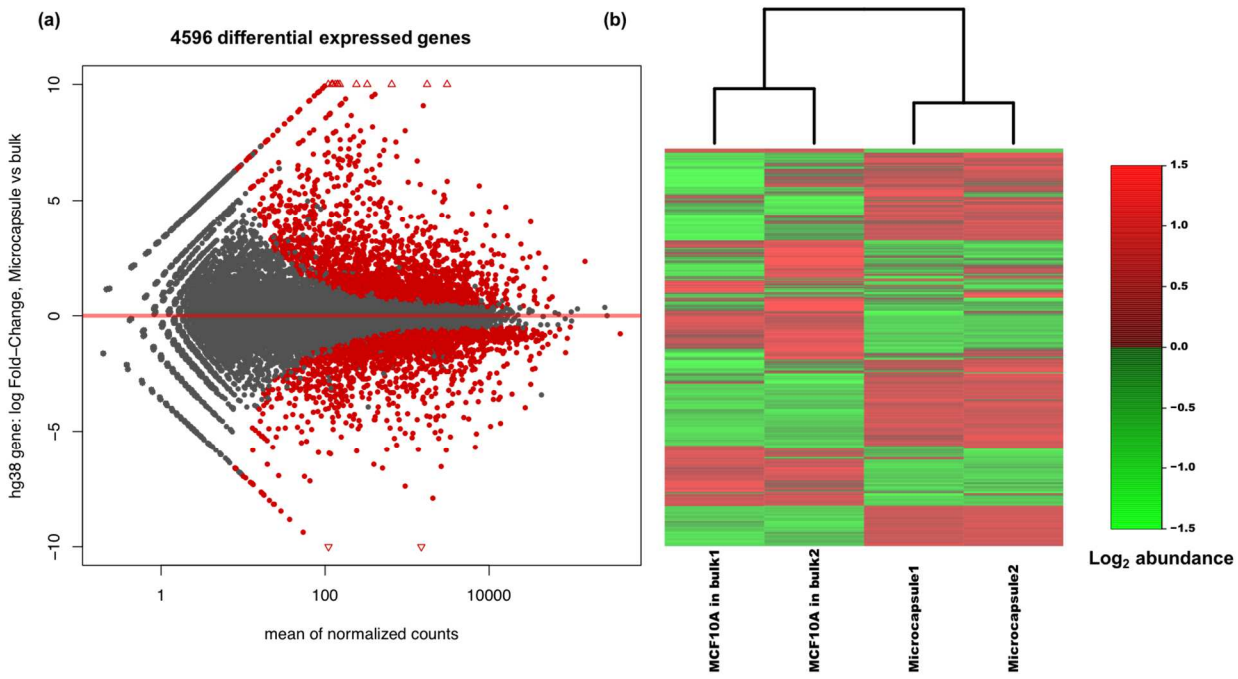

Figure 43, RNA-seq. from cells in dissolved microcapsules and in bulk.

(a) The MA plot for differential gene expression in fold-change of microcapsules over bulk. There are 4740 genes which are differentially expressed in microcapsules comparing with bulk. ($p<0.01$) (b) The heat map for the samples with 2 microcapsules and 2 bulks.

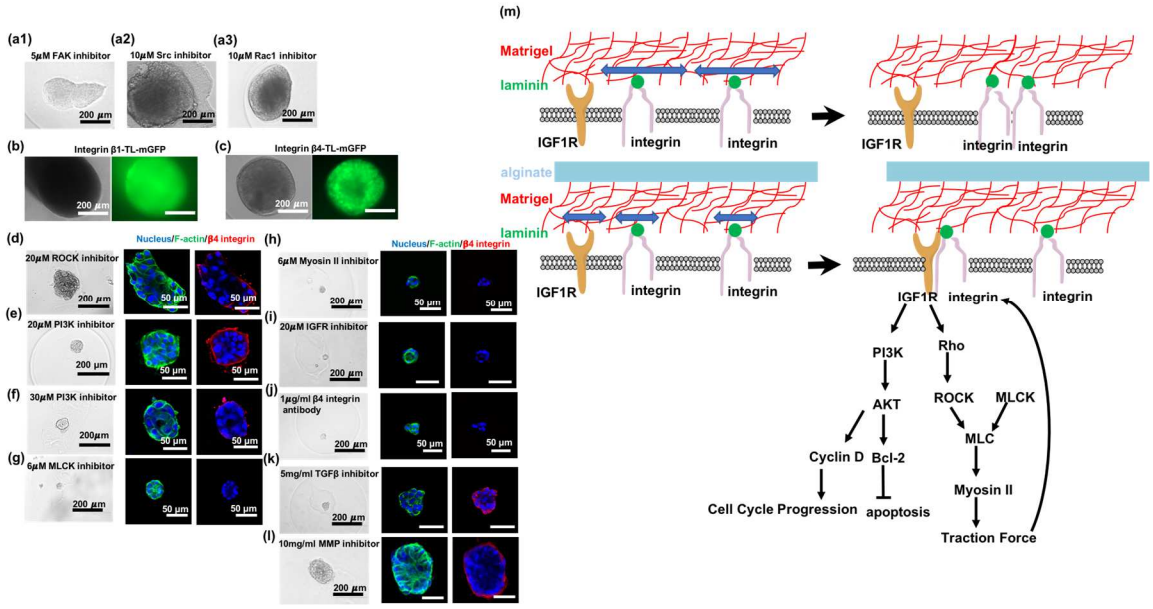

Figure 44, The drug inhibition and proposed mechanism for physical confinement.

(a) drugs for proteins (FAK, Src kinase, Rac1) in mechanotranduction signaling pathway. The encapsulated cells continuously grew with these inhibitors. (b) (c) MCF10A cells constitutively express GFP fused tail-less integrin β1 or β4 (TL). (d)(e) The encapsulated cell applied with ROCK and PI3K inhibitors did not grow to fill the core, but the inhibitors induce the integrin β4 localization. (f) With 30μM PI3K inhibitor, the encapsulated cell grew into acini-like structure with partial loss of integrin β4. (g)(h) Drugs for cytoskeleton, MLCK and myosin II inhibitors were applied for the cells in microcapsules. Acini-like structure was observed at day 40 without integrin β4 expression. (i) The encapsulated cells form acini structure with IGF1R inhibitor but lost integrin β4 expression. (j) Application of integrin β4 antibody ceases the growth of cells in the microcapsules. (k)(l) Inhibitors for TGFβ signaling pathway, such TGFβ receptor and MMP cease the over-growth signaling and induce the localization of integrin β4. (m) The signaling pathway is proposed for the physical confinement from RNA sequencing and confirmed by drug inhibitions.

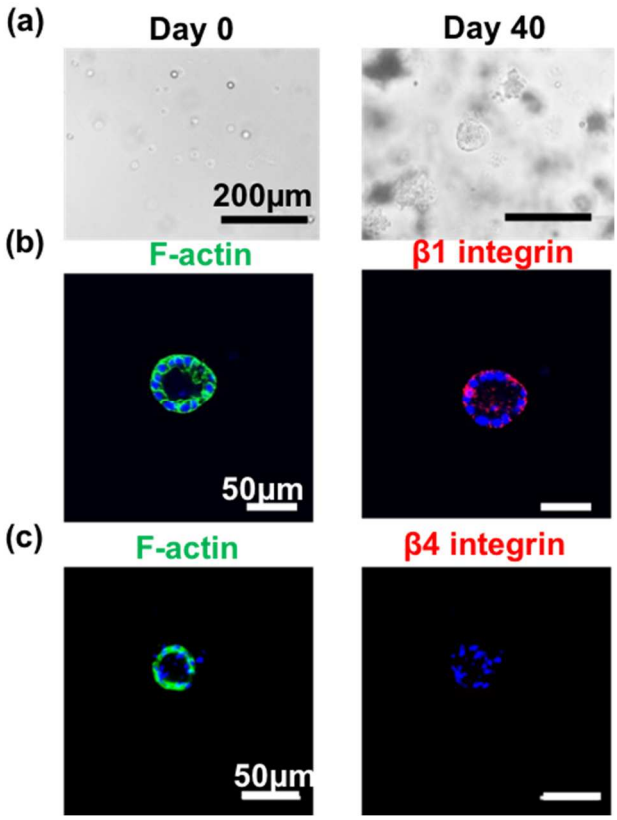

Figure 45, AG1024 (IGF1R inhibitor) in bulk as a control.

(a) 20μM AG1024 was applied for MCF10A cells in bulk Matrigel. (b)(c) Acini were observed with AG1024 at 40 days. The integrin β1 was localized on the surface, but integrin β4 did not express.

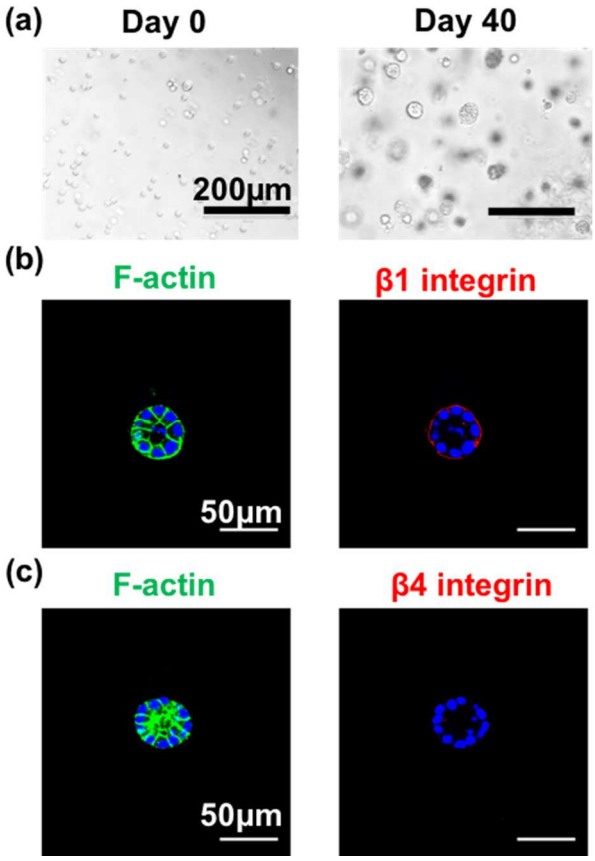

Figure 46, Integrin β4 antibody in bulk as a control.

(a) 1μg/ml antibody was applied for MCF10A cells in bulk Matrigel. (b)(c) polarized acini were observed with integrin β4 antibody at 40 days. The integrin β1 was localized on the surface, but integrin β4 did not express.

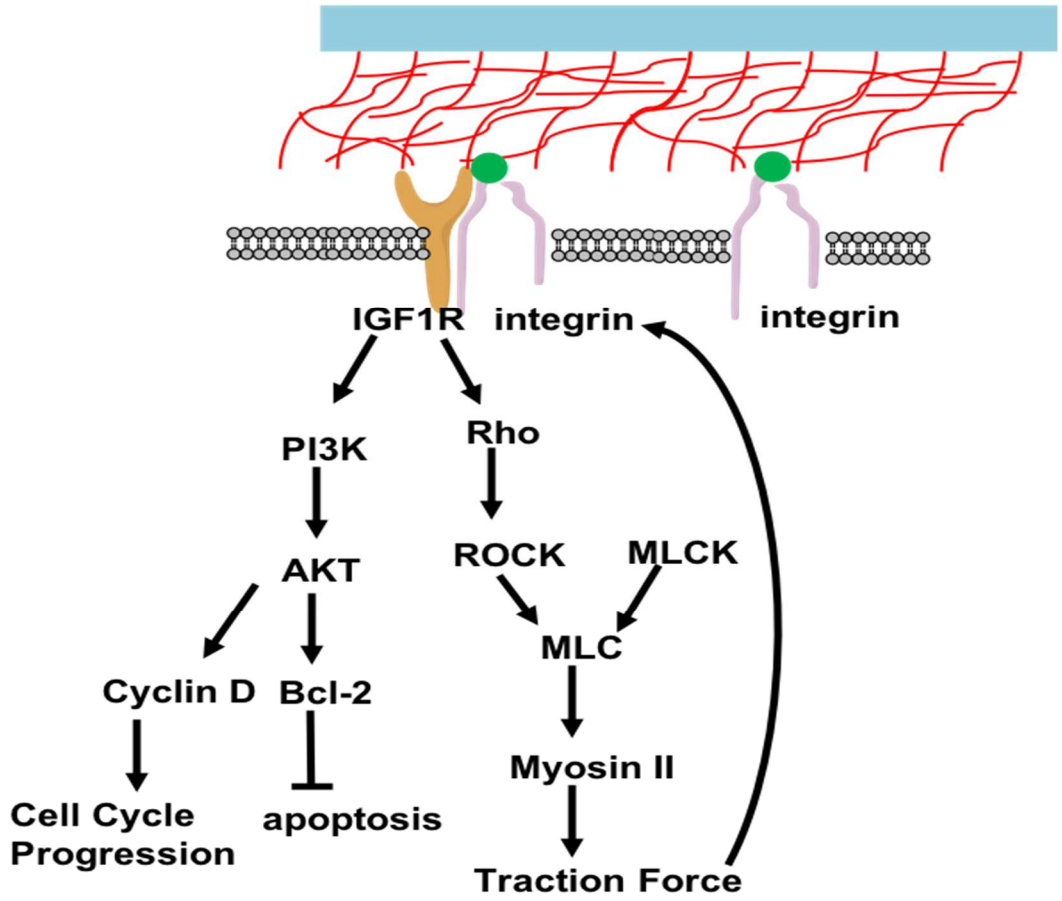

Figure 47, Proposed signaling pathways were regulated under physical confinement from GO enrichment analysis.

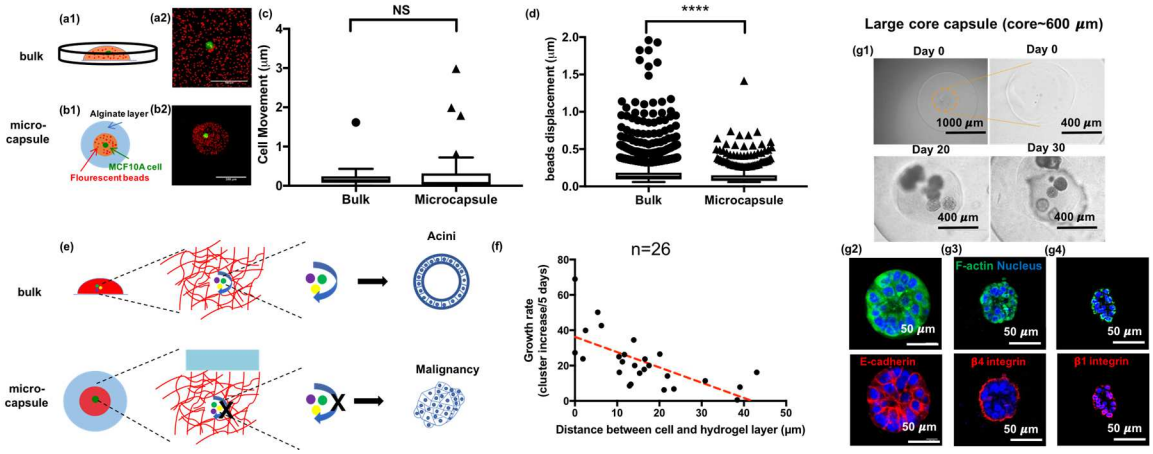

Figure 48, The physical confinement restricts the matrix fluctuation to disrupt the hemidesmosome formation.

(a)Reconstituted basement membrane matrix behaved differently in bulk and microcapsule by fluorescent beads binding with matrix. The Matrigel mixing with fluorescent beads (red) and GFP-expressing MCF10A cells (green) were pipetted in glass-bottom petri-dish and encapsulated in microcapsules for time-lapse confocal microscope. (a1) Schematic for cells in bulk condition. (a2) The z-projection of stacks for fluorescent beads and MCF10A cell in Matrigel. (b) One single MCF10A cell in pure Matrigel with red fluorescent beads was encapsulated in alginate microcapsule. (b1) Schematic for core-shell hydrogel microcapsule with fluorescent beads (b2) z projection for red microbeads and green cell in microcapsule. All scale bar is 100μm. (c) Cells behaved similar in bulk and microcapsules. (n=40, 56 stacked from five independent experiments, p=0.2993) (d) Bead displacement was significantly smaller in a confined microcapsule than in bulk where beads were freely moved without confinement. (n=8113, 732 stacked from five experiments, p<0.0001) (e) Schematic for how hydrogel confinement interrupts acini formation and induce malignancy transformation. (f) The relationship for growth rate versus distance between cell and alginate layer shows that cells received more growth signaling when they were close to the confined layer. (n=26) (g) When the core size increased to 600μm, the confinement effect decreased. The encapsulated cells form acini again in capsules, and integrins localized on the surface, in addition, E-cadherin fully expressed from these acini.

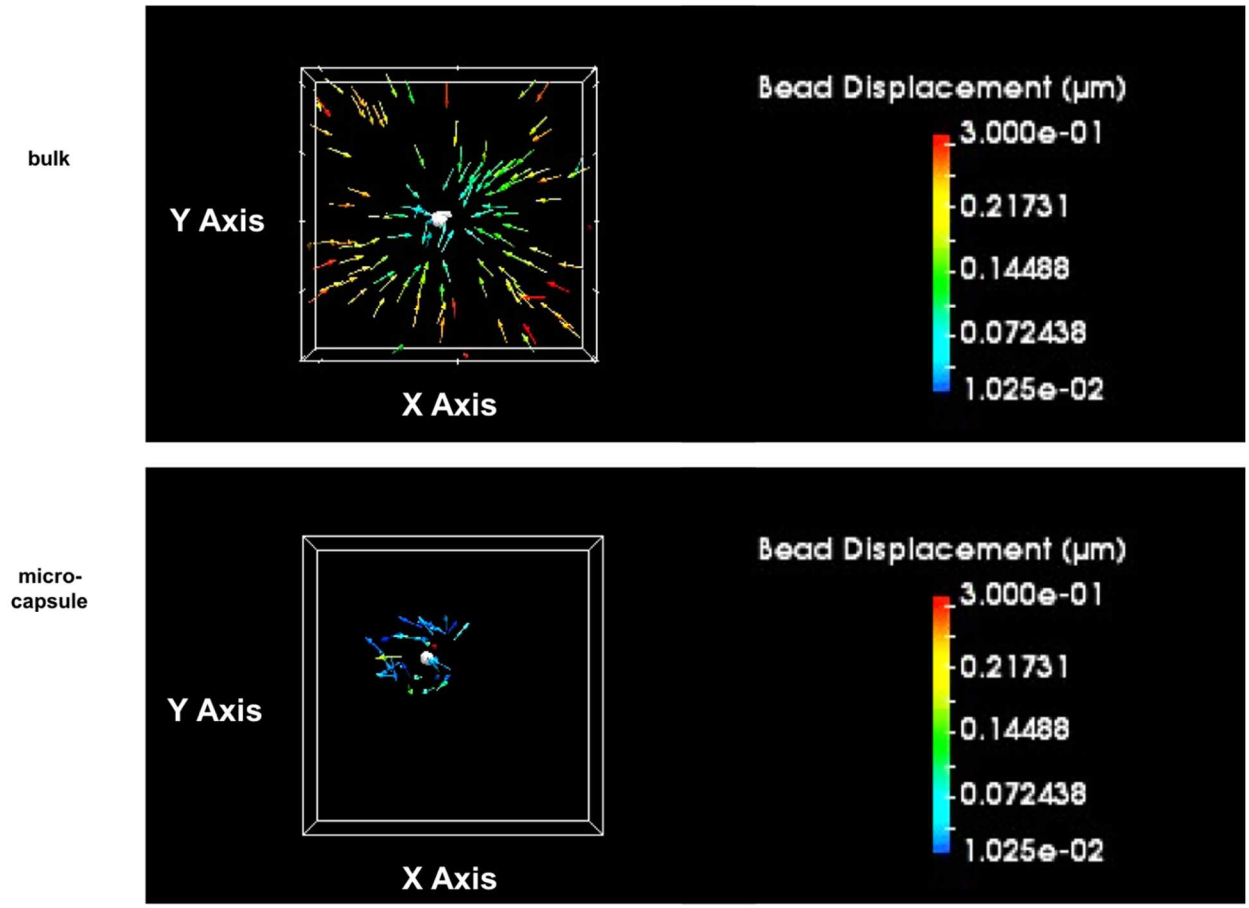

Figure 49, Beads movement in bulk and in microcapsule.

Each arrow represents the discrete displacement of a fluorescent bead binding to Matrigel matrix. Color code was applied to the arrow as the true magnitude for visualization.

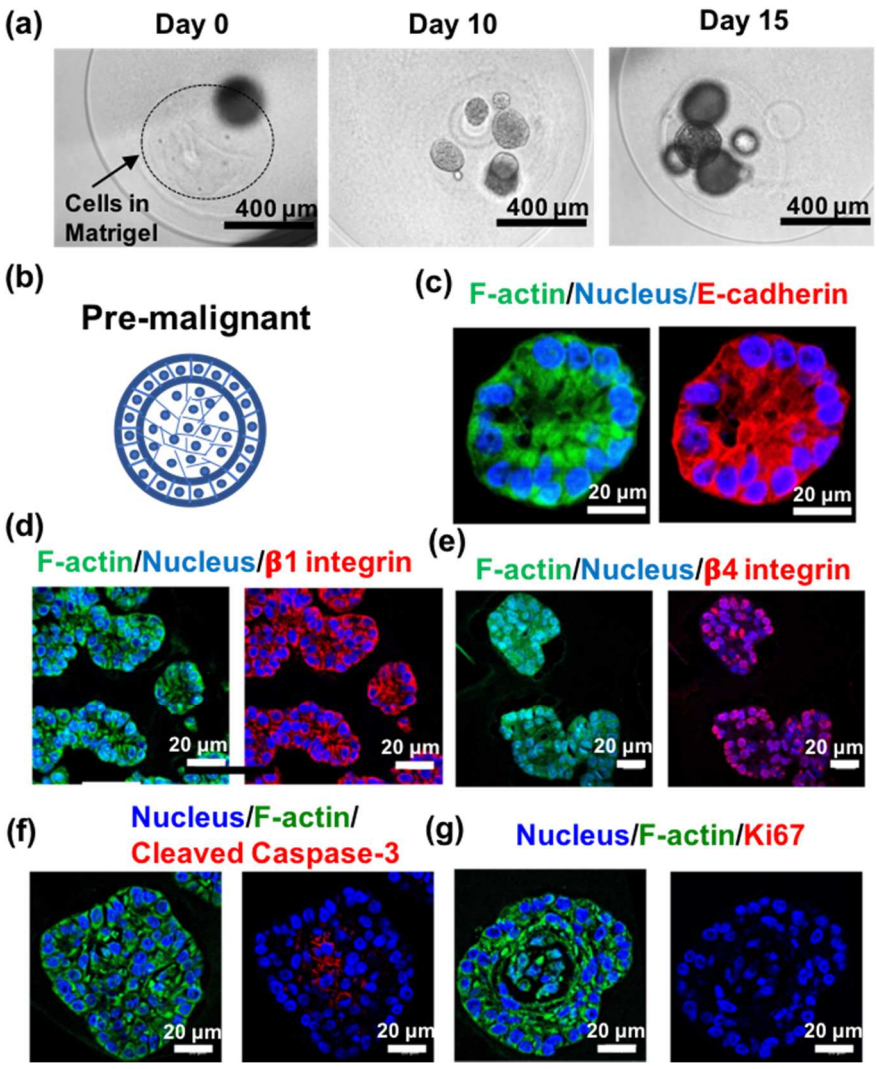

Figure 50, The MCF10A cells were confined in alginate capsules with 500μm core in diameter.

(a) The MCF10A cells grew in larger core to decrease the confinement effect and became pre-malignant state of mammary epithelium. (b) The schematic for pre-malignant state in mammary epithelium. (c) The immunofluorescent staining for F-actin and E-cadherin showed that these cells kept the E-cadherin expression in large core capsules. (d)(e) The integrin β1 and β4 localization were disrupted in large core capsules. (f)(g) The apoptosis and proliferation markers were characterized for acini formation.

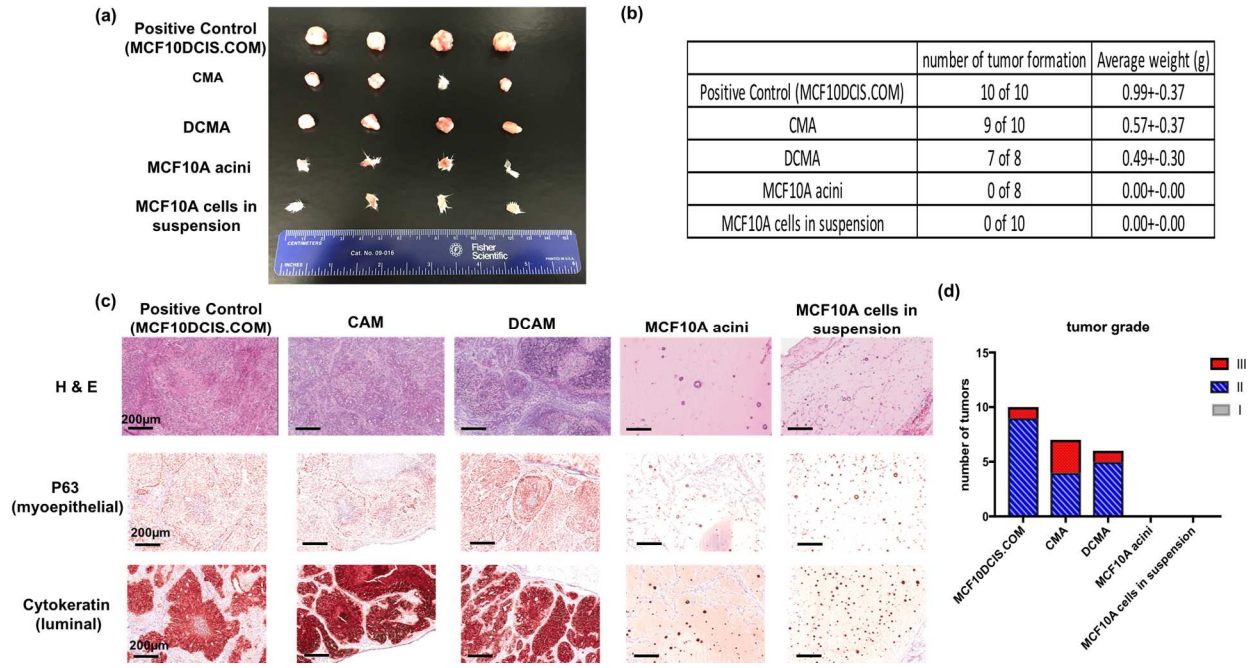

	number of tumor formation	Average weight (g)
Positive Control (MCF10DCIS.COM)	10 of 10	0.99+-0.37
CMA	9 of 10	0.57+-0.37
DCMA	7 of 8	0.49+-0.30
MCF10A acini	0 of 8	0.00+-0.00
MCF10A cells in suspension	0 of 10	0.00+-0.00

Figure 51, In-vivo xenograft and characterization.

(a) Among the five different groups (i.e. MCF10DCIS.COM, confined MCF10A cell aggregates or CMA, confined MCF10A single cells or DCMA, MCF10A acini and single MCF10A cells) that were injected into mammary fat of Scid-beige mice for xenograft (n=10), only MCF10DCIS.COM and CMA, or DCMA formed carcinomas. (b) Rate of tumor formation and the tumor weights from the five groups. (c) H&E and immunohistochemistry staining for all the five groups from xenograft. Differentiation markers, p63 (myoepithelial) and cytokeratin (luminal) markers in mammary epithelium were characterized. (d) The xenograft tumors were analyzed as carcinomas and graded by tumor size, necrosis, tubules and mitotic rate.

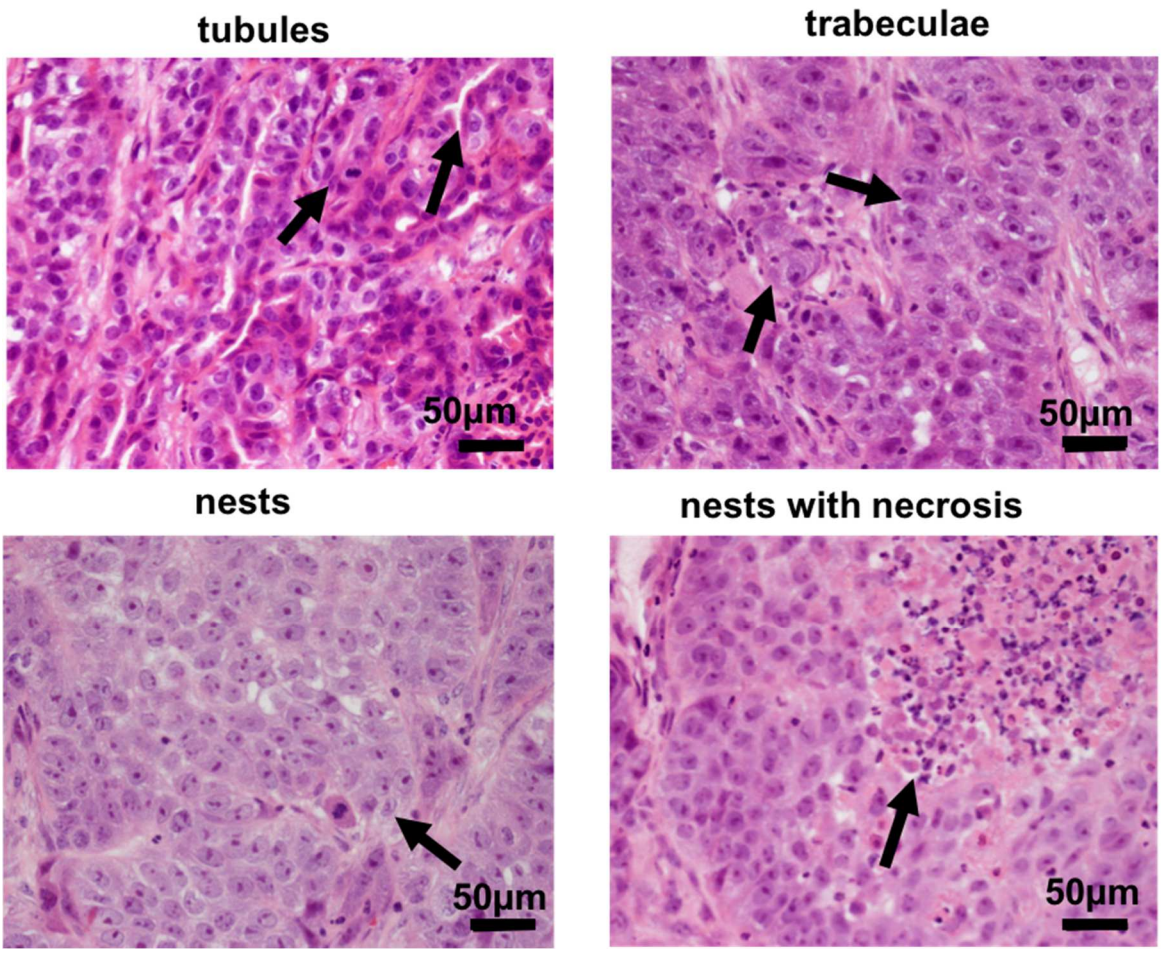

Figure 52, Four histological patterns in xenograft carcinomas, tubules, trabeculae, nests and nests with necrosis.

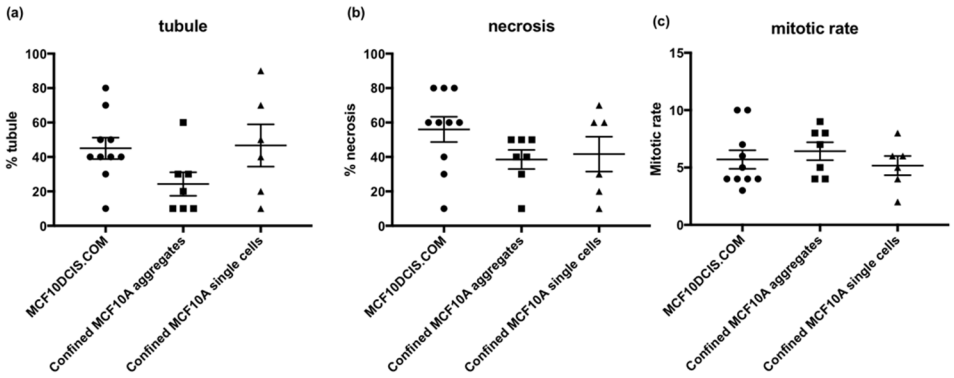

Figure 53, The histological analysis in tubule formation, necrosis and mitotic rate by H&E staining.

We calculated these features from MCF10DCIS.COM, confined MCF10A aggregates and confined MCF10A single cells (n=10, 7 ,6).

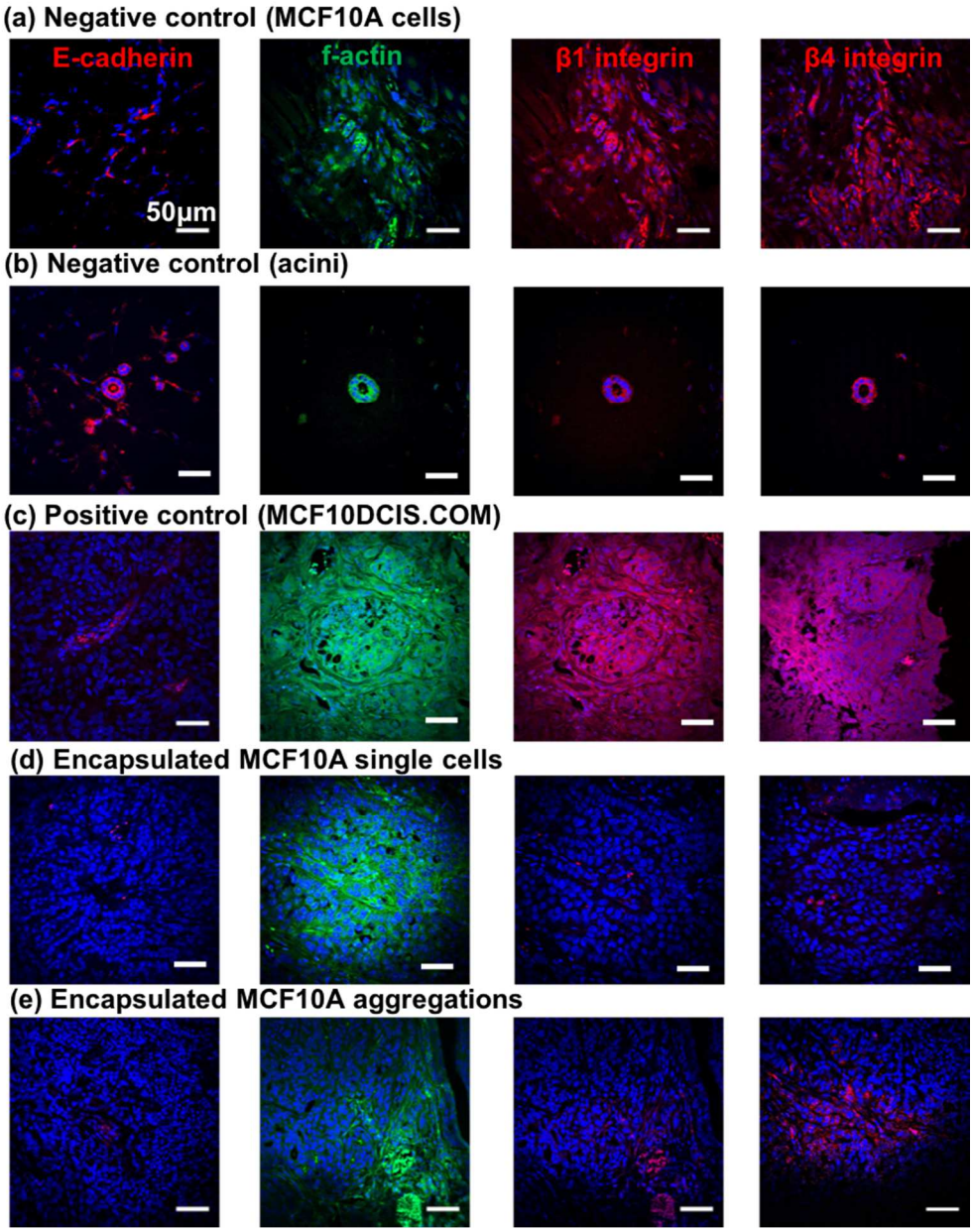

Figure 53, Immunofluorescent of E-cadherin, F-actin, integrin β1 and integrin β4 for xenograft samples.

(a)(b) MCF10A cells suspension and acini from xenograft shows E-cadherin expression, integrin β1 and β4. Interestingly, the acini maintained polarized structure after 4-6 weeks in mice. (c) section of MCF10DCIS.COM lost the expression of E-cadherin, and the localization of integrin β1 and β4 was disrupted. (d)(e) The E-cadherin was completely lost in encapsulated cells/aggregations from microcapsules, and the F-actin was partially lost. Moreover, similar expression of integrin β1 and integrin β4 were lost in xenograft.

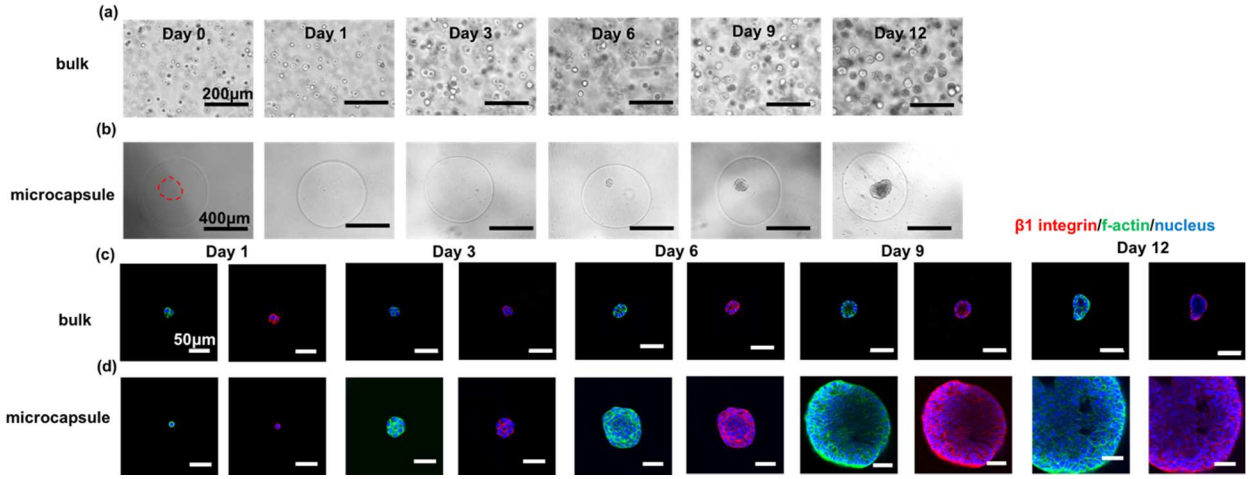

Figure 54, The cell growth in bulk and in microcapsules with time.

(a) The MCF10A cells in bulk grew with time. (b) The encapsulated MCF10A cell in microcapsules grew with time and filled the core in 12 days. (c)(d) The immunofluorescent staining for F-actin and integrin β1 of MCF10A cells in bulk and in microcapsules showed the integrin in bulk was localized after 12 days, but it was disrupted in microcapsules.

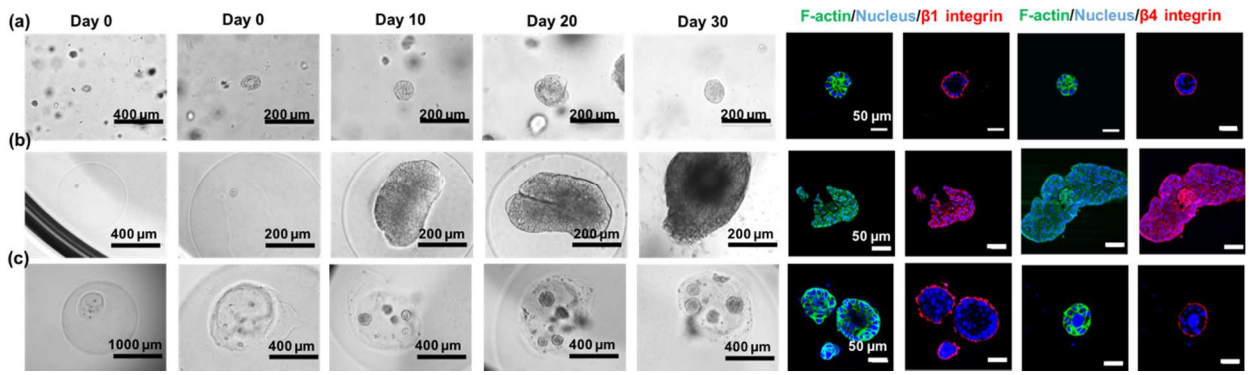

Figure 55, MCF10A acini encapsulation.

(a) acini from bulk Matrigel at day 40 were re-suspended in Matrigel and cultured for 30 days. The acini maintained polarized structure with localization of integrin β1 and integrin β4 (b) When the acini were encapsulated in microcapsules, the polarized structure including integrin localization were disrupted with uncontrolled growth. (c) The acini were encapsulated in capsule with 500μm core to decrease the confinement effect, these acini became larger and similar structure after 30 days. The integrin β1 and integrin β4 were still localized on the surface.

chromosome name	location	GRCh19	confined cells in microcapsules	cells in bulk
chr1	32519111-3219131	CCTCCCAAGTAGCTAGGACTA	CCTCCCAAGTAGCTAGGACTA	CCTCCCAAGTAGCTAGGACTA
chr2	203740000-203740020	CGTTTAGTGGCACGCTAAAAT	CGTTTAGTGGCACGCTAAAAT	CGTTTAGTGGCACGCTAAAAT
chr2	96936111-96936131	CACGCACCCAATCCCAGCTAC	CACGCACCCAATCCCAGCTAC	CACGCACCCAATCCCAGCTAC
chr3	183915218-183915238	GGTTCTCGCTATGTTGCCTAG	GGTTCTCGCTATGTTGCCTAG	GGTTCTCGCTATGTTGCCTAG
chr3	58409962-58409982	GTCATTTTACATAAGATCACA	GTCATTTTACCTAAGATCACA	GTCATTTTACCTAAGATCACA
chr5	150428389-150428409	CAGGGAAGAGCAGACTTTCAC	CAGGGAAGAGGAGACTTTCAC	CAGGGAAGAGGAGACTTTCAC
chr6	15493197-15493217	TACCTTGCCAATAATTCAGTA	TACCTTGCCAATAATTCAGTA	TACCTTGCCAATAATTCAGTA
chr7	66175864-66175874	GATCACCTGTAATCCCACCAT	GATCACCTGTAATCCCACCAT	GATCACCTGTAATCCCACCAT
chr7	86791612-86791632	CTGAGGTTAAGTGATCCTCC	CTGAGGTTAAGTGATCCTCC	CTGAGGTTAAGTGATCCTCC
chr8	21831239-21831259	ACTCCTGACAACTTTGAAGTT	ACTCCTGACACCTTTGAAGTT	ACTCCTGACACCTTTGAAGTT
chr9	35761472-35761492	TGCCTGGGTAACATGACAAAA	TGCCTGGGTAACATGACAAAA	TGCCTGGGTAACATGACAAAA
chr12	125834385-125834405	GGGATGACAGTGACCTTACGG	GGGATGACAGCGACCTTACGG	GGGATGACAGCGACCTTACGG
chr12	53568552-53568572	GCGACAGAGTGGGACTCCAT	GCGACAGAGTGGGACTCCAT	GGCGACAGAGTGGGACTCCAT
chr14	24762212-24762232	AGAAATGGAACGCAAGAGCC	AGAAATGGAACGCAAGAGCC	AGAAATGGAACGCAAGAGCC
chr15	44521463-44521483	AGAGAAACATAAATCTGGCTT	AGAGAAACATAAATCTGGCTT	AGAGAAACATAAATCTGGCTT
chr15	59373826-59373846	GCAGGAGGATAATTTGAGCCC	GCAGGAGGATAATTTGAGCCC	GCAGGAGGATAATTTGAGCCC
chr16	84537634-84537654	CCAGAGGCCCTTGTGCGAAGG	CCAGAGGCCCTTGTGCGAAGG	CCAGAGGCCCTTGTGCGAAGG
chr16	68385841-68385861	GTCAGCCCCACTTTGTCTGCT	GTCAGCCCCACTTTGTCTGCT	GTCAGCCCCACTTTGTCTGCT
chr18	20877282-20877302	GAGACCAGCCTGGCCAACACA	GAGACCAGCCTGGCCAACACA	GAGACCAGCCTGGCCAACACA
chr19	7712575-7712595	CCCCAACATCTTCCCCAAACC	CCCCAACATCTTCCCCAAACC	CCCCAACATCTTCCCCAAACC
chr20	61563590-61563610	TCCTGACACTTTGGGAGGCC	TCCTGACACTTTGGGAGGCC	TCCTGACACTTTGGGAGGCC
chr21	34666366-34666386	CTGCTGGCATAAGCTCTCACC	CTGCTGGCATGAGCTCTCACC	CTGCTGGCATGAGCTCTCACC
chr21	40553970-40553990	GATAAAACTATTGCATACGTG	GATAAAACTACTGCATACGTG	GATAAAACTACTGCATACGTG
chr22	18307624-18307644	GGGACTTCTGGAGCAAAGATA	GGGACTTCTGAAGCAAAGATA	GGGACTTCTGAAGCAAAGATA
chr22	38703352-38703372	CAGACCAGCCTGACCACCATG	CAGACCAGCCTGACCACCATG	CAGACCAGCCTGACCACCATG
chrX	118673318-118673338	AACCCGTCTCTACTAAAAATA	AACCCGTCTCTACTAAAAATA	AACCCGTCTCTACTAAAAATA

Table 3, The DNA sequencing for 26 potential locations on chromosome of cells from microcapsule and bulk. The sequencing results were compared with human reference genome.

CHAPTER 4: CONCLUSION AND FUTURE PERSPECTIVE

4.1 Conclusion

I have developed multiple compartmentalized hydrogel capsules with a tunable ECM support for cell encapsulation and scalable 3D cell culture. These capsules, rapidly produced by a one-step, multi-fluidic electrostatic co-spraying technique have a uniform spherical shape and nearly monodisperse size distribution. Importantly, the technique could fabricate the core-shell decoupled hydrogel capsules with a high production rate from 120 to 13,000 capsules per minute depending on the size of the capsule. This platform provides better scaffold in 3D cell culture and microtissue production because the spherical capsules have a higher surface area for mass transfer and the defined space of ECM to support the cellular growth and function.

First, the core-shell microcapsules are used to culture the cells within capsules in a stirred bioreactor for biomanufacturing because the alginate hydrogel layer could protect the encapsulated cells from the shear force. To prove this concept, I have successfully grown tumoroids and mouse small intestinal organoids in the alginate capsules in the bioreactor. The size of tumoroids could be controlled by the tunable volume of the ECM-supported core in the hydrogel capsules. More importantly, the large sized tumor (>600μm in diameter) could be easily produced by the core-shell hydrogel capsules due to the controllable core size and confined space. In organoid production, this hydrogel capsules not only enhance the expansion efficiency but also improve the cellular recovery from cryopreservation. Altogether, I demonstrated the core-shell hydrogel capsule as a new platform for scalable 3D cell culture and biomanufacturing.

Next, I used the same core-shell structure to create physical confinement by the hydrogel shell layer on the human mammary epithelial cells (MCF10A). I found that MCF10A cells which could form growth-arrested polarized acini in Matrigel, transformed into cancer-like cells within the same Matrigel material following confinement in hydrogel microcapsules. The confined cells exhibited a range of tumor-like behaviors, including uncontrolled cellular proliferation and invasion. Additionally, 4-6 weeks after transplantation into the mammary fad pads of immunocompromised mice, the confined cells formed large palpable masses that exhibited histological features similar to that of carcinomas. Taken together, the results suggest that physical confinement represents a previously unrecognized mechanism for malignancy induction in mammary epithelial cells and also provide a new, microcapsule-based, high throughput model system for testing new breast cancer therapeutics.

In this dissertation, I have demonstrated that the compartmentalized hydrogel capsules could be simply fabricated by one-step electrostatic co-spraying technique. The high-throughput nature of electrospraying technique allows hundreds or thousands of capsules to be rapidly produced for biomanufacturing application. Moreover, the capsule-based platform could be also applied to study the basic biology in breast cancer. In conclusion, the compartmentalized hydrogel capsules have many applications in not only industrial production but also fundamental biology research.

4.2 Future perspective

4.2.1 Applications of double core and triple layer hydrogel capsules

I have shown that different complex structure of hydrogel capsules (double core, triple layer) could be produced by the electrostatic co-spraying technique. However, I have not

demonstrated their practical applications. The next step is that to apply these structures in the basic biology research, for instance, to study cellular communication without contact. In general, several models could be used for cell-cell interaction, such as a transwell system or a conditioned medium which contains exosomes or microvesicles. Nevertheless, these methods could not represent the *in-vivo* condition due to the lack of 3D cell culture and continuous communication between each other. In the double core or triple layer hydrogel capsules, the cells could be seeded in different cores with appropriate ECM to support the 3D culture. Moreover, the interaction between different cells could be continuous because of the close distance between the cells in different compartments. Thus, these two platforms could be useful in the basic biology research, such as, cell paracrine co-culture study.

4.2.2 Physical confinement in stem cell growth and differentiation

I have shown that physical confinement plays an important role in malignant transformation of mammary epithelial cells. Additionally, the physical confinement could also be a factor in stem cell differentiation. For instance, when the organoids were encapsulated in the hydrogel capsules, I observed that the stemness was more highly expressed than the ones without confinement. Next, the exact mechanism for the effect of physical confinement on stem cell biology could be explored by using the same core-shell hydrogel microcapsule system in which the physical properties of hydrogel could be tuned by changing the hydrogel concentration and the crosslinking strength. Thus, the core-shell hydrogel microcapsules could be a versatile platform to study the physical confinement in stem cell growth and differentiation, further contributing to tissue engineering and therapeutic delivery.

Reference

1. Edmondson, R., Broglie, J. J., Adcock, A. F. & Yang, L. Three-dimensional cell culture systems and their applications in drug discovery and cell-based biosensors. *Assay Drug Dev. Technol.* **12,** 207–18 (2014).

2. Timmins, N. E. & Nielsen, L. K. Generation of multicellular tumor spheroids by the hanging-drop method. *Methods Mol Med* **140,** 141–151 (2007).

3. Tung, Y. C. *et al.* High-throughput 3D spheroid culture and drug testing using a 384 hanging drop array. *Analyst* **136,** 473–478 (2011).

4. Song, W. *et al.* Nanofibrous microposts and microwells of controlled shapes and their hybridization with hydrogels for cell encapsulation. *ACS Appl. Mater. Interfaces* **6,** 7038–7044 (2014).

5. Mosaad, E. O., Chambers, K. F., Futrega, K., Clements, J. A. & Doran, M. R. The Microwell-mesh: A high-throughput 3D prostate cancer spheroid and drug-testing platform. *Sci. Rep.* **8,** 253 (2018).

6. Choi, J. K., Agarwal, P., Huang, H., Zhao, S. & He, X. The crucial role of mechanical heterogeneity in regulating follicle development and ovulation with engineered ovarian microtissue. *Biomaterials* **35,** 5122–5128 (2014).

7. Marquis, M., Renard, D. & Cathala, B. Microfluidic Generation and Selective Degradation of Biopolymer-Based Janus Microbeads. *Biomacromolecules* **13,** 1197–1203 (2012).

8. Tan, W.-H. & Takeuchi, S. Monodisperse Alginate Hydrogel Microbeads for Cell

Encapsulation. *Adv. Mater.* **19,** 2696–2701 (2007).

9. Radtke, A. L. & Herbst-Kralovetz, M. M. Culturing and applications of rotating wall vessel bioreactor derived 3D epithelial cell models. *J Vis Exp* (2012). doi:10.3791/38683868 [pii]

10. Orive, G. *et al.* Cell encapsulation: Promise and progress. *Nat. Med.* **9,** 104–107 (2003).

11. Langer, R. & Tirrell, D. A. Designing materials for biology and medicine. *Nature* **428,** 487–492 (2004).

12. Lanza, R. P., Hayes, J. L. & Chick, W. L. Encapsulated cell technology. *Nat. Biotechnol.* **14,** 1107–1111 (1996).

13. Aebischer, P. *et al.* Intrathecal delivery of CNTF using encapsulated genetically modifiedxenogeneic cells in amyotrophic lateral sclerosis patients. *Nat. Med.* **2,** 696–699 (1996).

14. Dolgin, E. Encapsulate this. *Nat. Med.* **20,** 9–11 (2014).

15. Orive, G., Emerich, D. & De Vos, P. Encapsulate this: the do's and don'ts. *Nat. Med.* **20,** 233–233 (2014).

16. Place, E. S., Evans, N. D. & Stevens, M. M. Complexity in biomaterials for tissue engineering. *Nat. Mater.* **8,** 457–470 (2009).

17. Benoit, D. S. W., Schwartz, M. P., Durney, A. R. & Anseth, K. S. Small functional groups for controlled differentiation of hydrogel-encapsulated human mesenchymal stem cells. *Nat. Mater.* **7,** 816–823 (2008).

18. Lim, F. & Sun, A. M. Microencapsulated islets as bioartificial endocrine pancreas. *Science* **210,** 908–10 (1980).

19. Wang, T. *et al.* An encapsulation system for the immunoisolation of pancreatic islets. *Nat. Biotechnol.* **15,** 358–362 (1997).

20. Ma, M. *et al.* Core-Shell Hydrogel Microcapsules for Improved Islets Encapsulation. *Adv. Healthc. Mater.* **2,** 667–672 (2013).

21. Alessandri, K. *et al.* Cellular capsules as a tool for multicellular spheroid production and for investigating the mechanics of tumor progression in vitro. *Proc. Natl. Acad. Sci. U. S. A.* **110,** 14843–14848 (2013).

22. Wei Rao, Shuting Zhao, Jianhua Yu, Xiongbin Lu, Debra L. Zynger, X. H. Enhanced enrichment of prostate cancer stem-like cells with miniaturized 3D culture in liquid core-hydrogel shell microcapsules. *Biomaterials* **35,** 7762–7773 (2014).

23. Maeda, K., Onoe, H., Takinoue, M. & Takeuchi, S. Controlled Synthesis of 3D Multi-Compartmental Particles with Centrifuge-Based Microdroplet Formation from a Multi-Barrelled Capillary. *Adv. Mater.* **24,** 1340–1346 (2012).

24. Liu, Z. & Shum, H. C. Fabrication of uniform multi-compartment particles using microfludic electrospray technology for cell co-culture studies. *Biomicrofluidics* **7,** 44117 (2013).

25. Lutolf, M. P. & Hubbell, J. A. Synthetic biomaterials as instructive extracellular microenvironments for morphogenesis in tissue engineering. *Nat. Biotechnol.* **23,** 47–55 (2005).

26. Onoe, H. *et al.* Metre-long cell-laden microfibres exhibit tissue morphologies and functions. *Nat. Mater.* **12,** 584–590 (2013).

27. Trappmann, B. *et al.* Extracellular-matrix tethering regulates stem-cell fate. *Nat. Mater.* **11,** 642–649 (2012).

28. Chan, B. P., Hui, T. Y., Wong, M. Y., Yip, K. H. K. & Chan, G. C. F. Mesenchymal Stem Cell–Encapsulated Collagen Microspheres for Bone Tissue Engineering. *Tissue Eng. Part C Methods* **16,** 225–235 (2010).

29. Wan, J. & Jiandi. Microfluidic-Based Synthesis of Hydrogel Particles for Cell Microencapsulation and Cell-Based Drug Delivery. *Polymers (Basel).* **4,** 1084–1108 (2012).

30. Lahann, J. Recent Progress in Nano-biotechnology: Compartmentalized Micro- and Nanoparticles via Electrohydrodynamic Co-jetting. *Small* **7,** 1149–1156 (2011).

31. Chen, H., Zhao, Y., Song, Y. & Jiang, L. One-Step Multicomponent Encapsulation by Compound-Fluidic Electrospray. *J. Am. Chem. Soc.* **130,** 7800–7801 (2008).

32. Lima, A. C., Custódio, C. A., Alvarez-Lorenzo, C. & Mano, J. F. Biomimetic Methodology to Produce Polymeric Multilayered Particles for Biotechnological and Biomedical Applications. *Small* **9,** 2487–2492 (2013).

33. Williams, R. M., Zipfel, W. R. & Webb, W. W. Interpreting Second-Harmonic Generation Images of Collagen I Fibrils. *Biophys. J.* **88,** 1377–1386 (2005).

34. Friedrich, J., Seidel, C., Ebner, R. & Kunz-Schughart, L. A. Spheroid-based drug screen: considerations and practical approach. *Nat. Protoc.* **4,** 309–324 (2009).

35. Minchinton, A. I. & Tannock, I. F. Drug penetration in solid tumours. *Nat. Rev. Cancer* **6,** 583–592 (2006).

36. Nyga, A., Cheema, U. & Loizidou, M. 3D tumour models: novel in vitro approaches to cancer studies. *J. Cell Commun. Signal.* **5,** 239–248 (2011).

37. Carey, S. P., Starchenko, A., McGregor, A. L. & Reinhart-King, C. A. Leading malignant cells initiate collective epithelial cell invasion in a three-dimensional heterotypic tumor spheroid model. *Clin. Exp. Metastasis* **30,** 615–630 (2013).

38. Sommers, C. L., Byers, S. W., Thompson, E. W., Torri, J. A. & Gelmann, E. P. Differentiation state and invasiveness of human breast cancer cell lines. *Breast Cancer Res. Treat.* **31,** 325–335 (1994).

39. Pouysségur, J., Dayan, F. & Mazure, N. M. Hypoxia signalling in cancer and approaches to enforce tumour regression. *Nature* **441,** 437–443 (2006).

40. Carmeliet, P. & Jain, R. K. Angiogenesis in cancer and other diseases. *Nat. 2000 4076801* (2000).

41. Ýrr A. Mørch *, Ivan Donati, ‡, and Berit L. Strand & Skjåk-Bræk§, G. Effect of Ca2+, Ba2+, and Sr2+ on Alginate Microbeads. (2006). doi:10.1021/BM060010D

42. Napolitano, A. P., Chai, P., Dean, D. M. & Morgan, J. R. Dynamics of the self-assembly of complex cellular aggregates on micromolded nonadhesive hydrogels. *Tissue Eng* **13,** 2087–2094 (2007).

43. Abu-Absi, S. F., Hansen, L. K. & Hu, W.-S. Three-dimensional co-culture of hepatocytes and stellate cells. *Cytotechnology* **45,** 125–140 (2004).

44. Foty, R. A. & Steinberg, M. S. Cadherin-mediated cell-cell adhesion and tissue segregation in relation to malignancy. *Int. J. Dev. Biol.* **48,** 397–409 (2004).

45. Duguay, D., Foty, R. A. & Steinberg, M. S. Cadherin-mediated cell adhesion and tissue segregation: qualitative and quantitative determinants. *Dev. Biol.* **253,** 309–323 (2003).

46. Kaplowitz, N. Idiosyncratic drug hepatotoxicity. *Nat. Rev. Drug Discov.* **4,** 489–499 (2005).

47. Navarro, V. J. & Senior, J. R. Drug-Related Hepatotoxicity. *N. Engl. J. Med.* **354,** 731–739 (2006).

48. Guillouzo, A. Liver cell models in in vitro toxicology. *Environ. Health Perspect.* **106 Suppl 2,** 511–32 (1998).

49. LeCluyse, E. L. Human hepatocyte culture systems for the in vitro evaluation of cytochrome P450 expression and regulation. *Eur. J. Pharm. Sci.* **13,** 343–368 (2001).

50. Khetani, S. R. & Bhatia, S. N. Microscale culture of human liver cells for drug development. *Nat. Biotechnol.* **26,** 120–126 (2008).

51. Mizuguchi, T. *et al.* Enhanced proliferation and differentiation of rat hepatocytes cultured with bone marrow stromal cells. *J. Cell. Physiol.* **189,** 106–119 (2001).

52. Lin, C. Q. & Bissell, M. J. Multi-faceted regulation of cell differentiation by extracellular matrix. *FASEB J.* **7,** 737–43 (1993).

53. Stevens, K. R. *et al.* InVERT molding for scalable control of tissue microarchitecture. *Nat. Commun.* **4,** 1847 (2013).

54. Du, C., Narayanan, K., Leong, M. F. & Wan, A. C. A. Induced pluripotent stem cell-derived hepatocytes and endothelial cells in multi-component hydrogel fibers for liver tissue engineering. *Biomaterials* **35,** 6006–6014 (2014).

55. Rivron, N. C. *et al.* Tissue deformation spatially modulates VEGF signaling and angiogenesis. *Proc Natl Acad Sci U S A* **109,** 6886–6891 (2012).

56. Alajati, A. *et al.* Spheroid-based engineering of a human vasculature in mice. *Nat. Methods* **5,** 439–445 (2008).

57. Koike, N. *et al.* Creation of long-lasting blood vessels. *Nature* **428,** 138–139 (2004).

58. Bikfalvi, A. *et al.* Interaction of vasculotropin/vascular endothelial cell growth factor with human umbilical vein endothelial cells: Binding, internalization, degradation, and biological effects. *J. Cell. Physiol.* **149,** 50–59 (1991).

59. Bishop, E. T. *et al.* An in vitro model of angiogenesis: Basic features. *Angiogenesis* **3,** 335–344 (1999).

60. Zhong, Z.-F. *et al.* Anti-angiogenic effect of furanodiene on HUVECs in vitro and on zebrafish in vivo. *J. Ethnopharmacol.* **141,** 721–727 (2012).

61. Andrejecsk, J. W. *et al.* Paracrine exchanges of molecular signals between alginate-encapsulated pericytes and freely suspended endothelial cells within a 3D protein gel. *Biomaterials* **34,** 8899–8908 (2013).

62. Villaschi, S. & Nicosia, R. F. Paracrine interactions between fibroblasts and endothelial cells in a serum-free coculture model. Modulation of angiogenesis and collagen gel contraction. *Lab. Invest.* **71,** 291–9 (1994).

63. Lancaster, M. A. & Knoblich, J. A. Organogenesis in a dish: modeling development and disease using organoid technologies. *Science (80-.).* **345,** 1247125 (2014).

64. Sato, T. & Clevers, H. Growing self-organizing mini-guts from a single intestinal stem cell: mechanism and applications. *Science (80-.).* **340,** 1190–1194 (2013).

65. Armstrong, P. B. Cell sorting out: the self-assembly of tissues in vitro. *Crit Rev Biochem Mol Biol* **24,** 119–149 (1989).

66. Dahmann, C., Oates, A. C. & Brand, M. Boundary formation and maintenance in tissue development. *Nat Rev Genet* **12,** 43–55 (2011).

67. Weiss, P. & Taylor, A. C. Reconstitution of Complete Organs from Single-Cell Suspensions of Chick Embryos in Advanced Stages of Differentiation. *Proc Natl Acad Sci U S A* **46,** 1177–1185 (1960).

68. Sinha, G. The organoid architect. *Science* **357,** 746–749 (2017).

69. Lancaster, M. A. *et al.* Cerebral organoids model human brain development and microcephaly. *Nature* **501,** 373–379 (2013).

70. Gjorevski, N. *et al.* Designer matrices for intestinal stem cell and organoid culture. *Nature* **539,** 560–564 (2016).

71. Sachs, N. & Clevers, H. Organoid cultures for the analysis of cancer phenotypes. *Curr. Opin. Genet. Dev.* **24,** 68–73 (2014).

72. Gao, D. *et al.* Organoid Cultures Derived from Patients with Advanced Prostate Cancer. *Cell* **159,** 176–187 (2014).

73. Sato, T. *et al.* Long-term Expansion of Epithelial Organoids From Human Colon, Adenoma, Adenocarcinoma, and Barrett's Epithelium. *Gastroenterology* **141,** 1762–1772 (2011).

74. Clevers, H. The intestinal crypt, a prototype stem cell compartment. *Cell* **154,** 274–284 (2013).

75. Sato, T. *et al.* Single Lgr5 stem cells build crypt-villus structures in vitro without a mesenchymal niche. *Nature* **459,** 262–265 (2009).

76. Sato, T. *et al.* Paneth cells constitute the niche for Lgr5 stem cells in intestinal crypts. *Nature* **469,** 415–418 (2011).

77. Spence, J. R. *et al.* Directed differentiation of human pluripotent stem cells into intestinal tissue in vitro. *Nature* **470,** 105–109 (2011).

78. Yui, S. *et al.* Functional engraftment of colon epithelium expanded in vitro from a single adult Lgr5(+) stem cell. *Nat Med* **18,** 618–623 (2012).

79. Zimmermann, B. Lung organoid culture. *Differentiation* **36,** 86–109 (1987).

80. Lee, J. H. *et al.* Lung stem cell differentiation in mice directed by endothelial cells via a BMP4-NFATc1-thrombospondin-1 axis. *Cell* **156,** 440–455 (2014).

81. Huch, M. *et al.* In vitro expansion of single Lgr5+ liver stem cells induced by Wnt-driven regeneration. *Nature* **494,** 247–250 (2013).

82. Takebe, T. *et al.* Vascularized and functional human liver from an iPSC-derived organ bud transplant. *Nature* **499,** 481–484 (2013).

83. Eiraku, M. *et al.* Self-organizing optic-cup morphogenesis in three-dimensional culture. *Nature* **472,** 51–56 (2011).

84. Nakano, T. *et al.* Self-formation of optic cups and storable stratified neural retina from human ESCs. *Cell Stem Cell* **10,** 771–785 (2012).

85. Kadoshima, T. *et al.* Self-organization of axial polarity, inside-out layer pattern, and species-specific progenitor dynamics in human ES cell-derived neocortex. *Proc Natl Acad Sci U S A* **110,** 20284–20289 (2013).

86. Takasato, M. *et al.* Directing human embryonic stem cell differentiation towards a renal lineage generates a self-organizing kidney. *Nat Cell Biol* **16,** 118–126 (2014).

87. Dekkers, J. F. *et al.* A functional CFTR assay using primary cystic fibrosis intestinal organoids. *Nat. Med.* **19,** 939–945 (2013).

88. Li, M. L. *et al.* Influence of a reconstituted basement membrane and its components on casein gene expression and secretion in mouse mammary epithelial cells. *Proc Natl Acad Sci U S A* **84,** 136–140 (1987).

89. Greggio, C. *et al.* Artificial three-dimensional niches deconstruct pancreas development in vitro. *Development* **140,** 4452–4462 (2013).

90. Lei, Y. & Schaffer, D. V. A fully defined and scalable 3D culture system for human pluripotent stem cell expansion and differentiation. *Proc. Natl. Acad. Sci. U. S. A.* **110,** E5039-48 (2013).

91. Kirouac, D. C. & Zandstra, P. W. The Systematic Production of Cells for Cell Therapies. *Cell Stem Cell* **3,** 369–381 (2008).

92. Desbordes, S. C. & Studer, L. Adapting human pluripotent stem cells to high-throughput and high-content screening. *Nat. Protoc.* **8,** 111–130 (2012).

93. Giwa, S. *et al.* The promise of organ and tissue preservation to transform medicine. *Nat. Biotechnol.* **35,** 530–542 (2017).

94. Popa, E. G. *et al.* Cryopreservation of cell laden natural origin hydrogels for cartilage regeneration strategies. *Soft Matter* **9,** 875–885 (2013).

95. Manuchehrabadi, N. *et al.* Improved tissue cryopreservation using inductive heating of magnetic nanoparticles. *Sci. Transl. Med.* **9,** eaah4586 (2017).

96. Zhang, W., Yang, G., Zhang, A., Xu, L. X. & He, X. Preferential vitrification of water in small alginate microcapsules significantly augments cell cryopreservation by vitrification. *Biomed. Microdevices* **12,** 89–96 (2010).

97. Huang, H. *et al.* Alginate Hydrogel Microencapsulation Inhibits Devitrification and Enables Large-Volume Low-CPA Cell Vitrification. *Adv. Funct. Mater.* **25,** 6839–6850 (2015).

98. Lu, Y.-C. *et al.* Designing compartmentalized hydrogel microparticles for cell encapsulation and scalable 3D cell culture. *J. Mater. Chem. B* **3,** 353–360 (2015).

99. Cheng, C.-Y. *et al.* miR-34 Cooperates with p53 in Suppression of Prostate Cancer by Joint Regulation of Stem Cell Compartment. *Cell Rep.* **6,** 1000–1007 (2017).

100. Sato, T. *et al.* Single Lgr5 stem cells build crypt-villus structures in vitro without a mesenchymal niche. *Nature* **459,** 262–5 (2009).

101. Mahe, M. M. *et al.* Establishment of Gastrointestinal Epithelial Organoids. in *Current Protocols in Mouse Biology* (2013). doi:10.1002/9780470942390.mo130179

102. Raj, A., van den Bogaard, P., Rifkin, S. A., van Oudenaarden, A. & Tyagi, S. Imaging individual mRNA molecules using multiple singly labeled probes. *Nat. Methods* **5,** 877–879 (2008).

103. Grün, D. *et al.* Single-cell messenger RNA sequencing reveals rare intestinal cell types. *Nature* **525,** 251–255 (2015).

104. Barker, N. *et al.* Lgr5(+ve) stem cells drive self-renewal in the stomach and build long-lived gastric units in vitro. *Cell Stem Cell* **6,** 25–36 (2010).

105. Wang, D. H. & Souza, R. F. Transcommitment: Paving the Way to Barrett's Metaplasia. in *Stem Cells, Pre-neoplasia, and Early Cancer of the Upper Gastrointestinal Tract* (eds. Jansen, M. & Wright, N. A.) 183–212 (Springer International Publishing, 2016). doi:10.1007/978-3-319-41388-4_10

106. Agarwal, P. *et al.* A Biomimetic Core-Shell Platform for Miniaturized 3D Cell and Tissue Engineering. *Part. Part. Syst. Charact.* **32,** 809–816 (2015).

107. Gjorevski, N. *et al.* Designer matrices for intestinal stem cell and organoid culture. *Nat. Publ. Gr.* **539,** (2016).

108. Agarwal, P. *et al.* One-step microfluidic generation of pre-hatching embryo-like core–shell microcapsules for miniaturized 3D culture of pluripotent stem cells. *Lab Chip* **13,** 4525 (2013).

109. Zhao, S. *et al.* Coaxial electrospray of liquid core–hydrogel shell microcapsules for

encapsulation and miniaturized 3D culture of pluripotent stem cells. *Integr. Biol.* **6,** 874–884 (2014).

110. Zhao, S. *et al.* Bioengineering of injectable encapsulated aggregates of pluripotent stem cells for therapy of myocardial infarction. *Nat. Commun.* **7,** 13306 (2016).

111. Choi, J. K. *et al.* The crucial role of zona pellucida in cryopreservation of oocytes by vitrification. *Cryobiology* **71,** 350–355 (2015).

112. Xue, X. & Shah, Y. M. In vitro organoid culture of primary mouse colon tumors. *J. Vis. Exp.* e50210 (2013). doi:10.3791/50210

113. Miyoshi, H. & Stappenbeck, T. S. In vitro expansion and genetic modification of gastrointestinal stem cells in spheroid culture. *Nat. Protoc.* **8,** 2471–82 (2013).

114. Chua, C. W. *et al.* Culture of mouse prostate organoids. *Nat. Protoc. Exch.* (2014).

115. DeSantis, C. E., Ma, J., Goding Sauer, A., Newman, L. A. & Jemal, A. Breast cancer statistics, 2017, racial disparity in mortality by state. *CA. Cancer J. Clin.* **67,** 439–448 (2017).

116. Page, D. L. & Lagios, M. D. Pathology and clinical evolution of ductal carcinoma in situ (DCIS) of the breast. *Cancer Lett* **86,** 1–4 (1994).

117. Ellis, I. O. Intraductal proliferative lesions of the breast: morphology, associated risk and molecular biology. *Mod Pathol* **23 Suppl 2,** S1-7 (2010).

118. Silverstein, M. J. *et al.* A prognostic index for ductal carcinoma in situ of the breast. *Cancer* **77,** 2267–2274 (1996).

119. Place, A. E., Jin Huh, S. & Polyak, K. The microenvironment in breast cancer progression: biology and implications for treatment. *Breast Cancer Res.* **13,** 227 (2011).

120. Chavez, K. J., Garimella, S. V. & Lipkowitz, S. Triple negative breast cancer cell lines: One tool in the search for better treatment of triple negative breast cancer. *Breast Dis.* **32,** 35–48 (2011).

121. Bauer, K. R., Brown, M., Cress, R. D., Parise, C. A. & Caggiano, V. Descriptive analysis of estrogen receptor (ER)-negative, progesterone receptor (PR)-negative, and HER2-negative invasive breast cancer, the so-called triple-negative phenotype. *Cancer* **109,** 1721–1728 (2007).

122. Debnath, J., Muthuswamy, S. K. & Brugge, J. S. Morphogenesis and oncogenesis of MCF-10A mammary epithelial acini grown in three-dimensional basement membrane cultures. *Methods* **30,** 256–268 (2003).

123. Qu, Y. *et al.* Evaluation of MCF10A as a reliable model for normal human mammary epithelial cells. *PLoS One* **10,** 1–16 (2015).

124. Santner, S. J. *et al.* Malignant MCF10CA1 cell lines derived from premalignant human breast epithelial MCF10AT cells. *Breast Cancer Res. Treat.* **65,** 101–10 (2001).

125. Dawson, P. J., Wolman, S. R., Tait, L., Heppner, G. H. & Miller, F. R. MCF10AT: a model for the evolution of cancer from proliferative breast disease. *Am. J. Pathol.* **148,** 313–9 (1996).

126. Visvader, J. E. Keeping abreast of the mammary epithelial hierarchy and breast tumorigenesis. *Genes Dev.* **23,** 2563–77 (2009).

127. Polyak, K. Breast cancer: origins and evolution. *J. Clin. Invest.* **117,** 3155–63 (2007).

128. Levental, K. R. *et al.* Matrix Crosslinking Forces Tumor Progression by Enhancing Integrin Signaling. *Cell* **139,** 891–906 (2009).

129. Paszek, M. J. M. J. J. *et al.* Tensional homeostasis and the malignant phenotype. *Cancer Cell* **8,** 241–254 (2005).

130. Chaudhuri, O. *et al.* Extracellular matrix stiffness and composition jointly regulate the induction of malignant phenotypes in mammary epithelium. *Nat. Mater.* **13,** 1–35 (2014).

131. Rakha, E. A. *et al.* Prognostic significance of Nottingham histologic grade in invasive breast carcinoma. *J. Clin. Oncol.* **26,** 3153–8 (2008).

132. Hall, M. S. *et al.* Fibrous nonlinear elasticity enables positive mechanical feedback between cells and ECMs. *Proc. Natl. Acad. Sci. U. S. A.* **113,** 14043–14048 (2016).

133. Feng, X. Z., Hall, M. S., Wu, M. M. & Hui, C. Y. An adaptive algorithm for tracking 3D bead displacements: application in biological experiments. *Meas. Sci. Technol.* **25,** (2014).

134. Patro, R., Duggal, G., Love, M. I., Irizarry, R. A. & Kingsford, C. Salmon provides fast and bias-aware quantification of transcript expression. *Nat. Methods* **14,** 417–419 (2017).

135. Love, M. I., Huber, W. & Anders, S. Moderated estimation of fold change and dispersion for RNA-seq data with DESeq2. *Genome Biol.* **15,** 550 (2014).

136. Soofi, S. S., Last, J. A., Liliensiek, S. J., Nealey, P. F. & Murphy, C. J. The elastic modulus of Matrigel as determined by atomic force microscopy. *J. Struct. Biol.* **167,** 216–9 (2009).

137. Liberti, M. V & Locasale, J. W. The Warburg Effect: How Does it Benefit Cancer Cells? *Trends Biochem. Sci.* **41,** 211–218 (2016).

138. Tsai, J. H. & Yang, J. Epithelial-mesenchymal plasticity in carcinoma metastasis. *Genes Dev.* **27,** 2192–206 (2013).

139. Ashburner, M. *et al.* Gene Ontology: tool for the unification of biology. *Nat. Genet.* **25,** 25–29 (2000).

140. Cedano Prieto, D. M. *et al.* Direct integrin binding to insulin-like growth factor-2 through the C-domain is required for insulin-like growth factor receptor type 1 (IGF1R) signaling. *PLoS One* **12,** e0184285 (2017).

141. Kocatürk, B. & Versteeg, H. H. Orthotopic injection of breast cancer cells into the mammary fat pad of mice to study tumor growth. *J. Vis. Exp.* (2015). doi:10.3791/51967

142. McElwee, J. L. *et al.* Identification of PADI2 as a potential breast cancer biomarker and therapeutic target. *BMC Cancer* **12,** 500 (2012).

143. Boyd, N. F. *et al.* Mammographic density and the risk and detection of breast cancer. *N Engl J Med* **356,** 227–236 (2007).

144. Boyd, N. F. *et al.* Mammographic Density: A Heritable Risk Factor for Breast Cancer. in 343–360 (Humana Press, 2009). doi:10.1007/978-1-60327-492-0_15

145. Wang, H., Lacoche, S., Huang, L., Xue, B. & Muthuswamy, S. K. Rotational motion during three-dimensional morphogenesis of mammary epithelial acini relates to laminin matrix assembly. *Proc. Natl. Acad. Sci. U. S. A.* **110,** 163–168 (2013).

146. Underwood, J. M. *et al.* The ultrastructure of MCF-10A acini. *J. Cell. Physiol.* **208,** 141–148 (2006).

147. Milholland, B. *et al.* Differences between germline and somatic mutation rates in humans and mice. *Nat. Commun.* **8,** 15183 (2017).

148. Pisco, A. O., d'Herouel, A. F. & Huang, S. Conceptual Confusion: the case of Epigenetics. *bioRxiv* 053009 (2016). doi:10.1101/053009

149. Fujita, M. *et al.* Cross-talk between integrin α6β4 and insulin-like growth factor-1 receptor (IGF1R) through direct α6β4 binding to IGF1 and subsequent α6β4-IGF1-IGF1R ternary complex formation in anchorage-independent conditions. *J. Biol. Chem.* **287,** 12491–500 (2012).

150. Shaw, L. M. Identification of insulin receptor substrate 1 (IRS-1) and IRS-2 as signaling intermediates in the alpha6beta4 integrin-dependent activation of phosphoinositide 3-OH kinase and promotion of invasion. *Mol. Cell. Biol.* **21,** 5082–93 (2001).

151. Elston, C. W. THE ASSESSMENT OF HISTOLOGICAL DIFFERENTIATION IN BREAST CANCER. *ANZ J. Surg.* **54,** 11–15 (1984).

152. Page, D. L. & Lagios, M. D. Pathology and clinical evolution of ductal carcinoma in situ (DCIS) of the breast. *Cancer Lett* **86,** 1–4 (1994).